Title
The Theory of Thermal, Thermoelectric and Electrical Transport Properties of Graphene

Author
Ugarte, Vincent Ike

Publication Date
2010

Peer reviewed|Thesis/dissertation

UNIVERSITY OF CALIFORNIA
RIVERSIDE

The Theory of Thermal, Thermoelectric and Electrical Transport Properties of Graphene

A Dissertation submitted in partial satisfaction
of the requirements for the degree of

Doctor of Philosophy

in

Physics

by

Vincent Ike Ugarte

December 2010

Dissertation Committee:

Dr. Chandra Varma, Chairperson
Dr. Vivek Aji
Dr. Jin Shi

The Dissertation of Vincent Ike Ugarte is approved:

Committee Chairperson

University of California, Riverside

Acknowledgments

First, I would like to thank my advisor, Professor Chandra M. Varma for supervising my academic research. Also I would like to thank my committee members Professor Vivek Aji and Professor Jin Shi for helping me with my academic research. Furthermore, I would like to thank Professor Jin Shi, Peng Wei and Deqi Wang for useful discussions and sharing their experimental data which was the instrumental in guiding my academic research. Last but not least, I like to thank my family and friends for there support.

To my Mother, family, and friends for all the support.

ABSTRACT OF THE DISSERTATION

The Theory of Thermal, Thermoelectric and Electrical Transport Properties of Graphene

by

Vincent Ike Ugarte

Doctor of Philosophy, Graduate Program in Physics
University of California, Riverside, December 2010
Dr. Chandra Varma, Chairperson

Motivated by the experimental measurement of transport properties such as electrical and hall conductivity, thermopower and Nernst, I present a study of longitudinal and transverse transport in graphene for the dilute limit of impurities. The temperature and carrier density dependence in this system display a number of anomalous properties that can be related to three effects: 1) emergence of "chirality", 2) vanishing density of states at the chemical potential in the ideal undoped (zero gate voltage) systems and 3) nature of scattering. In an attempt to theoretically understand these anomalous transport properties, I use the theory of quantum transport in a two-dimensional system with Unitary(lattice vacancy) and screened Coulomb(charge impurity in the underlining substrate) scatterers. I show for a system such as graphene, the type of scattering potential has a profound effect on all transport properties, even though both types of potentials induce low energy states that yield a finite density of states at zero energy. My results are compared with experimental data for both types of scatterer and I show for a single set of impurity parameters all transport properties can be reproduced to agree qualitative with the features observed in experimental data.

Contents

List of Figures

List of Tables

Chapter 1

Introduction

1.1 Introduction to Graphene

Graphene is a two dimensional material made of carbon atoms arranged in a honeycomb lattice structure. The honeycomb lattice is made of two interpenetrating Bravais lattices which have the symmetry of equilateral triangles. The atoms comprising the triangular sub-lattices are labeled as A(Blue) and B(Yellow) in figure 1.1. The crystal structure is a consequence of the sp^2 symmetry of the carbon's hybridized orbitals. In graphene the four valence electrons of each carbon($1s^2 2s^2 2p^2$) atom hybridize to form three sp^2 orbitals and one p_z orbit. The hybridized orbitals form sigma-bonds with the three neighboring carbon atoms leaving the pi-bond(p_z orbit) half filled. The electrons that form the three sigma bonds do not contribute to transport properties[1, 2].

In the tight binding formalism the Hamiltonian for graphene with nearest- and next-nearest-neighbor hopping is

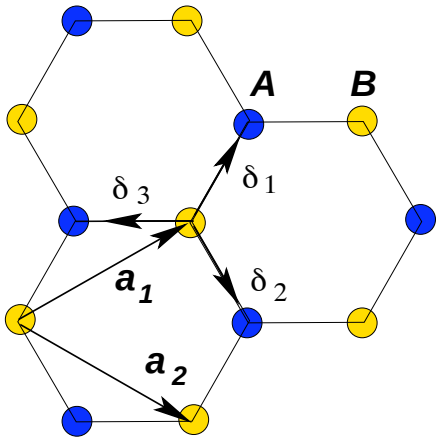

Figure 1.1: A sketch of the honeycomb lattice structure of graphene was adapted from Ref.[3]. Here the vectors connecting any atom to its nearest neighbor are: $\delta_1 = \frac{a_0}{2}(1, \sqrt{3}, 0)$, $\delta_2 = \frac{a_0}{2}(1, -\sqrt{3}, 0)$, $\delta_3 = -a_0(1, 0, 0)$ where a_0 is the lattice spacing. The two sub-lattices consisting of A and B atoms are arranged in a triangular lattice with primitive vectors: $a_1 = \frac{a_0}{2}(3, \sqrt{3}, 0)$ and $a_2 = \frac{a_0}{2}(3, -\sqrt{3}, 0)$.

$$\begin{aligned} H &= -t \sum_{<i,j>,\sigma} (a^\dagger_{i,\sigma} b_{j,\sigma} + h.c.) \\ &- t' \sum_{<<i,j>>,\sigma} (a^\dagger_{i,\sigma} a_{j,\sigma} + b^\dagger_{i,\sigma} b_{j,\sigma} + h.c.), \end{aligned} \tag{1.1}$$

where t is the nearest-neighbor hopping energy and t' is the next-nearest-neighbor hopping energy. The operators $\{a_{i,\sigma}, b_{i,\sigma}\}$ are the annihilation operators for an electron on A and B sub-lattice respectively. The band dispersion is [3, 2, 4]

$$\begin{aligned} E_{\overrightarrow{k}} &= \pm t\sqrt{3 + \phi(\overrightarrow{k})} - t'\phi(\overrightarrow{k}) \\ \phi(\overrightarrow{k}) &= 2\cos(\sqrt{3}k_y a_0) + 4\cos(\frac{\sqrt{3}}{2}k_y a_0)\cos(\frac{3}{2}k_x a_0), \end{aligned} \tag{1.2}$$

where the plus(minus) sign of the energy spectrum refers to the upper(lower) $\pi^*(\pi)$ bands. The p_z bands are referred to as $\pi^*(\pi)$ bands because graphene layers bond via π bonds to form graphite. Since there are two atoms per unit cell two energy bands are

obtained in the dispersion.

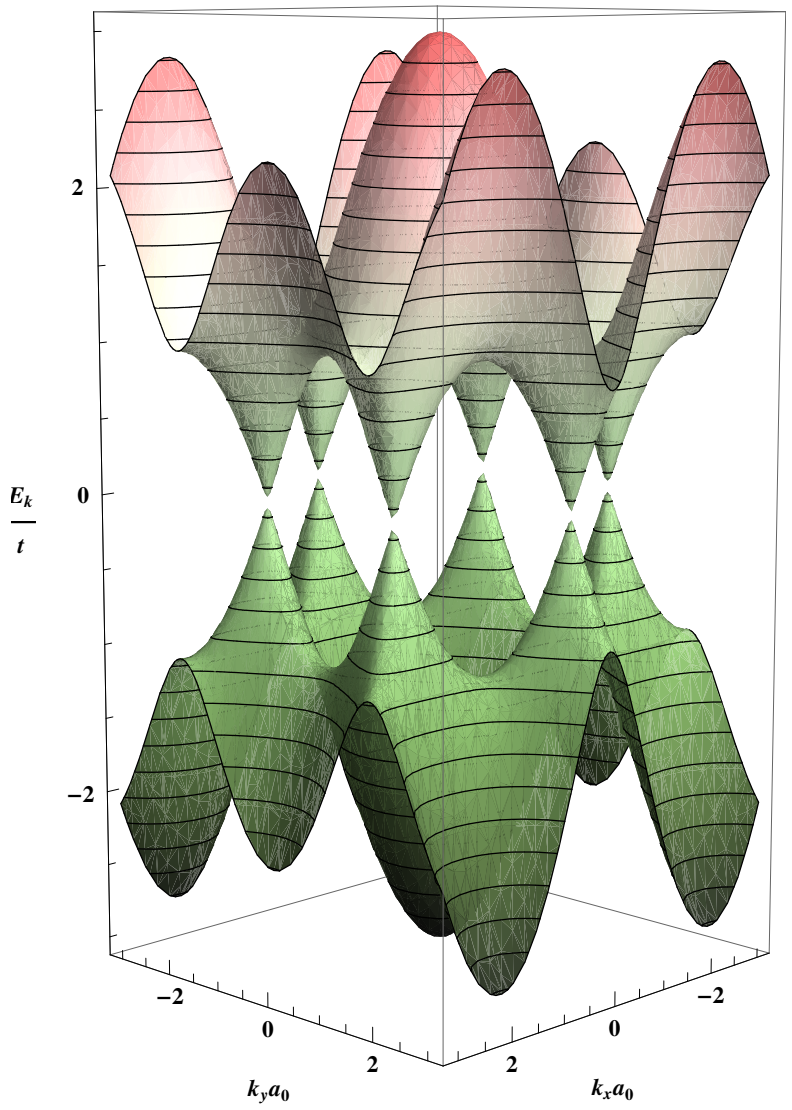

Figure 1.2: A plot of Electronic dispersion of un-doped graphene, here the parameter t' has been set to zero and the energy spectrum has been rescaled in term of t. The energy spectrum has six point where the hole and electron bands meet but only two point are inequivalent

Graphene's band structure has remarkable features: the hole and electron bands are not separated by a band gap and the two bands do not overlap. Unlike ordinary semiconductors where there is a finite band gap (typically of $O(eV)$), Graphene is a zero gap semiconductor. The hole and electron bands intersect at six points, but only two

points are inequivalent because the other points can be generated using reciprocal lattice vectors see figure (1.1). The two inequivalent band intersections are called Dirac points in the first Brillouin Zone and the electronic dispersion in the vicinity of these points have a linear rather then the typical parabolic dispersion found in most crystals.

1.1.1 Graphene Lattice In Reciprocal Space

In reciprocal space the two sub-lattices structure of graphene is shown for the first Brillouin zone in figure 1.1.1.

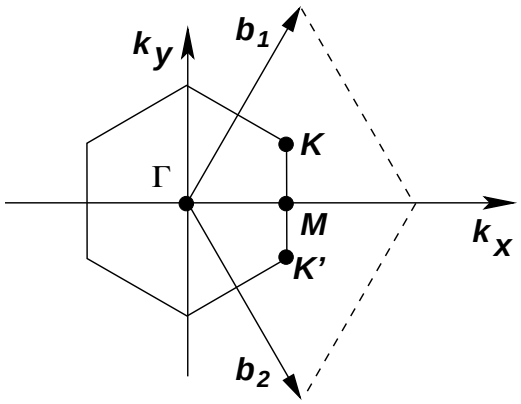

Figure 1.3: A sketch of graphene's first Brillouin Zone was adapted from Ref.[3]. Here the reciprocal lattice vectors are: $b_1 = \frac{2\pi}{3a_0}(1, \sqrt{3}, 0)$ and $b_2 = \frac{2\pi}{3a_0}(1, -\sqrt{3}, 0)$, where a_0 is the lattice spacing. The two vectors K and K' are the location of the Dirac points in reciprocal space: $K = \frac{2\pi}{3a_0}(1, \frac{1}{\sqrt{3}}, 0)$ and $K' = \frac{2\pi}{3a_0}(1, -\frac{1}{\sqrt{3}}, 0)$.

The two points K and K' are referred to as Dirac points and near these points the band dispersion of electrons can be simplified to the form $E_{\overrightarrow{q}} = \pm\hbar v_F|\overrightarrow{q}|$, where $\overrightarrow{q} = \{\overrightarrow{k} - \overrightarrow{K}, \overrightarrow{k} - \overrightarrow{K'}\}$ for each Dirac point respectively. The conical dispersion can be found by first substituting $\overrightarrow{k} = \overrightarrow{q} + \overrightarrow{K}^{(1,2)}$ in to eqn.1.2; here the wave-vectors $\overrightarrow{K}^{(1,2)}$ correspond to each Dirac points $\{K, K'\}$, $\overrightarrow{q}$ is a small wave-vector deviation from each Dirac point. After substituting $\overrightarrow{k} = \overrightarrow{q} + \overrightarrow{K}^{(1,2)}$ into $\phi(\overrightarrow{k})$ of eqn.1.2, $\phi(\overrightarrow{q})$ has the

following form

$$\begin{aligned}\phi(\overrightarrow{q}) &= -\cos(\sqrt{3}q_y a_0) \mp \sqrt{3}\sin(\sqrt{3}q_y a_0) \\ &- 2\left(\cos\left(\frac{\sqrt{3}}{2}q_y a_0\right) \mp \sqrt{3}\sin\left(\frac{\sqrt{3}}{2}q_y a_0\right)\right)\cos\left(\frac{3}{2}q_x a_0\right), \end{aligned} \tag{1.3}$$

here the following trig identities have been used to simplify $\phi(\overrightarrow{q})$.

$$\cos(x \pm y) = \cos x \cos y \mp \sin x \sin y \tag{1.4}$$

$$\cos\left(\frac{\pi}{3}\right) = -\cos\left(\frac{2\pi}{3}\right) = \frac{1}{2} \tag{1.5}$$

$$\sin\left(\frac{\pi}{3}\right) = \sin\left(\frac{2\pi}{3}\right) = \frac{\sqrt{3}}{2} \tag{1.6}$$

Taylor expanding $\phi(\overrightarrow{q})$ about $\overrightarrow{q} = 0$ and only including up to second order in $|\overrightarrow{q}|$ eqn.1.2 is

$$\begin{aligned} E_{\overrightarrow{k}} &= \pm\hbar v_F|\overrightarrow{q}| - \frac{\hbar^2|\overrightarrow{q}|^2}{2m_{eff}} + 3t' \\ \phi(\overrightarrow{k}) &= -3 + \frac{9(a_0|\overrightarrow{q}|)^2}{4}, \end{aligned} \tag{1.7}$$

where v_F is the Fermi velocity and is equal to $\frac{3ta_0}{2\hbar}$, m_{eff}^{-1} is the effective mass of electron in one of the triangular lattices and is equal to $\frac{9t'a_0^2}{2\hbar^2}$. Near these Dirac points the electrons low energy behavior is equivalent to two dimensional mass-less Dirac Fermions[5]. The low energy Hamiltonian for graphene near these Dirac points has the form

$$H = \hbar v_F \overrightarrow{\sigma} \cdot \overrightarrow{k}, \tag{1.8}$$

where $\overrightarrow{\sigma} = \{\sigma_x, \sigma_y, \sigma_z\}$ and σ_i's are Pauli matrices, v_F is the Fermi velocity. The Pauli matrices are defined as

$$\sigma_x = \begin{pmatrix} 0 & 1 \\ 1 & 0 \end{pmatrix}, \quad \sigma_y = \begin{pmatrix} 0 & -i \\ i & 0 \end{pmatrix}, \quad \sigma_z = \begin{pmatrix} 1 & 0 \\ 0 & -1 \end{pmatrix} \tag{1.9}$$

and the Fermi velocity in terms of band parameters is $v_F = \frac{3ta_0}{2\hbar}$. The low energy Hamiltonian is obtained for small deviations of momenta near the Dirac point. As such it is not valid for large values of the chemical potential away from half filling.

1.1.2 Inconsistency between Classical and Quantum Description of Graphene

Graphene's electronic properties exhibit unique features: experimental measurements of electrical conductivity varies linearly with carrier density and reaches a minimum conductivity near zero carrier density[6, 7, 5, 8]. Measurements of the density of states of graphene via $\frac{dI}{dV}$ and quantum capacitance have shown that the density of states is linear in energy down to a cutoff energy scale where it becomes nonzero[9, 10, 11]. If the low energy dispersion ($E_{\overrightarrow{k}} = \pm\hbar v_F|\overrightarrow{k}|$) is to be taken seriously, a theory must explain the inconsistency between classical and quantum description of graphene. In Boltzmann theory of transport the electrical conductivity at zero temperature has the form

$$\sigma(\varepsilon_F) = \frac{e^2 v_F^2}{2} N(\varepsilon_F)\tau(\varepsilon_F), \tag{1.10}$$

here ε_F is the Fermi energy and $\tau(\varepsilon_F)$ is the transport time. In order for the classical descriptions of electrical conductivity to be consistent with experiments either the density states must be finite at the node or the transport time is inversely proportional to energy. Experiments have shown that near the Dirac point the density of states does

not go to zero[9, 10, 11], which supports the first explanation for a finite electrical conductivity. The puzzling problem is that the density of states in the vicinity of the Dirac point is linear and has the form

$$N(\varepsilon) = \frac{|\varepsilon|}{\pi v_F^2 \hbar^2}, \tag{1.11}$$

which indicates that experimentally the density of states should vanishes at the Dirac point. A possible classical explanation for both of these unique features is charge puddles; these puddles mask the Dirac point by providing a finite charge distribution, i.e., charge puddles provide a cut-off energy scale where the linear density of states becomes a constant. Alternatively, the minimum conductivity can be explained without modifying the density of states by using short-ranged unitary scatterers. The corresponding scattering rate of short-ranged unitary scatterers is also linear in energy, yielding an electrical conductivity that is independent of carrier density[12]. However, short-ranged unitary scatterers do not explain the finite density of states unless quantum effect such as resonance are included.

The problem with these models is that experiments have shown at large carrier densities the electrical conductivity varies linearly with carrier density[6, 7, 5, 8]. This implies either the source of charge puddles provides an energy dependent transport rate or the scattering rate of short-ranged unitary scatterers has a more complex energy dependence. The linear carrier density dependence of electrical conductivity can be understood in the first model by assuming that charge scatterers provide the source of these charge inhomogeneities(puddles). The scattering rate for charge scatterers in the first order born approximation is inversely proportionally to energy[13]. Therefore, the transport rate is linear in energy. Using the transport rate of charge scatterer with the zero temperature form of the carrier density given by

$$n(\varepsilon_F) \quad = \quad sgn(\varepsilon_F)\frac{|\varepsilon_F|^2}{2\pi v_F^2\hbar^2}, \tag{1.12}$$

and eqn.(1.10), the electrical conductivity is a linear function of carrier density. Alternatively, short-ranged unitary scatterers can explain the linear dependence if the scattering rate is modified to the form

$$\tau^{-1}(\varepsilon_F) \quad = \quad \frac{\tau_0^{-1}\left(\frac{\varepsilon_F}{E_c}\right)}{1+\left(\frac{\varepsilon_F}{E_c}\right)^2}. \tag{1.13}$$

Here the constant τ_0^{-1} accounts for units and E_c is the energy scale at which the electrical conductivity becomes a linear function of carrier density. However, the scattering rate of short-ranged unitary scatterers does not have the form of eqn.1.13 unless many-body quantum effects are incorporated

Another problem with these schemes is for small carrier densities quantum correlation effects can become important in the regime were the coherence length of electrons is comparable to the impurity mean free path of electron. Quantum correlation effects can led to large corrections to conductivity, e.g., Anderson localization is a particular example where quantum correlation between electrons in forward and backward time trajectories destructively interfere. As a result electron in these corresponding time trajectories can be weakly localized. The effect of quantum correlations on transport is extremely important near the Dirac point since the carrier density is zero, i.e., the density of states is small and for a particular impurity concentrations, the electrons coherence length can be comparable to the impurity mean free path of electron.

Theoretical studies have been done to determine if localization is possible in graphene[14, 15]. These studies have shown that the chirality of the wave function allows

for all energy states to be connected by continuous variation of the wave function phases. However, the chirality can be broken for potentials that modify sp^2 hybrid orbitals to sp^3, e.g., exposing graphene to hydrogen or NO_2 gas[15]. Since localization can be understood as the energy level spacing becoming larger then energy variation attributed to changing the phase of the wave function, Dirac Fermions cannot be localized unless the chiral symmetry is broken.

In summary, the quantum chemistry of hybrid orbitals has provided a material with rich physical features. A comprehensive understanding of how various scattering types effect transport in graphene will yield important information for the developments of new technologies. In this thesis transport in bulk graphene is studied for both unitary scatterers(short range scatters) and Coulomb scatterers(long range scatters) in the self impurity averaged formalism.

Chapter 2

Quantum Transport Theory In a Weak Magnetic Field

2.1 Introduction

Classical transport in metals is understood within the Boltzmann theory. The transport coefficients are obtained using linear Boltzmann equation that relies on the following two assumptions: (1) the change in the electron distribution function in an external field is a small perturbation on the equilibrium distribution and only degrees of freedom of order $\frac{T}{\varepsilon_F}$ are affected and (2) an equilibrium distribution function is achieved through scattering of impurities. The fact that strongly interacting metals can be described as a system of weakly interacting quasiparticles, i.e. the Landau paradigm, is the reason for the remarkable success of the Boltzmann approach.

Boltzmann Theory is a single-electron transport theory and does not take into account many-body effects such as interference, localization and tunneling. In this chapter a brief introduction to Quantum Transport Theory is given with an emphasis on the weak magnetic field regime for longitudinal and transverse Electrical, Thermoelectric

and Thermal conductivities. In section 2.2 an introduction to the impurity averaged Green's function is given with a discussion of regimes where the full Green's function can be approximated by the impurity averaged Green's function. An outline of how to perform the self-impurity averaging is given in section 2.2.1 with examples. The formalism of the full Green's in weak magnetic field is presented in section 2.2 with an emphasis on the impurity averaged regime, followed by a short summary of the regime of validity for the approximation.

The Kubo formalism is presented in section 2.3. The form of each type of current operator is presented in section 2.4. In section 2.5 a short discussion of the Khodas-Finkelstein Formalism is given[16] followed by a derivation of correlation function in sections(2.5.1, 2.5.2, 2.5.3). See the appendix for a detailed analysis of the Khodas-Finkelstein approach applied to graphene for each type of transport conductivites.

2.2 Impurity Self-Average Greens Function

We begin with the discussion of the impurity average Greens function, which is our primary tool in investigating transport properties. For a more detailed review of the impurity self-averaged Greens function see reference[17] and references there in.

For systems where impurities are located at random but definite positions $\overrightarrow{R}_i, \quad i = 1, \ldots, N'$ an impurity self-averaging can be performed. Assuming identical impurities are randomly distributed throughout the system with a small mean impurity concentration ($n_i = \frac{N_i}{V}$), i.e., the system is in the dilute limit, the sole important macroscopic parameter in perturbation theory is the impurity concentration. The impurity self-averaged Greens can be obtained by averaging the Full Green's function over all im-

purity states. The equation that governs the Full Green's function is derived using the Schwinger-Dyson equation[18, 19, 20, 21]. The Schwinger-Dyson equation in momentum and Matsubara frequency space for static impurities is:

$$G_{\sigma,\overrightarrow{R}_i}(\overrightarrow{k}, \overrightarrow{k}', i\omega) =$$

$$G^0_{\sigma,\overrightarrow{R}_i}(\overrightarrow{k}, \overrightarrow{k}', i\omega) + G^0_{\sigma,\overrightarrow{R}_i}(\overrightarrow{k}, i\omega) \sum_{\overrightarrow{k}'',\sigma} U(\overrightarrow{k} - \overrightarrow{k}'') G_{\sigma,\overrightarrow{R}_i}(\overrightarrow{k}'', \overrightarrow{k}', i\omega) \quad (2.1)$$

where $G_{\sigma,\overrightarrow{R}_i}(\overrightarrow{k}, \overrightarrow{k}', i\omega)$ is the full Green's function, $G^0_\sigma(\overrightarrow{k}, \overrightarrow{k}', i\omega)$ is the unperturbed Green's function, and the impurity potential is

$$U(\overrightarrow{k} - \overrightarrow{k}'') = U_{imp}(\overrightarrow{k} - \overrightarrow{k}'') \frac{1}{V} \sum_{\overrightarrow{R}_i} e^{-\frac{i}{\hbar}(\overrightarrow{k} - \overrightarrow{k}'') \cdot \overrightarrow{R}_i} \quad (2.2)$$

The general solution to the Schwinger-Dyson equation can be obtained by iterating eqn.2.1 until all possible scattering events have been included. Such a procedure is extremely difficult and physical insight is needed to identify the dominant contributions.

2.2.1 Impurity Self-Average Technique

In the dilute limit, the primary contributions come from all events that scatter off a single impurity. The nature of the impurity dictates the maximum number of times a particle can scatter off a single impurity. For example screened Coulomb scatterers have a typical screening length of the order lattice constant and are weak scatterers. For such an impurity it is sufficient to include only two scattering events. However for strong scatterers, such as unitary potentials, the maximum number of times a particle can scatter off a single impurity is infinite. The infinite sums that are obtained from the Schwinger-Dyson equation for strong scatterers can be greatly simplified by averaging over all impurities. The impurity potential of eqn.2.2 averaged over all impurities is

$$U(\overrightarrow{k'}, i\omega) \quad = \quad U_{imp}(\overrightarrow{k} - \overrightarrow{k}', i\omega) N_{imp} \delta_{(\overrightarrow{k} = \overrightarrow{k}')} \tag{2.3}$$

where the total number of impurities is N_{imp} is given by

$$< \frac{1}{V} \sum_{\overrightarrow{R}_i} e^{-\frac{i}{\hbar}(\overrightarrow{k} - \overrightarrow{k}'') \cdot \overrightarrow{R}_i} > \quad = \quad N_{imp} \delta_{(\overrightarrow{k} = \overrightarrow{k}'')} \tag{2.4}$$

For large samples higher order scattering terms when averaged are approximately $(U_{imp}(\overrightarrow{k} - \overrightarrow{k}'') N_{imp})^m \delta_{(\overrightarrow{k} = \overrightarrow{k}_2)} \ldots \delta_{(\overrightarrow{k}_{m-1} = \overrightarrow{k}'')}$, where m is the order of scattering events; for a details explanation of how to average over impurities see references [17]. The resulting impurity self-averaged Schwinger-Dyson equation is

$$G_\sigma(\overrightarrow{k}, i\omega) = G^0_\sigma(\overrightarrow{k}, i\omega) + G^0_\sigma(\overrightarrow{k}, i\omega) \Sigma(i\omega) G_\sigma(\overrightarrow{k}, i\omega) \tag{2.5}$$

where the functions $G_\sigma(\overrightarrow{k}, i\omega)$ is the impurity self-averaged Green's function, $G^0_\sigma(\overrightarrow{k}, i\omega)$ is the unperturbed Green's function, and $\Sigma(i\omega)$ is the self energy. The impurity self-averaging technique is valid for sample sizes much larger than the coherence length of electrons. The self energy must be calculated in the full self-consistent Born approximation (FSBA) to account for many-body effects. The self energy for screened Coulomb scatterers in full self-consistent born approximation to first order has the form:

$$\Sigma_{CS}(i\omega) \quad = \quad \frac{n_i}{V} \sum_{\overrightarrow{k'}} |U(\overrightarrow{k'}, i\omega)|^2 G(\overrightarrow{k'}, i\omega) \tag{2.6}$$

$$U(\overrightarrow{k'}, i\omega) \quad = \quad \frac{(2\pi e^2)/(\kappa \epsilon_0)}{|\overrightarrow{k} - \overrightarrow{k'}| + q_{TF}(\overrightarrow{k'}, i\omega)} \delta_{(\overrightarrow{k} = \overrightarrow{k}')} \tag{2.7}$$

where n_i is the concentration of charge impurities, e is the charge of an electron, V is the volume, ϵ_0 is the vacuum permittivity, κ is the permittivity of the substrate, and the function $q_{TF}(\overrightarrow{k}', i\omega)$ is the inverse Thomas Fermi screening length. In the regime of strong short range scatterers the infinite sums that are obtained from iterating eqn.2.1 leading to

$$\begin{aligned} G_\sigma(\overrightarrow{k}, i\omega) = G^0_\sigma(\overrightarrow{k}, i\omega) + G^0_\sigma(\overrightarrow{k}, i\omega)\frac{n_i}{V}\sum_{\overrightarrow{k'}} U(\overrightarrow{k'}, i\omega)G_\sigma(\overrightarrow{k}', i\omega) \\ + G^0_\sigma(\overrightarrow{k}, i\omega)n_i(\frac{1}{V}\sum_{\overrightarrow{k'}} U(\overrightarrow{k'}, i\omega)G_\sigma(\overrightarrow{k}', i\omega))^2 \\ + G^0_\sigma(\overrightarrow{k}, i\omega)n_i(\frac{1}{V}\sum_{\overrightarrow{k'}} U(\overrightarrow{k'}, i\omega)G_\sigma(\overrightarrow{k}', i\omega))^3 + \ldots \end{aligned} \tag{2.8}$$

The self energy for unitary scatterers in full self-consistent born approximation can be found by comparing eqns(2.5,2.8) to have the form

$$\begin{aligned} \Sigma(i\omega) = \frac{n_i}{V}\sum_{\overrightarrow{k'}} U(\overrightarrow{k'}, i\omega)G_\sigma(\overrightarrow{k}', i\omega) + n_i(\frac{1}{V}\sum_{\overrightarrow{k'}} U(\overrightarrow{k'}, i\omega)G_\sigma(\overrightarrow{k}', i\omega))^2 \\ + n_i(\frac{1}{V}\sum_{\overrightarrow{k'}} U(\overrightarrow{k'}, i\omega)G_\sigma(\overrightarrow{k}', i\omega))^3 + n_i(\frac{1}{V}\sum_{\overrightarrow{k'}} U(\overrightarrow{k'}, i\omega)G_\sigma(\overrightarrow{k}', i\omega))^4 + \ldots \end{aligned} \tag{2.9}$$

The self energy can be simplified by using the following mathematical expression.

$$\frac{x}{1-x} = x + x^2 + x^3 + x^4 + x^5 + x^6 + x^7 + x^8 + \ldots. \tag{2.10}$$

The self energy for unitary scatterers has the form

$$\Sigma_{US}(i\omega) = \frac{n_{Imp}U_0}{1 - U_0\overline{G}(i\omega - \Sigma_{US}(i\omega))}$$
$$\overline{G}(i\omega - \Sigma_{US}(i\omega)) = \frac{1}{V}\sum_{\overrightarrow{k}} G(i\omega - \Sigma_{US}(i\omega)), \tag{2.11}$$

where we have assumed delta s-wave scatterers with a magnitude of U_0.

2.2.2 Approximations of the Full Greens Function in a Weak Magnetic Field

In a weak magnetic field, $\omega_c\tau < 1$(here ω_c is the cyclotron frequency and τ is the mean free time), the Landau quantization can be neglected and the following Green's function can be used as a approximation for the full Green's function[22, 23, 24, 25, 26]:

$$G_\sigma(\overrightarrow{r}, \overrightarrow{r}', B) = \exp\{-\frac{ie}{c}\int_{\overrightarrow{r}}^{\overrightarrow{r}'} d\overrightarrow{r}'' \cdot A(\overrightarrow{r}'')\} G_\sigma(\overrightarrow{r} - \overrightarrow{r}', B = 0) \tag{2.12}$$

where $G_\sigma(\overrightarrow{r} - \overrightarrow{r}', B = 0)$ is the Green function in zero magnetic field and $A(\overrightarrow{r}'')$ is the vector potential. The approximation for the full Green's function was originally due to Schwinger (see reference[26] for details). The full Green's function in the presence of impurities with a weak magnetic field can be obtained from impurity self-averaged Green's function due to the simple form of eqn.2.12. The phase factor of eqn.2.12 is the flux contribution to the Green's along the path $\overrightarrow{r} \rightarrow \overrightarrow{r}'$. Since all scattering paths are continuous, all information about the impurity position is lost in the sum over the different paths, i.e., the impurity self-averaging technique is applied only to the Green function in zero magnetic field.

In summary the approximations of the full Green's function made in both sections (2.1, 2.2) are valid only in the following regime:

$$(I) \quad \frac{N_i}{V} << 1 \quad , \qquad w_c\tau << 1 \tag{2.13}$$

here N_i is the number of impurities, V is the volume, ω_c is the cyclotron frequency, and τ is the mean free time. The dilute limit of impurities ($\frac{N_i}{V} << 1$) restricts the sample size to be much larger than the coherence length of electrons. The restriction placed on the magnetic field ($w_c\tau << 1$) guarantees momentum is still a good quantum number.

2.3 Kubo Formalism

In this section we introduce the Kubo Formalism and different types of current-current correlation function needed to calculate Electrical, Thermoelectric, and Thermal transport coefficients. In linear response theory it has been proven by Green and Kubo[27] that transport coefficients are related to the time dependence of equilibrium fluctuations in the conjugate currents. In the dc limit, the Kubo Formulas have the general form

$$L^R_{i,k}(q,\Omega) \quad = \quad \frac{\Pi^{\alpha,\beta}_{i,k}(q,\Omega+i\delta)}{\Omega}. \tag{2.14}$$

Here the $\Pi^{\alpha,\beta}_{i,k}(q,\Omega+i\delta)$ is the retarded current-current correlation function and is defined in momentum and Matsubara frequency space as:

$$\Pi^{\alpha,\beta}_{i,k}(q,i\Omega_m) \quad = \quad \frac{-i}{V}\int_0^\beta d\tau e^{i\Omega_m\tau} < T_\tau j_{\alpha,i}(\tau,q) j^\dagger_{\beta,k}(\tau,0) > \tag{2.15}$$

where $j_{\alpha,i}(\tau,q)$ is the current density operator, α refers to the type of current density and i refers to the components.

2.4 Current Density Operator

In physics, the conservation of a physical quantity is a statement of a particular symmetry of the system. For an example, if a physical system behaves the same under translation operation $\overrightarrow{R} \rightarrow \overrightarrow{R} + \overrightarrow{\delta}$, then it is symmetric under continuous translation and the law of conservation of linear momentum is obtained. Conservation laws themselves are necessary for calculations of physical measurable quantities. Noether's theorem is important because it gives a practical method of how to obtain equations that uphold conservation laws. These conservation equation are found by assuming the system's Lagrangian is invariant for a small variation in the symmetry of interest, if the system's Lagrangian has changed the variation must be zero and the conservation equation is found.

However, Noether's theorem which is applicable to continuous symmetries can be used in systems that have discrete symmetries. In systems of discrete symmetries conservation equations are found in the same manner but the deviation in the Lagrangian must be transformed using a basis function that characterizes each discrete symmetry. For an example in condensed matter systems discrete symmetries of crystals are characterized by wannier function, therefore, the Noether construction of the conservation equation is obtained from a transformation that uses Wannier functions as a basis.

The symmetries and associated conservation laws used in transport are as follows: the global gauge invariance of the electromagnetic field is the symmetry that is associated with charge conservation, while the time invariance of a system is associated with energy conservation. The conservation equations for both conservation laws are called continuity equations and have the following form

$$\frac{\partial \rho_e}{\partial t} = \overrightarrow{\nabla_r} \cdot j_e \tag{2.16}$$

$$\frac{\partial \rho_E}{\partial t} = \overrightarrow{\nabla_r} \cdot j_E \tag{2.17}$$

where ρ_e is the charge density, ρ_E is the energy density, j_e is the charge current density, and j_E is the energy current density. In the following chapters only dc transport is being investigated in the regime where static impurities are the primary scattering mechanism. The current densities are greatly simplified in the static impurities regime and have already been derived in the reference [28] to have the form:

$$j_{e,\alpha}(r,t) = \\ -\frac{ie}{2m}(\Psi^\dagger(r,t)(\overrightarrow{\nabla}_r^\alpha \Psi(r,t)) - (\overrightarrow{\nabla}_r^\alpha \Psi^\dagger(r,t))\Psi(r,t)) - \frac{e^2 \overrightarrow{A}_r^\alpha}{m}\Psi^\dagger(r,t)\Psi(r,t) \tag{2.18}$$

$$j_{E,\alpha}(r,t) = \\ \frac{-i}{2m}\left(\left(\frac{\partial \Psi^\dagger(r,t)}{\partial t}\right)(\overrightarrow{\nabla}_r^\alpha \Psi(r,t)) + ((\overrightarrow{\nabla}_r^\alpha \Psi^\dagger(r,t))\left(\frac{\partial \Psi(r,t)}{\partial t}\right)\right) \\ \frac{-e\overrightarrow{A}_r^\alpha}{2m}\left(\left(\frac{\partial \Psi^\dagger(r,t)}{\partial t}\right)\Psi(r,t) - \Psi^\dagger(r,t)\left(\frac{\partial \Psi(r,t)}{\partial t}\right)\right) \tag{2.19}$$

where $j_{e,\alpha}(r,t)$ and $j_{E,\alpha}(r,t)$ are the electrical and energy current densities, $\{\psi, \psi^\dagger\}$ are the fermion annihilations and creation operators and $\overrightarrow{A}_r$ is the vector potential.

2.5 Khodas-Finkelstein Formalism

In eqns.(2.18, 2.19) the explicit form of the vector potential is needed to investigate transport quantities. When the current densities of eqns. (2.18, 2.19) are inserted

directly into the Kubo formula complications arise due to the very singular natural of the vector potential. Singular terms in the current-current correlation functions must be canceled properly with there corresponding conjugate equilibrium fluctuations. The method developed by Khodas-Finkelstein handles the cancelation process of these singular terms in a general manner and will be used in our analysis.

The key points of the Khodas-Finkelstein Formalism are as follows[16]. In a weak magnetic the contribution to Hall conductivity is due the diamagnetic part of the current operator and the differentiation of the phase factors in eqn.2.12. The phase factors contribution can be used in two ways: the formation of gauge invariant closed loops gives a general method of canceling all singular terms in the current-current correlation function of eqn.2.15, while terms that do not yield closed loops are included in the diamagnetic terms of eqns.(2.18, 2.19). The extension of the diamagnetic part of the current operator is a consequence of the phase accumulation of the wave function in the magnetic field due to the Lorentz force. In the following sections a derivation of the correlation functions used in the calculating Electrical, Thermoelectric, and Thermal conductivity quantities in this thesis is presented.

2.5.1 Charge-Charge Current Correlation Tensor in a Homogeneous Magnetic Field

In this section we follow the method developed by Khodas and Finkel'stein to calculate the Hall coefficient. We define the electrical current density in the the presence of a homogeneous magnetic field and derive charge-charge current correlation tensor in the presence of a finite range disorder. The electrical current density [16] is

$$j_{e,\alpha}(r_i,t) = \lim_{\substack{r_i'\to r_i \\ t'\to t}} \frac{e}{2m}[(-i\overrightarrow{\nabla}^{\alpha}_{r_i'} - e\overrightarrow{A}^{\alpha}_{r_i'}) - (-i\overrightarrow{\nabla}^{\alpha}_{r_i} + e\overrightarrow{A}^{\alpha}_{r_i})]\Psi^{\dagger}(r_i,t)\Psi(r_i',t'), \quad (2.20)$$

while the charge-charge current correlation tensor is

$$\Pi^{e,e}_{\alpha,\beta}(r_i,r_f;\tau) =$$

$$< T_{\tau}(\lim_{\substack{r_i'\to r_i \\ \tau'\to\tau}} \frac{e}{2m}[(-i\overrightarrow{\nabla}^{\alpha}_{r_i'} - e\overrightarrow{A}^{\alpha}_{r_i'}) - (-i\overrightarrow{\nabla}^{\alpha}_{r_i} + e\overrightarrow{A}^{\alpha}_{r_i})]\Psi^{\dagger}(r_i,\tau)\Psi(r_i',\tau'))$$

$$\times (\lim_{r_f'\to r_f} \frac{e}{2m}[(i\overrightarrow{\nabla}^{\beta}_{r_f'} - e\overrightarrow{A}^{\beta}_{r_f'}) - (i\overrightarrow{\nabla}^{\beta}_{r_f} + e\overrightarrow{A}^{\beta}_{r_f})]\Psi^{\dagger}(r_f',0)\Psi(r_f,0)) > . \quad (2.21)$$

In the presence of a magnetic field the Greens function is defined as $G(r_1,r_2,\tau) = exp(\frac{ie}{c}\Phi(r_1,r_2))\widetilde{G}_{r_1-r_2}(\tau)$, where $\widetilde{G}_{r_1-r_2}(\tau)$ is the gauge invariant Greens function, and the exponential factor accounts for the phase acquired by the particle along the path $\overrightarrow{r}_i \to \overrightarrow{r}_f$[22, 23, 24, 25, 26, 16]. Choosing the vector potential as $\overrightarrow{A} = \frac{1}{2}\overrightarrow{B}\times\overrightarrow{r}$ and using the form of the phase factor of the exponential of the Green's function $\Phi(r_1,r_2) = \int_{r_1}^{r_2}\overrightarrow{A}(\overrightarrow{r})d\overrightarrow{r}$, eqn.2.21 can be written as

$$\Pi^{e,e}_{\alpha,\beta}(r_i,r_f;\tau)=\Pi^{e,e,1}_{\alpha,\beta}(r_i,r_f;\tau)+\Pi^{e,e,2}_{\alpha,\beta}(r_i,r_f;\tau)+\Pi^{e,e,3}_{\alpha,\beta}(r_i,r_f;\tau)+\Pi^{e,e,4}_{\alpha,\beta}(r_i,r_f;\tau)$$

$$\Pi^{e,e,1}_{\alpha,\beta}(r_i,r_f;\tau)=$$
$$\frac{-e^2}{4m^2}[(-i\overrightarrow{\nabla}_{r_i}-\frac{e\overrightarrow{B}}{2c}\times(\overrightarrow{r_i}-\overrightarrow{r_f}))^{\alpha}(i\overrightarrow{\nabla}_{r_f}+\frac{e\overrightarrow{B}}{2c}\times(\overrightarrow{r_i}-\overrightarrow{r_f}))^{\beta}\widetilde{G}_{r_i-r_f}(\tau)](\widetilde{G}_{r_f-r_i}(-\tau))$$

$$\Pi^{e,e,2}_{\alpha,\beta}(r_i,r_f;\tau)=$$
$$\frac{-e^2}{4m^2}(\widetilde{G}_{r_i-r_f}(\tau))[(-i\overrightarrow{\nabla}_{r_i}+\frac{e\overrightarrow{B}}{2c}\times(\overrightarrow{r_i}-\overrightarrow{r_f}))^{\alpha}(i\overrightarrow{\nabla}_{r_f}-\frac{e\overrightarrow{B}}{2c}\times(\overrightarrow{r_i}-\overrightarrow{r_f}))^{\beta}\widetilde{G}_{r_f-r_i}(-\tau)$$

$$\Pi^{e,e,3}_{\alpha,\beta}(r_i,r_f;\tau)=$$
$$\frac{e^2}{4m^2}[(-i\overrightarrow{\nabla}_{r_i}-\frac{e\overrightarrow{B}}{2c}\times(\overrightarrow{r_i}-\overrightarrow{r_f}))^{\alpha}\widetilde{G}_{r_i-r_f}(\tau)][(i\overrightarrow{\nabla}_{r_f}-\frac{e\overrightarrow{B}}{2c}\times(\overrightarrow{r_i}-\overrightarrow{r_f}))^{\beta}\widetilde{G}_{r_f-r_i}(-\tau)]$$

$$\Pi^{e,e,4}_{\alpha,\beta}(r_i,r_f;\tau)=$$
$$\frac{e^2}{4m^2}[(-i\overrightarrow{\nabla}_{r_i}+\frac{e\overrightarrow{B}}{2c}\times(\overrightarrow{r_i}-\overrightarrow{r_f}))^{\alpha}\widetilde{G}_{r_f-r_i}(-\tau)][(i\overrightarrow{\nabla}_{r_f}+\frac{e\overrightarrow{B}}{2c}\times(\overrightarrow{r_i}-\overrightarrow{r_f}))^{\beta}(\widetilde{G}_{r_i-r_f}(\tau))] \tag{2.22}$$

Define $\overrightarrow{R}=\overrightarrow{r}_i-\overrightarrow{r}_f$ and taking a fourier transform of each of these correlation functions and labeling $\overrightarrow{K}=\overrightarrow{p}+\overrightarrow{q}$ we get

$$\Pi^{e,e}_{\alpha,\beta}(\overrightarrow{q};i\Omega) = \Pi^{e,e,1}_{\alpha,\beta}(\overrightarrow{q};i\Omega) + \Pi^{e,e,2}_{\alpha,\beta}(\overrightarrow{q};i\Omega) + \Pi^{e,e,3}_{\alpha,\beta}(\overrightarrow{q};i\Omega) + \Pi^{e,e,4}_{\alpha,\beta}(\overrightarrow{q};i\Omega)$$

$$\Pi^{e,e,1}_{\alpha,\beta}(\overrightarrow{q};i\Omega) =$$
$$\frac{e^2}{4m^2\beta}\sum_{\overrightarrow{p},iw_n}[(\overrightarrow{K}+i\frac{e\overrightarrow{B}}{2c}\times\overrightarrow{\nabla}_{\overrightarrow{K}})^{\alpha}(\overrightarrow{K}-i\frac{e\overrightarrow{B}}{2c}\times\overrightarrow{\nabla}_{\overrightarrow{K}})^{\beta}\widetilde{G}_{\overrightarrow{K}}(iw_n+i\Omega)](\widetilde{G}_{\overrightarrow{p}}(iw_n))$$

$$\Pi^{e,e,2}_{\alpha,\beta}(\overrightarrow{q};i\Omega) =$$
$$\frac{e^2}{4m^2\beta}\sum_{\overrightarrow{p},iw_n}\widetilde{G}_{\overrightarrow{K}}(iw_n+i\Omega)[(-\overrightarrow{p}+i\frac{e\overrightarrow{B}}{2c}\times\overrightarrow{\nabla}_{\overrightarrow{p}})^{\alpha}(-\overrightarrow{p}-i\frac{e\overrightarrow{B}}{2c}\times\overrightarrow{\nabla}_{\overrightarrow{p}})^{\beta}\widetilde{G}_{\overrightarrow{p}}(iw_n)]$$

$$\Pi^{e,e,3}_{\alpha,\beta}(\overrightarrow{q};i\Omega) =$$
$$\frac{-e^2}{4m^2\beta}\sum_{\overrightarrow{p},iw_n}[(\overrightarrow{K}+i\frac{e\overrightarrow{B}}{2c}\times\overrightarrow{\nabla}_{\overrightarrow{K}})^{\alpha}\widetilde{G}_{\overrightarrow{K}}(iw_n+i\Omega)][(-\overrightarrow{p}-i\frac{e\overrightarrow{B}}{2c}\times\overrightarrow{\nabla}_{\overrightarrow{p}})^{\beta}(\widetilde{G}_{\overrightarrow{p}}(iw_n))]$$

$$\Pi^{e,e,4}_{\alpha,\beta}(\overrightarrow{q};i\Omega) =$$
$$\frac{-e^2}{4m^2\beta}\sum_{\overrightarrow{p},iw_n}[(-\overrightarrow{p}+i\frac{e\overrightarrow{B}}{2c}\times\overrightarrow{\nabla}_{\overrightarrow{p}})^{\alpha}\widetilde{G}_{\overrightarrow{p}}(iw_n)][(\overrightarrow{K}-i\frac{e\overrightarrow{B}}{2c}\times\overrightarrow{\nabla}_{\overrightarrow{K}})^{\beta}(\widetilde{G}_{\overrightarrow{K}}(iw_n+i\Omega))] \tag{2.23}$$

To first order in magnetic field (assumed to be in the positive z direction) the diagonal and off diagonal terms are

$$\Pi^{e,e}_{x,x}(\overrightarrow{q}\to 0;i\Omega) = \frac{e^2}{\beta}\sum_{\overrightarrow{p},iw_n}\{(\overrightarrow{v}^2_{\overrightarrow{p},x})\widetilde{G}_{\overrightarrow{p}}(iw_n+i\Omega)\widetilde{G}_{\overrightarrow{p}}(iw_n)\} \tag{2.24}$$

$$\Pi^{e,e}_{x,y}(\overrightarrow{q}\to 0;i\Omega) =$$
$$\frac{-e^3 i|\overrightarrow{B}|}{4c\beta m}\sum_{\overrightarrow{p},iw_n}(\overrightarrow{v}_{\overrightarrow{p},x})\{\frac{\partial\widetilde{G}_{\overrightarrow{p}}(iw_n+i\Omega)}{\partial p_x}\widetilde{G}_{\overrightarrow{p}}(iw_n)-\widetilde{G}_{\overrightarrow{p}}(iw_n+i\Omega)\frac{\partial\widetilde{G}_{\overrightarrow{p}}(iw_n)}{\partial p_x}\}$$
$$+\frac{-e^3 i|\overrightarrow{B}|}{4c\beta m}\sum_{\overrightarrow{p},iw_n}(\overrightarrow{v}_{\overrightarrow{p},y})\{\frac{\partial\widetilde{G}_{\overrightarrow{p}}(iw_n+i\Omega)}{\partial p_y}\widetilde{G}_{\overrightarrow{p}}(iw_n)-\widetilde{G}_{\overrightarrow{p}}(iw_n+i\Omega)\frac{\partial\widetilde{G}_{\overrightarrow{p}}(iw_n)}{\partial p_y}\} \tag{2.25}$$

Using these general forms of the charge-charge current correlation tensor in the Kubo formula of eqn.2.14, the electrical conductivity tensor can be found for a given model in the dilute impurity limit. The dc electrical conductivity tensor can be found from the electrical conductivity by taking the real part in the limit $\Omega \to 0$.

2.5.2 Energy-Charge Current Correlation Tensor in a Homogeneous Magnetic Field

In this section we follow a similar approach in calculating the energy-charge current correlation tensor as we did for charge-charge current correlation tensor in the previous section. The current densities are defined as [16, 28]

$$j_{e,\alpha}(r_i,t) = \lim_{\substack{r_i'\to r_i \\ t'\to t}} \frac{e}{2m}[(-i\overrightarrow{\nabla}^{\alpha}_{r_i'} - e\overrightarrow{A}^{\alpha}_{r_i'}) - (-i\overrightarrow{\nabla}^{\alpha}_{r_i} + e\overrightarrow{A}^{\alpha}_{r_i})]\Psi^{\dagger}(r_i,t)\Psi(r_i',t') \quad (2.26)$$

$$j_{E,\alpha}(r_i,t) = \lim_{\substack{r_i'\to r_i \\ t'\to t}} \frac{1}{2m}[(-i\overrightarrow{\nabla}^{\alpha}_{r_i'} - e\overrightarrow{A}^{\alpha}_{r_i'})\frac{\partial}{\partial t} + (-i\overrightarrow{\nabla}^{\alpha}_{r_i} + e\overrightarrow{A}^{\alpha}_{r_i})\frac{\partial}{\partial t'}]\Psi^{\dagger}(r_i,t)\Psi(r_i',t') \quad (2.27)$$

Letting $t \to i\tau$ the energy current density becomes

$$j_{E,\alpha}(r_i,t) = \lim_{\substack{r_i'\to r_i \\ \tau'\to \tau}} \frac{i}{2m}[(-i\overrightarrow{\nabla}^{\alpha}_{r_i'} - e\overrightarrow{A}^{\alpha}_{r_i'})\frac{\partial}{\partial \tau} + (-i\overrightarrow{\nabla}^{\alpha}_{r_i} + e\overrightarrow{A}^{\alpha}_{r_i})\frac{\partial}{\partial \tau'}]\Psi^{\dagger}(r_i,\tau)\Psi(r_i',\tau') \quad (2.28)$$

The correlation function that determines the thermoelectric response is

$$\Pi^{E,e}_{\alpha,\beta}(r_i, r_f; \tau) =$$

$$< T_\tau(\lim_{\substack{r_i' \to r_i \\ \tau' \to \tau}} \frac{i}{2m}[(-i\overrightarrow{\nabla}^{\alpha}_{r_i'} - e\overrightarrow{A}^{\alpha}_{r_i'})\frac{\partial}{\partial \tau} + (-i\overrightarrow{\nabla}^{\alpha}_{r_i} + e\overrightarrow{A}^{\alpha}_{r_i})\frac{\partial}{\partial \tau'}]\Psi^\dagger(r_i, \tau)\Psi(r_i', \tau'))$$

$$\times (\lim_{r_f' \to r_f} \frac{e}{2m}[(i\overrightarrow{\nabla}^{\beta}_{r_f'} - e\overrightarrow{A}^{\beta}_{r_f'}) - (i\overrightarrow{\nabla}^{\beta}_{r_f} + e\overrightarrow{A}^{\beta}_{r_f})]\Psi^\dagger(r_f', 0)\Psi(r_f, 0)) > \quad (2.29)$$

Since we have terms that depend on the derivative with respect to τ, we use the equations of motion to determine the Greens functions. Using the following identity:

$$\frac{\partial}{\partial \tau}G(r_1, r_2, \pm\tau) \quad = \quad \pm\delta(\tau)\delta(r_1 - r_2) + \quad < \quad T_\tau \frac{\partial}{\partial \tau}\Psi(r_1, \tau)\Psi^\dagger(r_2, 0) \quad > \quad (2.30)$$

Eqn.2.29 can be rewritten in terms of Green's functions to be

$$\Pi^{E,e}_{\alpha,\beta}(r_i,r_f;\tau)=\Pi^{E,e,1}_{\alpha,\beta}(r_i,r_f;\tau)+\Pi^{E,e,2}_{\alpha,\beta}(r_i,r_f;\tau)+\Pi^{E,e,3}_{\alpha,\beta}(r_i,r_f;\tau)+\Pi^{E,e,4}_{\alpha,\beta}(r_i,r_f;\tau)$$

$$\Pi^{E,e,1}_{\alpha,\beta}(r_i,r_f;\tau)=$$

$$\frac{ei}{4m^2}[(i\overrightarrow{\nabla}_{r_i}-\frac{e\overrightarrow{B}}{2c}\times(\overrightarrow{r_f}-\overrightarrow{r_i}))^{\alpha}(i\overrightarrow{\nabla}_{r_f}-\frac{e\overrightarrow{B}}{2c}\times(\overrightarrow{r_f}-\overrightarrow{r_i}))^{\beta}\widetilde{G}_{r_i-r_f}(\tau)](\frac{\partial\widetilde{G}_{r_f-r_i}(-\tau)}{\partial\tau})$$
$$-\frac{ei}{4m^2}[(i\overrightarrow{\nabla}_{r_i}-\frac{e\overrightarrow{B}}{2c}\times(\overrightarrow{r_f}-\overrightarrow{r_i}))^{\alpha}(i\overrightarrow{\nabla}_{r_f}-\frac{e\overrightarrow{B}}{2c}\times(\overrightarrow{r_f}-\overrightarrow{r_i}))^{\beta}\widetilde{G}_{r_i-r_f}(\tau)](\delta(-\tau)\delta(r_f-r_i))$$

$$\Pi^{E,e,2}_{\alpha,\beta}(r_i,r_f;\tau)=$$

$$\frac{-ei}{4m^2}(\frac{\partial\widetilde{G}_{r_i-r_f}(\tau)}{\partial\tau})[(i\overrightarrow{\nabla}_{r_i}+\frac{e\overrightarrow{B}}{2c}\times(\overrightarrow{r_f}-\overrightarrow{r_i}))^{\alpha}(i\overrightarrow{\nabla}_{r_f}+\frac{e\overrightarrow{B}}{2c}\times(\overrightarrow{r_f}-\overrightarrow{r_i}))^{\beta}\widetilde{G}_{r_f-r_i}(-\tau)$$
$$+\frac{-ei}{4m^2}(\delta(\tau)\delta(r_i-r_f))[(i\overrightarrow{\nabla}_{r_i}+\frac{e\overrightarrow{B}}{2c}\times(\overrightarrow{r_f}-\overrightarrow{r_i}))^{\alpha}(i\overrightarrow{\nabla}_{r_f}+\frac{e\overrightarrow{B}}{2c}\times(\overrightarrow{r_f}-\overrightarrow{r_i}))^{\beta}\widetilde{G}_{r_f-r_i}(-\tau)$$

$$\Pi^{E,e,3}_{\alpha,\beta}(r_i,r_f;\tau)=$$

$$\frac{-ei}{4m^2}[(i\overrightarrow{\nabla}_{r_i}-\frac{e\overrightarrow{B}}{2c}\times(\overrightarrow{r_f}-\overrightarrow{r_i}))^{\alpha}\widetilde{G}_{r_i-r_f}(\tau)][(i\overrightarrow{\nabla}_{r_f}+\frac{e\overrightarrow{B}}{2c}\times(\overrightarrow{r_f}-\overrightarrow{r_i}))^{\beta}(\frac{\partial\widetilde{G}_{r_f-r_i}(-\tau)}{\partial\tau})]$$
$$+\frac{ei}{4m^2}[(i\overrightarrow{\nabla}_{r_i}-\frac{e\overrightarrow{B}}{2c}\times(\overrightarrow{r_f}-\overrightarrow{r_i}))^{\alpha}\widetilde{G}_{r_i-r_f}(\tau)][(i\overrightarrow{\nabla}_{r_f}+\frac{e\overrightarrow{B}}{2c}\times(\overrightarrow{r_f}-\overrightarrow{r_i}))^{\beta}(\delta(-\tau)\delta(r_f-r_i))]$$

$$\Pi^{E,e,4}_{\alpha,\beta}(r_i,r_f;\tau)=$$

$$\frac{ei}{4m^2}[(i\overrightarrow{\nabla}_{r_i}+\frac{e\overrightarrow{B}}{2c}\times(\overrightarrow{r_f}-\overrightarrow{r_i}))^{\alpha}\widetilde{G}_{r_f-r_i}(-\tau)][(i\overrightarrow{\nabla}_{r_f}-\frac{e\overrightarrow{B}}{2c}\times(\overrightarrow{r_f}-\overrightarrow{r_i}))^{\beta}(\frac{\partial\widetilde{G}_{r_i-r_f}(\tau)}{\partial\tau})]$$
$$+\frac{ei}{4m^2}[(i\overrightarrow{\nabla}_{r_i}+\frac{e\overrightarrow{B}}{2c}\times(\overrightarrow{r_f}-\overrightarrow{r_i}))^{\alpha}\widetilde{G}_{r_f-r_i}(-\tau)][(i\overrightarrow{\nabla}_{r_f}-\frac{e\overrightarrow{B}}{2c}\times(\overrightarrow{r_f}-\overrightarrow{r_i}))^{\beta}(\delta(\tau)\delta(r_i-r_f))]$$

(2.31)

In momentum space, with the definition $\overrightarrow{K}=\overrightarrow{p}+\overrightarrow{q}$, we get

$$\Pi^{E,e}_{\alpha,\beta}(\overrightarrow{q};i\Omega)=\Pi^{E,e,1}_{\alpha,\beta}(\overrightarrow{q};i\Omega)+\Pi^{E,e,2}_{\alpha,\beta}(\overrightarrow{q};i\Omega)+\Pi^{E,e,3}_{\alpha,\beta}(\overrightarrow{q};i\Omega)+\Pi^{E,e,4}_{\alpha,\beta}(\overrightarrow{q};i\Omega)$$

$$\Pi^{E,e,1}_{\alpha,\beta}(\overrightarrow{q};i\Omega)=$$

$$\frac{-ei}{4m^2\beta}\sum_{\overrightarrow{p},iw_n}[(-\overrightarrow{K}-i\frac{e\overrightarrow{B}}{2c}\times\overrightarrow{\nabla}_{\overrightarrow{K}})^{\alpha}(\overrightarrow{K}-i\frac{e\overrightarrow{B}}{2c}\times\overrightarrow{\nabla}_{\overrightarrow{K}})^{\beta}\widetilde{G}_{\overrightarrow{K}}(iw_n+i\Omega)](-iw_n\widetilde{G}_{\overrightarrow{p}}(iw_n))$$
$$+\frac{ei}{4m^2\beta}\sum_{\overrightarrow{p},iw_n}[(-\overrightarrow{K}-i\frac{e\overrightarrow{B}}{2c}\times\overrightarrow{\nabla}_{\overrightarrow{K}})^{\alpha}(\overrightarrow{K}-i\frac{e\overrightarrow{B}}{2c}\times\overrightarrow{\nabla}_{\overrightarrow{K}})^{\beta}\widetilde{G}_{\overrightarrow{K}}(iw_n+i\Omega)]$$

$$\Pi^{E,e,2}_{\alpha,\beta}(\overrightarrow{q};i\Omega)=$$

$$\frac{ei}{4m^2\beta}\sum_{\overrightarrow{p},iw_n}(iw_n+i\Omega)\widetilde{G}_{\overrightarrow{K}}(iw_n+i\Omega)[(-\overrightarrow{p}+i\frac{e\overrightarrow{B}}{2c}\times\overrightarrow{\nabla}_{\overrightarrow{p}})^{\alpha}(\overrightarrow{p}+i\frac{e\overrightarrow{B}}{2c}\times\overrightarrow{\nabla}_{\overrightarrow{p}})^{\beta}\widetilde{G}_{\overrightarrow{p}}(iw_n)]$$
$$+\frac{ei}{4m^2\beta}\sum_{\overrightarrow{p},iw_n}[(-\overrightarrow{p}+i\frac{e\overrightarrow{B}}{2c}\times\overrightarrow{\nabla}_{\overrightarrow{p}})^{\alpha}(\overrightarrow{p}+i\frac{e\overrightarrow{B}}{2c}\times\overrightarrow{\nabla}_{\overrightarrow{p}})^{\beta}\widetilde{G}_{\overrightarrow{p}}(iw_n)]$$

$$\Pi^{E,e,3}_{\alpha,\beta}(\overrightarrow{q};i\Omega)=$$

$$\frac{ei}{4m^2\beta}\sum_{\overrightarrow{p},iw_n}[(-\overrightarrow{K}-i\frac{e\overrightarrow{B}}{2c}\times\overrightarrow{\nabla}_{\overrightarrow{K}})^{\alpha}\widetilde{G}_{\overrightarrow{K}}(iw_n+i\Omega)][(-\overrightarrow{p}-i\frac{e\overrightarrow{B}}{2c}\times\overrightarrow{\nabla}_{\overrightarrow{p}})^{\beta}(-iw_n\widetilde{G}_{\overrightarrow{p}}(iw_n))]$$
$$-\frac{ei}{4m^2\beta}\sum_{\overrightarrow{p},iw_n}[(-\overrightarrow{K}-i\frac{e\overrightarrow{B}}{2c}\times\overrightarrow{\nabla}_{\overrightarrow{K}})^{\alpha}\widetilde{G}_{\overrightarrow{K}}(iw_n+i\Omega)][(-\overrightarrow{p}-i\frac{e\overrightarrow{B}}{2c}\times\overrightarrow{\nabla}_{\overrightarrow{p}})^{\beta}(1)]$$

$$\Pi^{E,e,4}_{\alpha,\beta}(\overrightarrow{q};i\Omega)=$$

$$\frac{-ei}{4m^2\beta}\sum_{\overrightarrow{p},iw_n}[(\overrightarrow{p}-i\frac{e\overrightarrow{B}}{2c}\times\overrightarrow{\nabla}_{\overrightarrow{p}})^{\alpha}\widetilde{G}_{\overrightarrow{p}}(iw_n)][(\overrightarrow{K}-i\frac{e\overrightarrow{B}}{2c}\times\overrightarrow{\nabla}_{\overrightarrow{K}})^{\beta}((iw_n+i\Omega)\widetilde{G}_{\overrightarrow{K}}(iw_n+i\Omega))]$$
$$+\frac{-ei}{4m^2\beta}\sum_{\overrightarrow{p},iw_n}[(\overrightarrow{p}-i\frac{e\overrightarrow{B}}{2c}\times\overrightarrow{\nabla}_{\overrightarrow{p}})^{\alpha}\widetilde{G}_{\overrightarrow{p}}(iw_n)][(\overrightarrow{K}-i\frac{e\overrightarrow{B}}{2c}\times\overrightarrow{\nabla}_{\overrightarrow{K}})^{\beta}(1)]$$

(2.32)

To first order in magnetic field the diagonal and off diagonal terms of the energy-charge current correlation tensor are

$$\Pi^{E,e}_{x,x}(\overrightarrow{q}\rightarrow 0;i\Omega)=$$

$$\frac{-ei}{\beta}\sum_{\overrightarrow{p},iw_n}\{((iw_n+\frac{i\Omega}{2})\overrightarrow{v}^2_{\overrightarrow{p},x})\widetilde{G}_{\overrightarrow{p}}(iw_n+i\Omega)\widetilde{G}_{\overrightarrow{p}}(iw_n)+\overrightarrow{v}^2_{\overrightarrow{p},x}\frac{\widetilde{G}_{\overrightarrow{p}}(iw_n+i\Omega)+\widetilde{G}_{\overrightarrow{p}}(iw_n)}{2}\} \tag{2.33}$$

$$\Pi^{E,e}_{x,y}(\overrightarrow{q}\rightarrow 0;i\Omega)=$$

$$\frac{-e^2|\overrightarrow{B}|}{4c\beta m}\sum_{\overrightarrow{p},iw_n}(iw_n+\frac{i\Omega}{2})(\overrightarrow{v}_{\overrightarrow{p},x})\{\frac{\partial\widetilde{G}_{\overrightarrow{p}}(iw_n+i\Omega)}{\partial p_x}\widetilde{G}_{\overrightarrow{p}}(iw_n)-\widetilde{G}_{\overrightarrow{p}}(iw_n+i\Omega)\frac{\partial\widetilde{G}_{\overrightarrow{p}}(iw_n)}{\partial p_x}\}$$

$$+\frac{-e^2|\overrightarrow{B}|}{4c\beta m}\sum_{\overrightarrow{p},iw_n}(iw_n+\frac{i\Omega}{2})(\overrightarrow{v}_{\overrightarrow{p},y})\{\frac{\partial\widetilde{G}_{\overrightarrow{p}}(iw_n+i\Omega)}{\partial p_y}\widetilde{G}_{\overrightarrow{p}}(iw_n)-\widetilde{G}_{\overrightarrow{p}}(iw_n+i\Omega)\frac{\partial\widetilde{G}_{\overrightarrow{p}}(iw_n)}{\partial p_y}\}$$

$$+\frac{-e^2|\overrightarrow{B}|}{4c\beta m}\sum_{\overrightarrow{p},iw_n}\{\frac{i\Omega}{2}\widetilde{G}_{\overrightarrow{p}}(iw_n+i\Omega)\widetilde{G}_{\overrightarrow{p}}(iw_n)-\widetilde{G}_{\overrightarrow{p}}(iw_n+i\Omega)+\widetilde{G}_{\overrightarrow{p}}(iw_n)\} \tag{2.34}$$

Using these general forms of the energy-charge current correlation tensor and the Kubo formula of eqn.2.14 minus the electrical conductivity tensor rescaled by the ratio $\frac{\mu}{e}$(μ is the chemical potential and e is the charge of the electron), the thermoelectric conductivity tensor can be found for a given model in the dilute impurity limit. The dc thermoelectric conductivity tensor is found by taking the real part in the limit $\Omega\rightarrow 0$ of the thermoelectric conductivity tensor.

2.5.3 Energy-Energy Current Correlation Tensor in a Homogeneous Magnetic Field

In this section we calculate the energy-energy current correlation tensor as we did for the charge-charge and energy-charge current correlation tensors in the previous sections. The energy-energy current correlation tensor is

$$\Pi^{E,E}_{\alpha,\beta}(r_i, r_f; \tau_i, \tau_f) =$$

$$< T_\tau(\lim_{\substack{r'_i \to r_i \\ \tau'_i \to \tau_i}} \frac{i}{2m}[(-i\overrightarrow{\nabla}^{\alpha}_{r'_i} - e\overrightarrow{A}^{\alpha}_{r'_i})\frac{\partial}{\partial\tau_i} + (-i\overrightarrow{\nabla}^{\alpha}_{r_i} + e\overrightarrow{A}^{\alpha}_{r_i})\frac{\partial}{\partial\tau'_i}]\Psi^\dagger(r_i, \tau_i)\Psi(r'_i, \tau'_i))$$

$$\times (\lim_{\substack{r'_f \to r_f \\ \tau'_f \to \tau_f}} \frac{i}{2m}[(i\overrightarrow{\nabla}^{\beta}_{r'_f} - e\overrightarrow{A}^{\beta}_{r'_f})\frac{\partial}{\partial\tau_f} + (i\overrightarrow{\nabla}^{\beta}_{r_f} + e\overrightarrow{A}^{\beta}_{r_f})\frac{\partial}{\partial\tau'_f}]\Psi^\dagger(r'_f, \tau'_f)\Psi(r_f, \tau_f)) > \quad (2.35)$$

Since we have terms that depend on different order derivatives with respect to τ, we use the equations of motion to determine the greens functions. Using the following identity for terms in Eqn.2.35 that involve first order derivatives in τ:

$$\frac{\partial}{\partial\tau}G(r_1, r_2, \pm\tau) \quad = \quad \pm\delta(\tau)\delta(r_1 - r_2) + \quad < \quad T_\tau\frac{\partial}{\partial\tau}\Psi(r_1, \tau)\Psi^\dagger(r_2, 0) \quad > \quad (2.36)$$

and the following identity for terms in Eqn.2.35 that involve second order derivatives in τ,

$$\frac{\partial^2}{\partial\tau^2}G(r_1, r_2, \tau) \; + \; \delta(r_1 - r_2)\frac{\partial}{\partial\tau}\delta(\tau) \quad =< \quad T_\tau\frac{\partial\Psi(r_1, \tau_1)}{\partial\tau_1}\frac{\partial\Psi^\dagger(r_2, \tau_2)}{\partial\tau_2} \quad > \quad (2.37)$$

Eqn.2.35 can be rewritten in terms of Green's functions to be

$$\Pi^{E,E}_{\alpha,\beta}(r_i,r_f;\tau)=\Pi^{E,E,1}_{\alpha,\beta}(r_i,r_f;\tau)+\Pi^{E,E,2}_{\alpha,\beta}(r_i,r_f;\tau)+\Pi^{E,E,3}_{\alpha,\beta}(r_i,r_f;\tau)+\Pi^{E,E,4}_{\alpha,\beta}(r_i,r_f;\tau)$$

$$\Pi^{E,E,1}_{\alpha,\beta}(r_i,r_f;\tau)=$$

$$\frac{-1}{4m^2}[(-i\overrightarrow{\nabla}_{r_i}+\frac{e\overrightarrow{B}}{2c}\times(\overrightarrow{r_f}-\overrightarrow{r_i}))^{\alpha}(i\overrightarrow{\nabla}_{r_f}-\frac{e\overrightarrow{B}}{2c}\times(\overrightarrow{r_f}-\overrightarrow{r_i}))^{\beta}\widetilde{G}_{r_i-r_f}(\tau)](\frac{\partial^2\widetilde{G}_{r_f-r_i}(-\tau)}{\partial\tau^2})$$
$$+\frac{-1}{4m^2}[(-i\overrightarrow{\nabla}_{r_i}+\frac{e\overrightarrow{B}}{2c}\times(\overrightarrow{r_f}-\overrightarrow{r_i}))^{\alpha}(i\overrightarrow{\nabla}_{r_f}-\frac{e\overrightarrow{B}}{2c}\times(\overrightarrow{r_f}-\overrightarrow{r_i}))^{\beta}\widetilde{G}_{r_i-r_f}(\tau)](\delta(r_i-r_f)\frac{\partial\delta(-\tau)}{\partial\tau})$$

$$\Pi^{E,E,2}_{\alpha,\beta}(r_i,r_f;\tau)=$$

$$\frac{-1}{4m^2}(\frac{\partial^2\widetilde{G}_{r_i-r_f}(\tau)}{\partial\tau^2})[(-i\overrightarrow{\nabla}_{r_i}-\frac{e\overrightarrow{B}}{2c}\times(\overrightarrow{r_f}-\overrightarrow{r_i}))^{\alpha}(i\overrightarrow{\nabla}_{r_f}+\frac{e\overrightarrow{B}}{2c}\times(\overrightarrow{r_f}-\overrightarrow{r_i}))^{\beta}\widetilde{G}_{r_f-r_i}(-\tau)$$
$$+\frac{1}{4m^2}(\delta(r_i-r_f)\frac{\partial\delta(\tau)}{\partial\tau})[(-i\overrightarrow{\nabla}_{r_i}-\frac{e\overrightarrow{B}}{2c}\times(\overrightarrow{r_f}-\overrightarrow{r_i}))^{\alpha}(i\overrightarrow{\nabla}_{r_f}+\frac{e\overrightarrow{B}}{2c}\times(\overrightarrow{r_f}-\overrightarrow{r_i}))^{\beta}\widetilde{G}_{r_f-r_i}(-\tau)$$

$$\Pi^{E,E,3}_{\alpha,\beta}(r_i,r_f;\tau)=$$

$$\frac{-1}{4m^2}[(-i\overrightarrow{\nabla}_{r_i}+\frac{e\overrightarrow{B}}{2c}\times(\overrightarrow{r_f}-\overrightarrow{r_i}))^{\alpha}(\frac{\partial\widetilde{G}_{r_i-r_f}(\tau)}{\partial\tau})][(i\overrightarrow{\nabla}_{r_f}+\frac{e\overrightarrow{B}}{2c}\times(\overrightarrow{r_f}-\overrightarrow{r_i}))^{\beta}(\frac{\partial\widetilde{G}_{r_f-r_i}(-\tau)}{\partial\tau})]$$
$$+\frac{1}{4m^2}[(-i\overrightarrow{\nabla}_{r_i}+\frac{e\overrightarrow{B}}{2c}\times(\overrightarrow{r_f}-\overrightarrow{r_i}))^{\alpha}(\frac{\partial\widetilde{G}_{r_i-r_f}(\tau)}{\partial\tau})][(i\overrightarrow{\nabla}_{r_f}+\frac{e\overrightarrow{B}}{2c}\times(\overrightarrow{r_f}-\overrightarrow{r_i}))^{\beta}(\delta(\tau)\delta(r_i-r_f))]$$
$$+\frac{-1}{4m^2}[(-i\overrightarrow{\nabla}_{r_i}+\frac{e\overrightarrow{B}}{2c}\times(\overrightarrow{r_f}-\overrightarrow{r_i}))^{\alpha}(\delta(\tau)\delta(r_i-r_f))][(i\overrightarrow{\nabla}_{r_f}+\frac{e\overrightarrow{B}}{2c}\times(\overrightarrow{r_f}-\overrightarrow{r_i}))^{\beta}(\frac{\partial\widetilde{G}_{r_f-r_i}(-\tau)}{\partial\tau})]$$
$$+\frac{1}{4m^2}[(-i\overrightarrow{\nabla}_{r_i}+\frac{e\overrightarrow{B}}{2c}\times(\overrightarrow{r_f}-\overrightarrow{r_i}))^{\alpha}(\delta(\tau)\delta(r_i-r_f))][(i\overrightarrow{\nabla}_{r_f}+\frac{e\overrightarrow{B}}{2c}\times(\overrightarrow{r_f}-\overrightarrow{r_i}))^{\beta}(\delta(\tau)\delta(r_i-r_f))]$$

$$\Pi^{E,E,4}_{\alpha,\beta}(r_i,r_f;\tau)=$$

$$\frac{-1}{4m^2}[(-i\overrightarrow{\nabla}_{r_i}-\frac{e\overrightarrow{B}}{2c}\times(\overrightarrow{r_f}-\overrightarrow{r_i}))^{\alpha}(\frac{\partial\widetilde{G}_{r_f-r_i}(-\tau)}{\partial\tau})][(i\overrightarrow{\nabla}_{r_f}-\frac{e\overrightarrow{B}}{2c}\times(\overrightarrow{r_f}-\overrightarrow{r_i}))^{\beta}(\frac{\partial\widetilde{G}_{r_i-r_f}(\tau)}{\partial\tau})]$$
$$+\frac{-1}{4m^2}[(-i\overrightarrow{\nabla}_{r_i}-\frac{e\overrightarrow{B}}{2c}\times(\overrightarrow{r_f}-\overrightarrow{r_i}))^{\alpha}(\frac{\partial\widetilde{G}_{r_f-r_i}(-\tau)}{\partial\tau})][(i\overrightarrow{\nabla}_{r_f}-\frac{e\overrightarrow{B}}{2c}\times(\overrightarrow{r_f}-\overrightarrow{r_i}))^{\beta}(\delta(\tau)\delta(r_i-r_f))]$$
$$+\frac{1}{4m^2}[(-i\overrightarrow{\nabla}_{r_i}-\frac{e\overrightarrow{B}}{2c}\times(\overrightarrow{r_f}-\overrightarrow{r_i}))^{\alpha}(\delta(-\tau)\delta(r_f-r_i))][(i\overrightarrow{\nabla}_{r_f}-\frac{e\overrightarrow{B}}{2c}\times(\overrightarrow{r_f}-\overrightarrow{r_i}))^{\beta}(\frac{\partial\widetilde{G}_{r_i-r_f}(\tau)}{\partial\tau})]$$
$$+\frac{1}{4m^2}[(-i\overrightarrow{\nabla}_{r_i}-\frac{e\overrightarrow{B}}{2c}\times(\overrightarrow{r_f}-\overrightarrow{r_i}))^{\alpha}(\delta(-\tau)\delta(r_f-r_i))][(i\overrightarrow{\nabla}_{r_f}-\frac{e\overrightarrow{B}}{2c}\times(\overrightarrow{r_f}-\overrightarrow{r_i}))^{\beta}(\delta(\tau)\delta(r_i-r_f))] \tag{2.38}$$

In momentum space, with the definition $\overrightarrow{K}=\overrightarrow{p}+\overrightarrow{q}$, we get

$$\Pi^{E,E}_{\alpha,\beta}(\overrightarrow{q};i\Omega)=\Pi^{E,E,1}_{\alpha,\beta}(\overrightarrow{q};i\Omega)+\Pi^{E,E,2}_{\alpha,\beta}(\overrightarrow{q};i\Omega)+\Pi^{E,E,3}_{\alpha,\beta}(\overrightarrow{q};i\Omega)+\Pi^{E,E,4}_{\alpha,\beta}(\overrightarrow{q};i\Omega)$$

$$\Pi^{E,E,1}_{\alpha,\beta}(\overrightarrow{q};i\Omega)=$$

$$\frac{1}{4m^2\beta}\sum_{\overrightarrow{p},iw_n}[(\overrightarrow{K}+\frac{ie\overrightarrow{B}}{2c}\times\overrightarrow{\nabla}_{\overrightarrow{K}})^{\alpha}(\overrightarrow{K}-\frac{ie\overrightarrow{B}}{2c}\times\overrightarrow{\nabla}_{\overrightarrow{K}})^{\beta}(\widetilde{G}_{\overrightarrow{K}}(iw_n+i\Omega))](iw_n)^2\widetilde{G}_{\overrightarrow{p}}(iw_n))$$
$$+\frac{1}{4m^2\beta}\sum_{\overrightarrow{p},iw_n}[(\overrightarrow{K}+\frac{ie\overrightarrow{B}}{2c}\times\overrightarrow{\nabla}_{\overrightarrow{K}})^{\alpha}(\overrightarrow{K}-\frac{ie\overrightarrow{B}}{2c}\times\overrightarrow{\nabla}_{\overrightarrow{K}})^{\beta}(\widetilde{G}_{\overrightarrow{K}}(iw_n+i\Omega))](-iw_n)$$

$$\Pi^{E,E,2}_{\alpha,\beta}(\overrightarrow{q};i\Omega)=$$

$$\frac{1}{4m^2\beta}\sum_{\overrightarrow{p},iw_n}((iw_n+i\Omega)^2\widetilde{G}_{\overrightarrow{K}}(iw_n+i\Omega))[(-\overrightarrow{p}+\frac{ie\overrightarrow{B}}{2c}\times\overrightarrow{\nabla}_{\overrightarrow{p}})^{\alpha}(-\overrightarrow{p}-\frac{ie\overrightarrow{B}}{2c}\times\overrightarrow{\nabla}_{\overrightarrow{p}})^{\beta}\widetilde{G}_{\overrightarrow{p}}(iw_n)]$$
$$-\frac{1}{4m^2\beta}\sum_{\overrightarrow{p},iw_n}(iw_n+i\Omega)[(-\overrightarrow{p}+\frac{ie\overrightarrow{B}}{2c}\times\overrightarrow{\nabla}_{\overrightarrow{p}})^{\alpha}(-\overrightarrow{p}-\frac{ie\overrightarrow{B}}{2c}\times\overrightarrow{\nabla}\overrightarrow{p})^{\beta}\widetilde{G}_{\overrightarrow{p}}(iw_n)]$$

$$\Pi^{E,E,3}_{\alpha,\beta}(\overrightarrow{q};i\Omega)=\frac{1}{4m^2\beta}\sum_{\overrightarrow{p},iw_n}[(\overrightarrow{K}+\frac{ie\overrightarrow{B}}{2c}\times\overrightarrow{\nabla}_{\overrightarrow{K}})^{\alpha}((iw_n+i\Omega)\widetilde{G}_{\overrightarrow{K}}(iw_n+i\Omega))]$$
$$\times[(-\overrightarrow{p}-\frac{ie\overrightarrow{B}}{2c}\times\overrightarrow{\nabla}_{\overrightarrow{p}})^{\beta}((-iw_n)\widetilde{G}_{\overrightarrow{p}}(iw_n))]$$
$$-\frac{1}{4m^2\beta}\sum_{\overrightarrow{p},iw_n}[(\overrightarrow{K}+\frac{ie\overrightarrow{B}}{2c}\times\overrightarrow{\nabla}_{\overrightarrow{K}})^{\alpha}((iw_n+i\Omega)\widetilde{G}_{\overrightarrow{K}}(iw_n+i\Omega))][(-\overrightarrow{p}-\frac{ie\overrightarrow{B}}{2c}\times\overrightarrow{\nabla}_{\overrightarrow{p}})^{\beta}(1)]$$
$$+\frac{1}{4m^2\beta}\sum_{\overrightarrow{p},iw_n}[(\overrightarrow{K}+\frac{ie\overrightarrow{B}}{2c}\times\overrightarrow{\nabla}_{\overrightarrow{K}})^{\alpha}(1)][(-\overrightarrow{p}-\frac{ie\overrightarrow{B}}{2c}\times\overrightarrow{\nabla}_{\overrightarrow{p}})^{\beta}((-iw_n)\widetilde{G}_{\overrightarrow{p}}(iw_n))]$$
$$-\frac{1}{4m^2\beta}\sum_{\overrightarrow{p},iw_n}[(\overrightarrow{K}+\frac{ie\overrightarrow{B}}{2c}\times\overrightarrow{\nabla}_{\overrightarrow{K}})^{\alpha}(1)][(-\overrightarrow{p}-\frac{ie\overrightarrow{B}}{2c}\times\overrightarrow{\nabla}_{\overrightarrow{p}})^{\beta}(1)]$$

$$\Pi^{E,E,4}_{\alpha,\beta}(\overrightarrow{q};i\Omega)=\frac{1}{4m^2\beta}\sum_{\overrightarrow{p},iw_n}[(-\overrightarrow{p}+\frac{ie\overrightarrow{B}}{2c}\times\overrightarrow{\nabla}_{\overrightarrow{p}})^{\alpha}((-iw_n)\widetilde{G}_{\overrightarrow{p}}(iw_n))]$$
$$\times[(\overrightarrow{K}-\frac{ie\overrightarrow{B}}{2c}\times\overrightarrow{\nabla}_{\overrightarrow{K}})^{\beta}((iw_n+i\Omega)\widetilde{G}_{\overrightarrow{p}}(iw_n+i\Omega))]$$
$$+\frac{1}{4m^2\beta}\sum_{\overrightarrow{p},iw_n}[(-\overrightarrow{p}+\frac{ie\overrightarrow{B}}{2c}\times\overrightarrow{\nabla}_{\overrightarrow{p}})^{\alpha}((-iw_n)\widetilde{G}_{\overrightarrow{p}}(iw_n))][(\overrightarrow{K}-\frac{ie\overrightarrow{B}}{2c}\times\overrightarrow{\nabla}_{\overrightarrow{K}})^{\beta}(1)]$$
$$-\frac{1}{4m^2\beta}\sum_{\overrightarrow{p},iw_n}[(-\overrightarrow{p}+\frac{ie\overrightarrow{B}}{2c}\times\overrightarrow{\nabla}_{\overrightarrow{p}})^{\alpha}(1)][(\overrightarrow{K}-\frac{ie\overrightarrow{B}}{2c}\times\overrightarrow{\nabla}_{\overrightarrow{K}})^{\beta}((iw_n+i\Omega)\widetilde{G}_{\overrightarrow{p}}(iw_n+i\Omega))]$$
$$-\frac{1}{4m^2\beta}\sum_{\overrightarrow{p},iw_n}[(-\overrightarrow{p}+\frac{ie\overrightarrow{B}}{2c}\times\overrightarrow{\nabla}_{\overrightarrow{p}})^{\alpha}(1)][(\overrightarrow{K}-\frac{ie\overrightarrow{B}}{2c}\times\overrightarrow{\nabla}_{\overrightarrow{K}})^{\beta}(1)]$$

(2.39)

To first order in magnetic field the energy-energy current correlation function has the form

$$\Pi^{E,E}_{x,x}(\overrightarrow{q}\rightarrow 0;i\Omega)=\frac{1}{\beta}\sum_{\overrightarrow{p},iw_n}\{(iw_n+\frac{i\Omega}{2})^2\overrightarrow{v}^2_{\overrightarrow{p},x}\widetilde{G}(\overrightarrow{p},iw_n+i\Omega)\widetilde{G}(\overrightarrow{p},iw_n)+\frac{\overrightarrow{v}^2_{\overrightarrow{p},x}}{2}\}$$
$$+\frac{1}{\beta}\sum_{\overrightarrow{p},iw_n}\{\frac{\overrightarrow{v}^2_{\overrightarrow{p},x}}{2}\frac{(iw_n+i\Omega)\widetilde{G}(\overrightarrow{p},iw_n+i\Omega)+iw_n\widetilde{G}(\overrightarrow{p},iw_n)}{2}\}$$
$$+\frac{1}{\beta}\sum_{\overrightarrow{p},iw_n}\{\frac{i\Omega\overrightarrow{v}^2_{\overrightarrow{p},x}}{2}\frac{\widetilde{G}(\overrightarrow{p},iw_n+i\Omega)-\widetilde{G}(\overrightarrow{p},iw_n)}{2}\} \quad (2.40)$$

$$\Pi^{E,E}_{x,y}(\overrightarrow{q}\rightarrow 0;i\Omega)=$$
$$\frac{-ie|\overrightarrow{B}|}{4c\beta m}\sum_{\overrightarrow{p},iw_n}(iw_n+\frac{i\Omega}{2})^2(\overrightarrow{v}_{\overrightarrow{p},x})\{\frac{\partial\widetilde{G}_{\overrightarrow{p}}(iw_n+i\Omega)}{\partial p_x}\widetilde{G}_{\overrightarrow{p}}(iw_n)-\widetilde{G}_{\overrightarrow{p}}(iw_n+i\Omega)\frac{\partial\widetilde{G}_{\overrightarrow{p}}(iw_n)}{\partial p_x}\}$$
$$+\frac{-ie|\overrightarrow{B}|}{4c\beta m}\sum_{\overrightarrow{p},iw_n}(iw_n+\frac{i\Omega}{2})^2(\overrightarrow{v}_{\overrightarrow{p},y})\{\frac{\partial\widetilde{G}_{\overrightarrow{p}}(iw_n+i\Omega)}{\partial p_y}\widetilde{G}_{\overrightarrow{p}}(iw_n)-\widetilde{G}_{\overrightarrow{p}}(iw_n+i\Omega)\frac{\partial\widetilde{G}_{\overrightarrow{p}}(iw_n)}{\partial p_y}\}$$
$$+\frac{-ie|\overrightarrow{B}|}{4c\beta m}\sum_{\overrightarrow{p},iw_n}(iw_n+\frac{i\Omega}{2})\{\frac{i\Omega}{2}\widetilde{G}_{\overrightarrow{p}}(iw_n+i\Omega)\widetilde{G}_{\overrightarrow{p}}(iw_n)-\widetilde{G}_{\overrightarrow{p}}(iw_n+i\Omega)+\widetilde{G}_{\overrightarrow{p}}(iw_n)\}$$

(2.41)

Using these general forms of the energy-energy current correlation tensor and the Kubo formula of eqn.2.14 the energy conductivity tensor can be found for a given model in the dilute impurity limit. The heat conductivity tensor is found by subtracting the thermoelectric conductivity tensor rescaled by the ratio $\frac{2\mu}{e}$(μ is the chemical potential and e is the charge of the electron) and adding the electrical conductivity tensor rescaled by the ratio $(\frac{\mu}{e})^2$ from the energy conductivity tensor. The dc heat conductivity tensor is found by taking the real part in the limit $\Omega\rightarrow 0$ of the heat conductivity tensor.

Chapter 3

Quantum Transport Theory of Graphene in a Weak Magnetic Field

3.1 Introduction

Motivated by the experimental measurement of electrical and hall conductivity, thermopower and Nernst effect, we calculate the longitudinal and transverse electrical and heat transport in graphene in the presence of unitary scatterers as well as charged impurities. The temperature and carrier density dependence in this system display a number of anomalous features that arise due to the relativistic nature of the low energy fermionic degrees of freedom. We derive the properties in detail including the effect of unitary and charged impurities self-consistently, and present tables giving the analytic expressions for all the transport properties in the limit of small and large temperature compared to the chemical potential and the scattering rates. We compare our results

with the available experimental data. While the qualitative variations with temperature and density of carriers or chemical potential of all transport properties can be reproduced, we find that a given set of parameters of the impurities fits the Hall conductivity, Thermopower and the Nernst effect quantitatively but cannot fit the conductivity quantitatively. On the other hand a single set of parameters for scattering from Coulomb impurities fits conductivity, hall resistance and thermopower but not Nernst.

An unusual new electronic structure and the possibility of graphene as the basis for technologies of the future has sparked an intense effort in its fabrication and characterization. A number of spectacular properties such as conductivity in the limit of zero carrier density [6, 7, 5, 8], perfect tunneling through potential barriers[29, 30, 31, 8] and quantum hall effect at room temperatures[32, 33] have already been observed. While the anomalous properties of electrical conductivity has received a lot of attention, data on thermopower, Hall conductivity and Nernst[34, 35, 36, 37] have now revealed temperature and gate voltage dependence which need to be understood consistently within a single transport theory. Excellent summary of the previous theoretical and experimental work have recently become available while this work was in progress [38, 39].

Graphene is a two dimensional allotrope of carbon with a hexagonal crystal structure. Since it is made up of two interpenetrating triangular sublattices, the unit cell has two atoms[2]. As long as the sublattice symmetry is preserved the two bands touch at two points in the Brillouin zone. In the vicinity of these points the hamiltonian is linear in momentum and has the structure of $\mathbf{k} \cdot \vec{\sigma}$ where $\mathbf{k}$ is the momentum and $\vec{\sigma} = \{\sigma^x, \sigma^y, \sigma^z\}$[32, 29]. The pauli matrices represent pseudospin with the two components referring to the two sublattices. The linear dispersion means that the electrons near these points in the Brillouin zone behave like relativistic massless particles in the absence of

impurities and are called Dirac points[32, 29]. For pure graphene the fermi surface is at the Dirac point and the density of states depends linearly on energy near the chemical potential. The vanishing density of states, the conservation of the operator $\mathbf{k}\cdot\vec{\sigma}$ and the existence of two zeroes (or equivalently) valleys in the band structure are responsible for a number of novel phenomena in graphene.

The most striking observation is that the electrical conductivity varies linearly with carrier density when the carrier density is not too small and that it is nonzero even when the carrier density goes to zero[6, 7, 5, 8]. Numerous attempts at explaining the latter has led to a number of different values for the minimum conductivity[40, 41, 42, 43, 44, 45, 4, 38, 39, 46, 47]. The reason for the different predictions can be traced to sensitivity of the results to the different approximation schemes and order of limits employed in the calculations. For example taking the zero frequency limit before the zero temperature limit does not commute with the limits taken in the opposite order. Introducing an additional scale, such as the scattering rate further complicates the order of limits providing a wide spread of possible values. Experimentally it is clear that the observed minima is not universal. Within a Boltzmann transport formalism a scattering rate inversely proportional to the energy can account for the observed linear dependence with respect to carrier density. One possible source of such scattering is long range Coulomb scatterers [38, 39, 48, 46]. While this theory works well for finite densities, the finite minimum conductivity requires new physics near the Dirac point. Based on the observation of charge inhomogeneity in this limit[49, 9, 50, 51], a possible resolution is that the Coulomb scatterers promote the formation of charge puddles. These puddles mask the approach to zero carrier density and provide an effective mechanism for minimum conductivity. Another possibility which we work out is due to the fact that for small charge densities, the effect of Coulomb scattering due

to point charged defects also needs to be calculated self-consistently.

Alternatively, a mechanism that can provide a similar dependence of scattering rate on energy is strong scatterers in the unitarity limit [4, 52]. Within this approach, the scatterers introduce resonances and, in the independent scattering approximation, an effective impurity band forms which provides a finite density of states in the vicinity of the node. The width of this impurity band is set by the density of scatterers and for energies larger that the impurity bandwidth the linear density of states is recovered. Crucially the same parameter, i.e. density of impurities sets both the band width and the scattering rate. Qualitatively a constant conductivity at low densities crossing over to a linear in carrier density behavior is expected. A similar result occurs for Coulomb scatters as well since for low carrier densities even weak impurity potentials can induce resonances at low energies as the density of states goes to zero.

In this chapter we provide the dependence of longitudinal and hall conductivity, thermopower, thermal conductivity and Nernst coefficient for various regimes in temperature, scattering rate and chemical potential for unitary scatterers as well as calculate the self-consistent scattering rate for Coulomb scatterers so as to compare the two cases. For a finite impurity bandwidth the leading contribution to conductivity at the node is indeed universal in the limit of zero temperature. For temperatures smaller than the impurity bandwidth, the correction to the universal value is of order $(T\tau/\hbar)^2$, where τ is the mean free path. In this regime agreement with observed thermopower and hall resistance is obtained, the results are weakly dependent on the impurity concentration. On the other hand the Nernst signal is extremely sensitive to the impurity concentration. The higher the mobility the larger is the Nernst signal.

In section 3.2.1 we derive the form of the impurity averaged self energy and discuss the nature of the effective dispersion and mean free path. A similar analysis

for long range Coulomb impurities is presented in section 3.3. The transport formalism used to derive the conductivities is discussed in section 3.4. The form of electrical conductivity and hall resistance is analyzed in section 3.5. Section 3.6 discusses the nature of thermoelectric properties. In section 3.7 we present the results for thermal transport. We compare our results for conductivity, hall coefficient, thermopower and Nernst with experimental data in section 3.8. The details of all calculations are available in the appendix. Many parts of our work have already appeared in separate works of many others as we note in the References; our contribution is primarily the comprehensive calculations and comparison with experiments of diverse transport properties. We present asymptotic analytic expressions for the various transport quantities in a set of tables; these may be especially useful since they readily provide physical basis for the experimental results.

3.2 Impurities Self Averaging Formalism and Carrier densities

The Hamiltonian for graphene in tight binding formalism is[2, 45]

$$H_0 = -t \sum_{<i,j>} (a_i^\dagger b_j + b_j^\dagger a_i) \tag{3.1}$$

Where t is the nearest neighbor hopping amplitude and is related to the fermi velocity by $v_F = \frac{3}{2}\frac{ta}{\hbar}$. The operators in the Hamiltonian $\{a_i^\dagger, b_j^\dagger\}$ represent electron creation operators on sites i and j in the graphene's honeycomb lattice which belong to the A and B sublattice respectively. The two atoms per unit cell leads to a 2×2 matrix for the Green's function of graphene. The two bands touch at two points in the Brillouin zone labelled by $\mathbf{K}$ and $\mathbf{K}'$. In the vicinity of these points the Greens function is[45]

$$G_\sigma(\overrightarrow{k}, i\omega) = \frac{1}{2}\sum_{\lambda=\pm 1} \frac{\begin{pmatrix} 1 & \lambda e^{i\Theta(\overrightarrow{k})} \\ \lambda e^{-i\Theta(\overrightarrow{k})} & 1 \end{pmatrix}}{i\omega - \lambda|\phi(\overrightarrow{k})|} \tag{3.2}$$

Where the function $\Theta(\overrightarrow{k})$ is equal to $-\frac{\pi}{6} + arg(k_x + ik_y)$ and the dispersion relation at the node is given by $\phi(\overrightarrow{k}) = \pm\hbar v_F|\overrightarrow{k}|$. In the presence of impurities we have an additional term in the Hamiltonian given by

$$H_{Imp} = \sum_{<i,\sigma>}^{N_A} V_i^A a_i^\dagger a_i + \sum_{<i,\sigma>}^{N_B} V_i^B b_i^\dagger b_i \tag{3.3}$$

In our analysis the model chosen is s-wave scatter potentials in the unitary limit. If the assumption is made that we have identical impurities randomly distributed throughout the system a impurity self-average Green's function can used as a approximate solution to the full Green's function of graphene. The impurity self-averaging is valid if the sample size is much larger than the coherence length of electrons which is the case for most experiment. In the dilute impurity limit scattering of single impurities dominate. The self energy must be calculated in the full self-consistent Born approximation (FSBA). The effect of the impurity states on transport quantities is to produce a finite conductivity at the at node as the carrier density is no longer zero. In the dilute limit of impurities the self energy in the full self-consistent born approximation is given by[45]

$$\Sigma_{FSBA}(i\omega) = \frac{n_{Imp}V}{1 - V\overline{G}(i\omega - \Sigma_{FSBA}(i\omega))} \tag{3.4}$$

$$\overline{G}(i\omega - \Sigma(i\omega)) = \frac{1}{N}\sum_{\overrightarrow{k}} G(i\omega - \Sigma(i\omega)) \tag{3.5}$$

For s-wave short range scatterers the self energy is momentum independent. The electronic Carrier density and the change in carrier density near the node due to a change

in chemical potential μ is given by

$$\frac{n(\mu,T)}{N_v N_s} = -\int \frac{d\varepsilon}{\pi}\frac{d\overrightarrow{k}}{(2\pi)^2} n_F(\varepsilon) ImG^R(\overrightarrow{k},\varepsilon) \tag{3.6}$$

$$\frac{\delta n(\mu,T)}{N_v N_s} = -\int d\mu' \int \frac{d\varepsilon}{\pi}\frac{d\overrightarrow{k}}{(2\pi)^2}\frac{\partial n_F}{\partial \mu'} ImG^R(\overrightarrow{k},\varepsilon) \tag{3.7}$$

where $\{N_v, N_s\}$ represent graphene's valley and spin degeneracies and G^R is the retarded Greens function. The integral over momentum of can be performed leading to

$$n(\mu,T) = -\int d\varepsilon \frac{< ImG^R(\varepsilon) >}{\pi^2\hbar^2 v_F^2} n_F(\varepsilon) \tag{3.8}$$

$$\delta n(\mu,T) = -\int d\mu' \int d\varepsilon \frac{< ImG^R(\varepsilon) >}{\pi^2\hbar^2 v_F^2}\frac{\partial n_F}{\partial \mu'} \tag{3.9}$$

$$\begin{aligned} < ImG^R(\varepsilon) > &= A\arctan(\frac{D^2+B^2-A^2}{2AB}) \\ &- A\arctan(\frac{B^2-A^2}{2AB}) \\ &+ \frac{B}{2}\ln(\frac{(D^2+B^2-A^2)^2+(2AB)^2}{(B^2-A^2)^2+(2AB)^2}) \end{aligned} \tag{3.10}$$

where D is the electronic band width and the functions $\{A(\varepsilon), B(\varepsilon)\}$ are given by $\{\varepsilon - Re\Sigma(\varepsilon), -Im\Sigma(\varepsilon)\}$.

3.2.1 Self Energy

In fig.3.1 we plot $|Im\Sigma|$ as a function of energy (ϵ) for several impurity concentrations. As the impurity concentration is increased the scattering rate (which is proportional to $|Im\Sigma|$) increases. It is weakly dependent on energy near the node crossing over to a $1/\epsilon$ dependence for large energies. The crossover scale is determined by the bandwidth (D) times the square root of the impurity concentration [53]. This crossover scale is

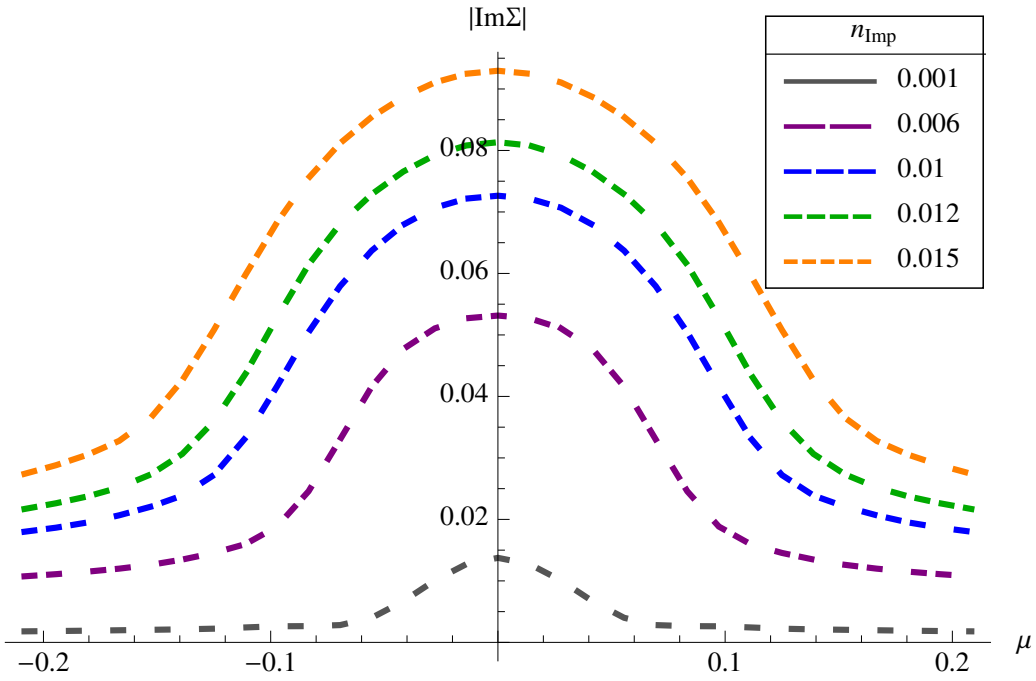

Figure 3.1: The absolute value of the imaginary part of the self energy is plotted as a function of the energy. The impurity concentration used to find the self energy curves is given in the legend.

the impurity band width. One can regard the effect of unitary scatters as producing resonances that fill in the density of states in the vicinity of the node. The linear density of states is recovered beyond the impurity band width. Unlike Born scattering, beyond the impurity band width the scattering rate remains inversely proportional to energy. Qualitatively, in this regime, the physics is similar to having weak Coulomb scatterers. Physical insight is gained by taking various limit of the change in electronic carrier density with respect to temperature, chemical potential and impurity band width.

$$\delta n_\mu \approx \frac{sgn(\mu)|\mu|^2}{2\pi\hbar^2 v_F^2}, \quad |\mu| >> |Im\Sigma(0)| >> T \tag{3.11}$$

$$\delta n_T \approx \frac{T\mu}{2\pi\hbar^2 v_F^2}, \quad T >> |\mu| >> |Im\Sigma(0)| \tag{3.12}$$

$$\delta n_{Im\Sigma} \approx \frac{\mu|Im\Sigma(0)|\ln(\frac{D^2}{|Im\Sigma|^2})}{\pi^2\hbar^2 v_F^2}, \quad |Im\Sigma(0)| >> |\mu| \tag{3.13}$$

In the limits above the electronic band size has been taken to be the largest energy scale and the real part of the self energy absorbed in a suitable redefinition of the chemical potential. In obtaining eqn.3.11 we have assumed that the imaginary part of the self energy is roughly constant upto the impurity band width with its value determined at zero energy.The integrals are approximated as $\int d\varepsilon \frac{\partial n_F(\varepsilon)}{\partial \mu}(\cdots) \rightarrow \int_{-T+\mu}^{T+\mu} \frac{d\varepsilon}{2T}(\cdots)$ and $\int d\varepsilon \frac{\partial n_F(\varepsilon)}{\partial \mu}(\cdots) \approx \int d\varepsilon \delta(\mu-\varepsilon)(\cdots) = (\cdots)|_{\varepsilon=\mu}$ at high and low temperatures respectively. Since $\delta n = \int d^2\mathbf{k} \int_0^\mu d\epsilon d\mathbf{k}\delta(\epsilon - \epsilon(\mathbf{k}))$ we can extract an effective dispersion relation in the different regimes

$$\hbar v_F k_F \approx |\mu|, \quad |\mu| >> |Im\Sigma|(0) >> T \tag{3.14}$$

$$\frac{\hbar^2 k_F^2}{2m^*} \approx |\mu|$$

$$m^* \approx \begin{cases} \frac{|Im\Sigma|\ln(\frac{D}{|Im\Sigma|})}{2\pi\hbar^2 v_F^2} & , |Im\Sigma(0)| >> |\mu| \\ \frac{T}{2v_F^2} & , T >> |\mu| >> |Im\Sigma(0)| \end{cases}$$

In the limit where $|\mu| >> |Im\Sigma| >> T$, the Dirac dispersion relation is preserved. In the other limits the dispersion is effectively that of a free electron with a mass determined by the dominant energy scale. Given this form we can use the effective dispersion in eqn.3.14 to calculate the longitudinal conductivites in various regimes[54].

$$\begin{aligned}
\sigma &\approx \frac{e^2}{h}\frac{T}{2|Im\Sigma|}, \quad T >> |\mu| >> |Im\Sigma| \\
\sigma &\approx \frac{e^2}{h}\frac{|\mu|}{2|Im\Sigma|}, \quad |\mu| >> |Im\Sigma| >> T \\
\sigma &\approx \frac{e^2}{h}\frac{2}{\pi}\ln|\frac{D}{Im\Sigma}|, |Im\Sigma| >> |\mu|
\end{aligned} \tag{3.15}$$

For small chemical potential we find that the conductivity is constant and depends logarithmically on the imaginary part of the self energy which in turn is proportional to the square root of the impurity concentration[53]. Thus, within this picture, we obtain a finite minimum conductivity which is not universal. As we increase the chemical potential, at low temperatures, we crossover to a regime where the conductivity scales as $\mu^2 \propto \delta n$ (note in this regime $Im\Sigma \propto 1/\mu$). Both these features are in qualitative agreement with observed data in graphene. There is also a constraint implicit here that the crossover scale is controlled by the same parameter that determines the value of the conductivity minimum.

3.2.2 Mean Free Path

We study the transport properties in weak magnetic fields where we are in the hydrodynamic limit ($\omega_c\tau \ll 1$). In fig.3.2 we plot the ratio of the mean free path to the cyclotron radius as a function of the chemical potential for a fixed magnetic field. The mean free path is roughly constant up to the impurity bandwidth which in this case is 0.09 eV. Beyond this scale the mean free path grows suggesting an energy dependent scattering rate that becomes smaller at higher energies. This behavior is consistent with the behavior of the imaginary part of the self energy. In the entire range shown the mean free path is much smaller than the magnetic length for a field of 8 Tesla, we are well within the hydrodynamic regime.

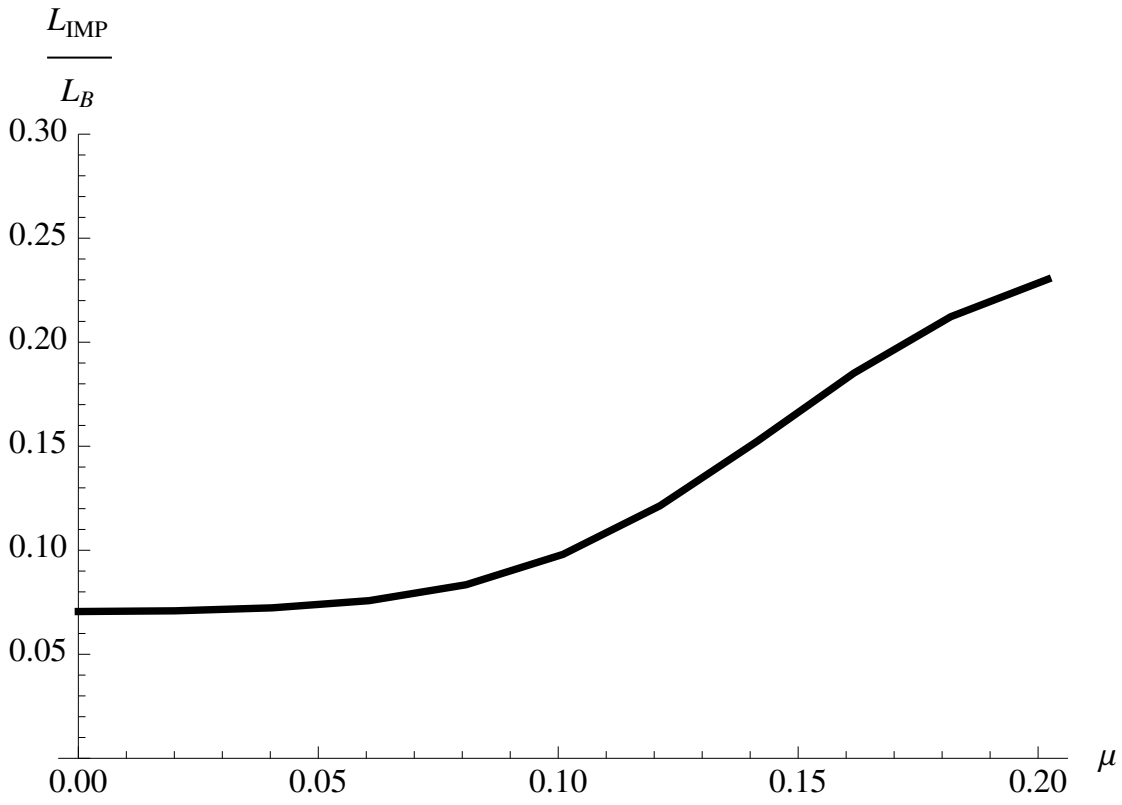

Figure 3.2: The mean free scattering length (L_{Imp}) in units of cyclotron radius (L_B) is plotted as a function of the chemical potential (μ). The impurity concentration is $n_i = 0.012$ and the cyclotron radius is calculated in an 8 Tesla magnetic field. The Fermi velocity used is $v_F = .8 * 10^6 m/sec$

Table 3.1: Carrier Density and Specific Heat

Quantity	$(I): T, \lvert\mu\rvert << \lvert\frac{\hbar}{2\tau}\rvert$	$(II): T, \lvert\frac{\hbar}{2\tau}\rvert << \lvert\mu\rvert$	$(III): \lvert\frac{\hbar}{2\tau}\rvert << \lvert\mu\rvert << T$	$(IV): \lvert\mu\rvert << \lvert\frac{\hbar}{2\tau}\rvert << T$
δn	$\frac{\mu\lvert Im\Sigma\rvert \ln(\frac{D^2}{\lvert Im\Sigma\rvert^2})}{\pi^2\hbar^2 v_F^2} + \cdots$	$\frac{sgn(\mu)\lvert\mu\rvert^2}{2\pi\hbar^2 v_F^2} + \cdots$	$\frac{T\mu}{2\pi\hbar^2 v_F^2} + \cdots$	$\frac{\mu\lvert Im\Sigma\rvert \ln(\frac{D^2}{\lvert Im\Sigma\rvert^2})}{\pi^2\hbar^2 v_F^2} + \cdots$
$\frac{c_v}{k_B}$	$\frac{\pi^2}{3}(\frac{k_B T\lvert Im\Sigma\rvert \ln(\frac{D^2}{\lvert Im\Sigma\rvert^2})}{\pi^2\hbar^2 v_F^2}) + \cdots$	$\frac{4\pi^2}{3}(\frac{k_B T\lvert\mu\rvert}{2\pi\hbar^2 v_F^2}) + \cdots$	$\frac{1}{2}(\frac{(k_B T)^2}{2\pi\hbar^2 v_F^2}) + \cdots$	$\frac{1}{3}(\frac{k_B T\lvert Im\Sigma\rvert \ln(\frac{D^2}{\lvert Im\Sigma\rvert^2})}{\pi^2\hbar^2 v_F^2}) + \cdots$

3.2.3 Specific heat

Thermoelectric transport coefficients, such as thermoelectric power, Nernst and thermal conductivity depend on the specific heat at constant volume. The energy density and specific heat in graphene in the presence of unitary scatterers are given by[54]

$$\frac{< E > (\mu, T)}{N_v N_s} = -\int \frac{d\varepsilon}{\pi} \frac{d\overrightarrow{k}}{(2\pi)^2} \varepsilon n_F(\varepsilon) ImG^R_{\overrightarrow{k}}(\varepsilon) \tag{3.16}$$

$$\frac{c_v(\mu, T)}{k_B N_v N_s} = -\int \frac{d\varepsilon}{\pi} \frac{d\overrightarrow{k}}{(2\pi)^2} \varepsilon \frac{\partial n_F}{\partial k_B T} ImG^R_{\overrightarrow{k}}(\varepsilon) \tag{3.17}$$

With the same approximations used to derive the conductivity above, the specific heat and electronic carrier density, to leading order in the appropriate small parameter, in different regimes are given in table 3.1. The specific heat divided by temperature is proportional to $\partial\delta n/\partial\mu$. This is natural as we expect the two quantities to be proportional to the density of states which in turn is the imaginary part of the self energy.

3.3 Coulomb Scatterers

In this section we consider the nature of scattering in the presence of charge impurities. We follow the same approach as in the case of unitary scatterers and compute

the self energy in the self consistent Born approximation.

To first order, within born approximation the self-energy due to screened Coulomb scatters has the form:

$$\Sigma(\overrightarrow{k}, i\omega_n) = \frac{n_i}{\Omega}\sum_{\overrightarrow{k'}} |U(\overrightarrow{k'}, \overrightarrow{k}, i\omega_n)|^2 G^0(\overrightarrow{k'}, i\omega_n) \tag{3.18}$$

$$U(\overrightarrow{k'}, \overrightarrow{k}, i\omega_n) = \frac{(2\pi e^2)/(\kappa\epsilon_0)}{|\overrightarrow{k} - \overrightarrow{k'}| + q_{TF}(\overrightarrow{k'}, i\omega_n)} \tag{3.19}$$

where n_i is the concentration of charge impurities, e is the charge of an electron, Ω is the area, ϵ_0 is the vacuum permittivity, $G^0(\overrightarrow{k'}, i\omega_n)$ is the greens function in the absence of impurities and κ is the permittivity of the substrate. The function $q_{TF}(\overrightarrow{k}, i\omega_n)$ is the inverse Thomas Fermi screening length. In general the self energy is a 2×2 matrix and must be handled in a self consistent manner. In order to correctly account for changes in the ground state energy the Green function in eq.(3.18) must be replaced by the full Green's function.

In the impurities self averaging formalism the self energy is diagonal and has the form:

$$\begin{aligned} \Sigma(i\omega_n) &= \frac{n_i}{\Omega}\sum_{\overrightarrow{k'}} \left|\frac{(2\pi e^2)/(\kappa\epsilon_0)}{k' + q_{TF}(i\omega_n)}\right|^2 G_{AA}(\overrightarrow{k'}, i\omega_n) \\ G_{AA}(\overrightarrow{k}, i\omega_n) &= \frac{i\omega_n - \Sigma(i\omega_n)}{(i\omega_n - \Sigma(i\omega_n))^2 - |\phi(\overrightarrow{k})|^2} \end{aligned} \tag{3.20}$$

Here we have made the assumption that the Total inverse Thomas Fermi screening length is the sum of a two terms: a energy dependent only term which can be related to the density of states by eqn.3.21 and a weak momentum dependent term which is proportional to momentum. The density of states and the energy dependent inverse Thomas Fermi screening length are given by

$$\begin{aligned} q_{TF}(i\omega_n) &= \frac{2\pi e^2}{\kappa\epsilon_0}\int d\varepsilon N(\varepsilon)\frac{\partial n_F}{\partial \mu} \\ N(\varepsilon) &= -\frac{< ImG^R(\varepsilon) >}{\pi^2\hbar^2 v_F^2} \end{aligned} \tag{3.21}$$

$$\begin{aligned} < ImG^R(\varepsilon) > &= A\arctan(\frac{D^2+B^2-A^2}{2AB}) \\ &- A\arctan(\frac{B^2-A^2}{2AB}) \\ &+ \frac{B}{2}\ln(\frac{(D^2+B^2-A^2)^2+(2AB)^2}{(B^2-A^2)^2+(2AB)^2}) \end{aligned} \tag{3.22}$$

To obtain the transport coefficients in the presence of Coulomb scatterers we substitute the scattering rate obtained here in expressions derived for unitary scatterers. An important point to emphasize is that the self consistency yields a finite screening length at the node while crossing over to the inverse fermi wave vector at large carrier densities. Thus the Coulomb potential is screened providing a mechanism for finite density of states and conductivity at zero bias.

The self energy is momentum independent at the node. For a finite impurity concentration eq.(3.20) is simplified to the form:

$$Im\Sigma(0) = \frac{n_i}{\Omega}\sum_{\vec{k}}\left|\frac{(2\pi e^2)/(\kappa\epsilon_0)}{k+q_{TF}(0)}\right|^2 \frac{-Im\Sigma(0)}{Im\Sigma^2(0)+|\phi(\vec{k})|^2} \tag{3.23}$$

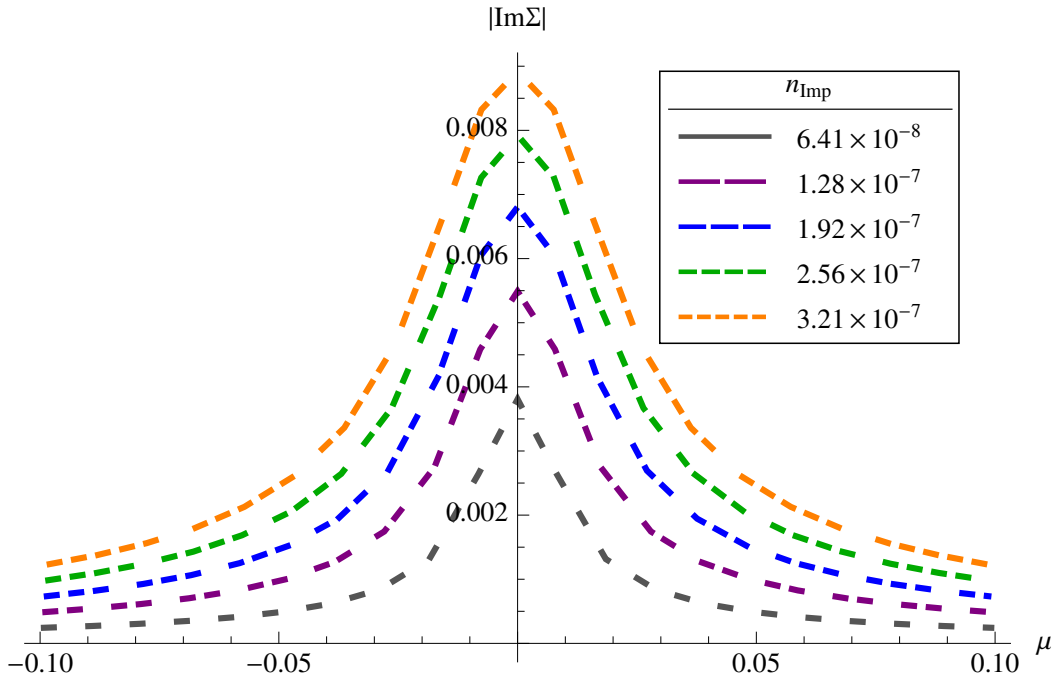

Figure 3.3: The absolute value of the imaginary part of the self energy is plotted as a function of the energy. The impurity concentration used to find the self energy curves is given in the legend.

The summation over momenta can be performed in closed form but the solution can only be obtained numerically. The screening obtained at zero energy allows us to approximate the self energy to be independent of momentum and compute its dependence on chemical potential. The results are shown in fig.3.3. We have chosen impurity concentrations that yield the best fit to the data analyzed. The only free parameter is the distance of the impurities from the graphene sheet. Unlike unitary scatterers, which are part of the graphene layer itself, the Coulomb scatterers are in the substrate. In these calculations we have assumed that the charged impurities are on the graphene sheet thus requiring a very small concentration to fit the data.

Qualitatively the imaginary part of the self energy is similar to that of unitary scatterers. At large carrier densities the scattering rate falls off as $1/\mu$. The divergence

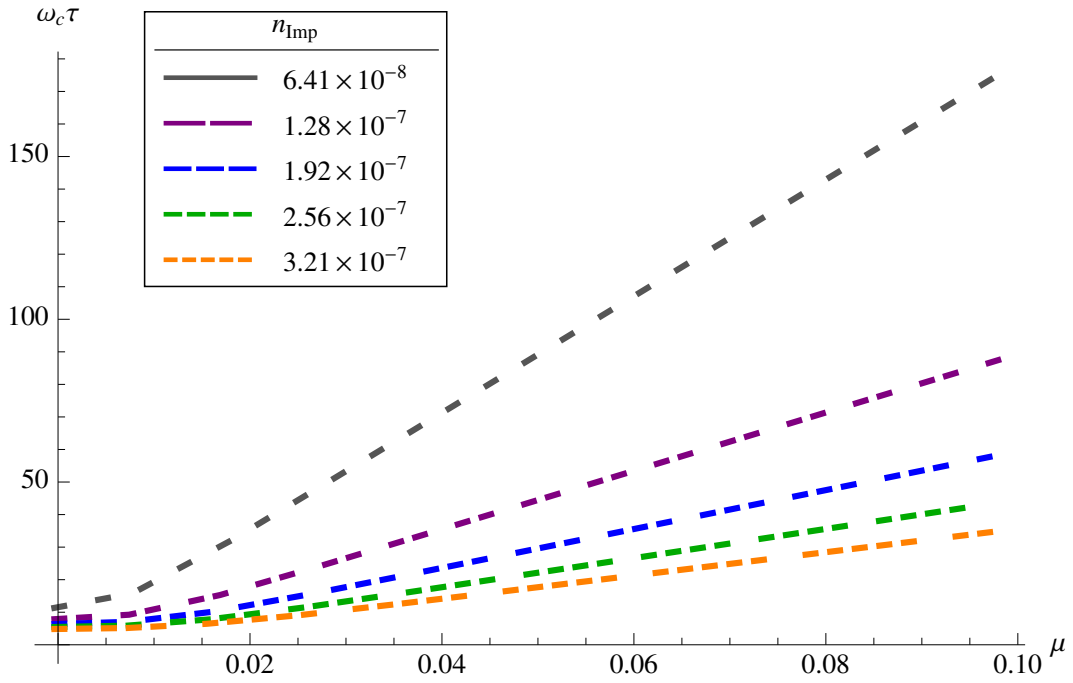

Figure 3.4: The ratio of the cyclotron energy ($\hbar\omega_c$) to the scattering rate is plotted as a function of the chemical potential at 8T.

at zero chemical potential is cutoff by the emergence of a finite screening length. The finite scattering rate is responsible for the observed minima in conductivity within this scenario. The existence of charge inhomogeneities at low bias has been experimentally observed and does lead finite conductivity at the dirac point. Whether the real space realization of this phenomena yields charge puddles is an open question that is beyond the scope of this work. Our analysis is valid in the hydrodynamic regime where $\omega_c\tau \ll 1$. For the range of charged impurities considered, this condition is violated when $8T$ field is applied as seen in fig.3.4. How the formation of Landau levels modifies the transport characteristics is beyond the scope of this study but the results presented are valid for smaller fields.

3.4 Transport Formalism

In response to applied electromagnetic fields and thermal gradients the electrical and heat current are induced. Within linear response these quantities are related as[54, 18]

$$\begin{aligned} \overrightarrow{G} &= \overrightarrow{E} + \overrightarrow{\nabla}(\frac{\mu}{e}) \\ \overrightarrow{J} &= (\sigma^{(0)})(\overrightarrow{E}) + (\beta^{(1)})(-\frac{\overrightarrow{\nabla}(T)}{T}) \\ \overrightarrow{J_Q} &= (\beta^{(2)})(\overrightarrow{E}) + (\kappa^{(3)})(-\frac{\overrightarrow{\nabla}(T)}{T}) \end{aligned} \tag{3.24}$$

where $\overrightarrow{J}$ is the charge current density, $\overrightarrow{J_Q}$ is the heat current density, $\sigma^{(0)}$ is the electrical conductivity, $\beta^{(1)} = \beta^{(2)}$ is the thermoelectric conductivity and $\kappa^{(3)}$ is the heat conductivity. The heat current density is related to the charge current density : $\overrightarrow{J_Q} = \overrightarrow{J_E} - \mu\overrightarrow{J}$, where $\overrightarrow{J_E}$ is the energy current density. Each of these conductivity tensors is computed using retarded current-current correlation function within the standard Kubo formalism. The current-current correlation function and current densities are given by[18, 16, 28]:

$$\begin{aligned} \Pi^{\alpha,\beta}_{i,k}(q, i\Omega_m) &= \frac{-i}{V}\int_0^\beta d\tau e^{i\Omega_m\tau} < T_\tau j_{\alpha,i}(\tau, q) j^\dagger_{\beta,k}(\tau, 0) > \\ j_{e,\alpha}(r_i, t) &= \lim_{\substack{r'_i \to r_i \\ t' \to t}} \frac{e}{2m}((-i\overrightarrow{\nabla}^\alpha_{r'_i} - e\overrightarrow{A}^\alpha_{r'_i}))\Psi^\dagger(r_i, t)\Psi(r'_i, t') \\ &- \lim_{\substack{r'_i \to r_i \\ t' \to t}} \frac{e}{2m}((-i\overrightarrow{\nabla}^\alpha_{r_i} + e\overrightarrow{A}^\alpha_{r_i}))\Psi^\dagger(r_i, t)\Psi(r'_i, t') \\ j_{E,\alpha}(r_i, t) &= \lim_{\substack{r'_i \to r_i \\ t' \to t}} \frac{1}{2m}((-i\overrightarrow{\nabla}^\alpha_{r'_i} - e\overrightarrow{A}^\alpha_{r'_i})\frac{\partial}{\partial t})\Psi^\dagger(r_i, t)\Psi(r'_i, t') \\ &+ \lim_{\substack{r'_i \to r_i \\ t' \to t}} \frac{1}{2m}((-i\overrightarrow{\nabla}^\alpha_{r_i} + e\overrightarrow{A}^\alpha_{r_i})\frac{\partial}{\partial t'})\Psi^\dagger(r_i, t)\Psi(r'_i, t') \end{aligned} \tag{3.25}$$

where $j_{\alpha,i}(\tau, q)$ is the current density operator, α refers to the type of current density, i

refers to the components, $j_{e,\alpha}(r_i,t)$ and $j_{E,\alpha}(r_i,t)$ are the electrical and energy current densities[28], $\{\psi,\psi^\dagger\}$ are the fermion annihilations and creation operators and $\overrightarrow{A}_r$ is the vector potential. The conductivities can be related to the appropriate current current correlation function. For closed boundary conditions, the thermoelectric transport coefficients , S, are related to the conductivities $\beta^{(1)}$ and $\sigma^{(0)}$:

$$\begin{aligned} S &= \frac{\beta^{(1)}}{T\sigma^{(0)}} \\ S_{xx} &= \frac{(\sigma^{(0)}_{xx})(\beta^{(1)}_{xx}) + (\sigma^{(0)}_{xy})(\beta^{(1)}_{xy})}{T*((\sigma^{(0)}_{xx})^2 + (\sigma^{(0)}_{xy})^2)} \\ e_y &= \frac{(\sigma^{(0)}_{xx})(\beta^{(1)}_{xy}) - (\sigma^{(0)}_{xy})(\beta^{(1)}_{xx})}{T*((\sigma^{(0)}_{xx})^2 + (\sigma^{(0)}_{xy})^2)} \\ \nu &= \frac{(\sigma^{(0)}_{xx})(\beta^{(1)}_{xy}) - (\sigma^{(0)}_{xy})(\beta^{(1)}_{xx})}{B*T*((\sigma^{(0)}_{xx})^2 + (\sigma^{(0)}_{xy})^2)} \end{aligned} \tag{3.26}$$

where S_{xx} is the thermopower and e_y is the Nernst[54, 18]. The Nernst coefficient ν is defined similarly to the hall coefficient but here the important quantity is the ratio of transverse electric field to longitudinal temperature gradient. Similarly the thermal transport coefficients can be obtained from[54, 18]

$$K = \frac{\kappa^{(3)}}{T} - \frac{\beta^{(2)}(\sigma^{(0)})^{-1}\beta^{(1)}}{T} \tag{3.27}$$

The components can be related to Nernst and thermopower:

$$\begin{aligned} K_{xx} &= \frac{\kappa^{(3)}_{xx}}{T} + \beta^{(1)}_{xy}e_y - \beta^{(1)}_{xx}S_{xx} \\ K_{xy} &= \frac{\kappa^{(3)}_{xy}}{T} - \beta^{(1)}_{xx}e_y - \beta^{(1)}_{xy}S_{xx} \end{aligned} \tag{3.28}$$

In metals the thermoelectric transport coefficients such as Nernst and thermopower are not large and generally do not contribute to thermal conductivity. The situation is more interesting in materials where the density of state vanishes, such as graphene and high

temperature superconductors. The focus of this paper is on the anomalous dependence on gate voltage and temperature of thermopower and Nernst, the latter being orders of magnitude larger than typical metals.

3.5 Electrical conductivity

In this section we discuss the formalism for calculating the electrical conductivity tensor and a comparison of our results with other theoretical studies is given. The electrical conductivity tensor is calculated using Kubo formula[18]:

$$\sigma_{i,j}(q,\Omega) = \frac{\Pi^{e,e}_{i,j}(q,\Omega+i\delta)}{\Omega} \tag{3.29}$$

where $\Pi^{e,e}_{i,j}$ is the current-current correlation function and the indices e referring to the vertex corresponding to charge current. Using the definition of the charge current density operator in eqn.3.25, the resulting current-current correlation function is:

$$\begin{aligned}\Pi^{e,e}_{\alpha,\beta}(r_i,r_f;\tau) = & < T_\tau(\lim_{\substack{r'_i\to r_i\\ \tau'\to\tau}} \frac{e}{2m}[(-i\overrightarrow{\nabla}^{\alpha}_{r'_i} - e\overrightarrow{A}^{\alpha}_{r'_i}) - (-i\overrightarrow{\nabla}^{\alpha}_{r_i} + e\overrightarrow{A}^{\alpha}_{r_i})]\Psi^\dagger(r_i,\tau)\Psi(r'_i,\tau')) \\ & (\lim_{r'_f\to r_f} \frac{e}{2m}[(i\overrightarrow{\nabla}^{\beta}_{r'_f} - e\overrightarrow{A}^{\beta}_{r'_f}) - (i\overrightarrow{\nabla}^{\beta}_{r_f} + e\overrightarrow{A}^{\beta}_{r_f})]\Psi^\dagger(r'_f,0)\Psi(r_f,0)) >\end{aligned} \tag{3.30}$$

The calculations are presented in the appendix. The conductivity in the presence of unitary scatterers is[4, 53, 55]

$$\sigma_{xx}^{DC} = \frac{N_v N_s e^2}{4\pi h} \int d\varepsilon \frac{\partial n_F}{\partial \mu} \sigma_{xx}^{K}(\varepsilon) \tag{3.31}$$

$$\sigma_{xy}^{DC} = \frac{N_v N_s e^3 |\overrightarrow{B}| v_F^2}{2c\pi} \int \frac{d\varepsilon}{\pi} \frac{\partial n_F(\varepsilon)}{\partial \mu} \sigma_{xy}^{K}(\varepsilon) \tag{3.32}$$

$$\sigma_{xx}^{K}(\varepsilon) = (1 + \frac{A^2 + B^2}{AB} \arctan \frac{A}{B}) \tag{3.33}$$

$$\sigma_{xy}^{K}(\varepsilon) = \frac{1}{8AB}(\frac{B^2 - A^2}{B^2 + A^2} - \frac{B^2 + A^2}{2AB} \arctan \frac{2AB}{B^2 - A^2}) - \frac{AB}{3(A^2 + B^2)^2} \tag{3.34}$$

The kernels of the electrical conductivity tensor have been defined in terms of the functions $\{A, B\} = \{\varepsilon - Re\Sigma(\varepsilon), -Im\Sigma(\varepsilon)\}$ (for details see appendix A). Defining $\sigma_0 = \frac{e^2}{\pi h}$ and $w_c^2 = \frac{2e|\overrightarrow{B}|v_F^2}{c\hbar}$, we analyze the dependence of conductivity in the four regimes described earlier.

3.5.1 Longitudinal and transverse electrical conductivities

The dependence of the longitudinal conductivity and hall resistance are shown in fig.3.5 and fig.3.6. Longitudinal conductivity has a minima at the node crossing over to a μ^2 (linear in charge density) dependence for large carrier densities. The crossover occurs at the impurity bandwidth. The hall coefficient is linear at the node and falls of as $1/\mu^2$ for large chemical potential.

Analytic expressions obtained in various asymptotic limits are shown in table 3.2. In the regime where $\{T << |\frac{\hbar}{2\tau}| << \mu\}$, the longitudinal electrical conductivity is a linear function of $\mu/|Im\Sigma|$. The slope in this regime is equal to half the conductivity quanta and agrees with the other theoretical results[4, 56, 55]. For unitary scatterers in this

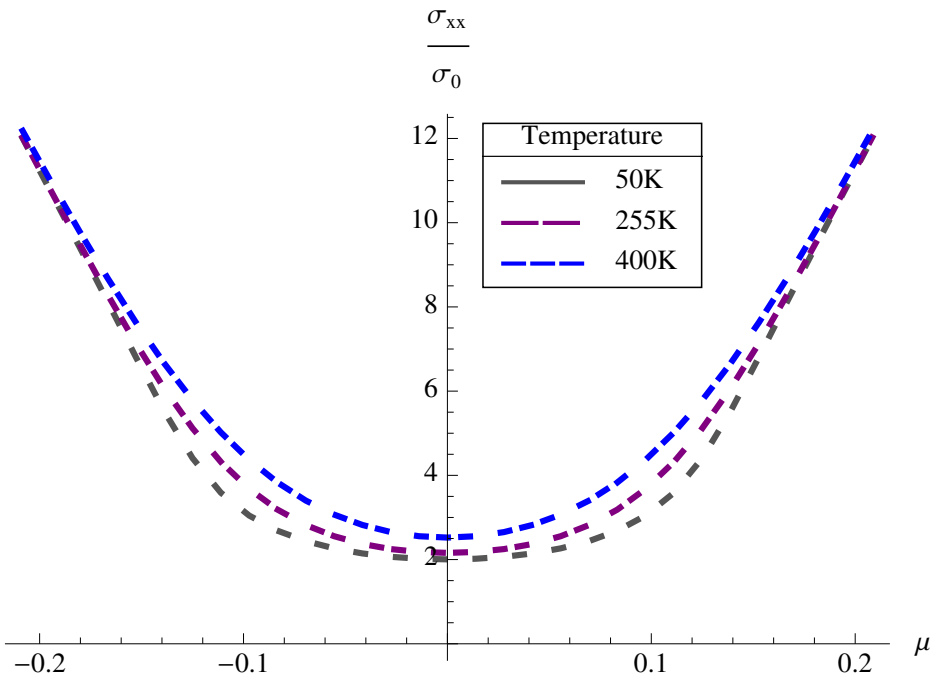

Figure 3.5: The diagonal electrical conductivity is plotted in units of $\frac{e^2}{\pi h}$ as a function of (μ). The impurity concentration is $n_i = 0.004$, while the temperature of each curve is given in the legend.

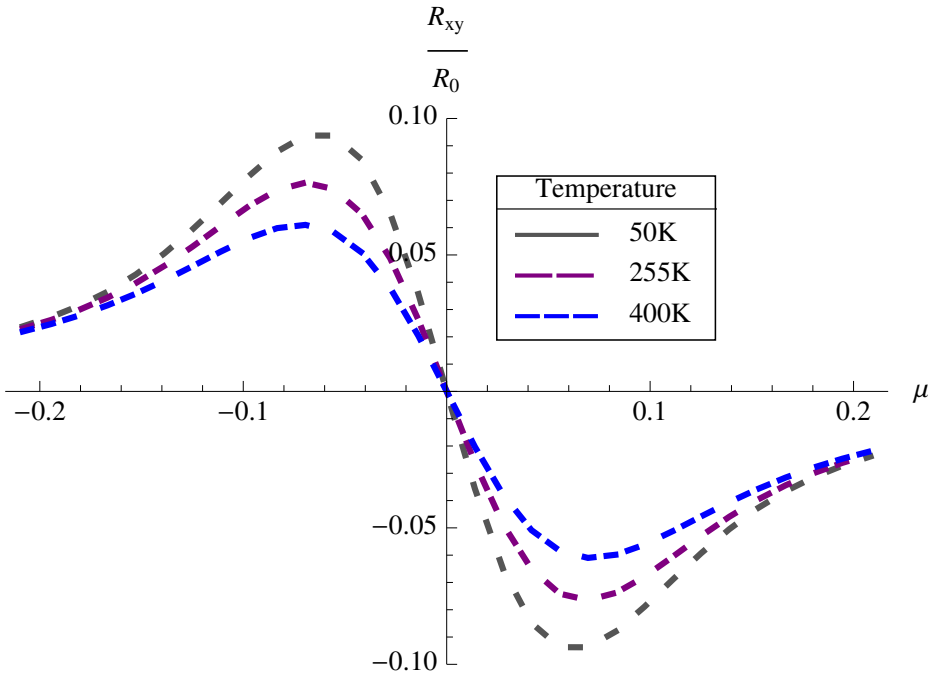

Figure 3.6: The Hall coefficient is plotted in units of $\frac{\pi h}{|B|e^2}$ as a function of chemical potential. The impurity concentration is $n_i = 0.012$, while the temperature of each curve is given in the legend.

Table 3.2: Electrical transport coefficients

Quantity	$(I): T, \lvert\mu\rvert < \lvert\frac{\hbar}{\tau}\rvert$	$(II): T, \lvert\frac{\hbar}{\tau}\rvert < \lvert\mu\rvert$	$(III): \lvert\frac{\hbar}{\tau}\rvert < \lvert\mu\rvert < T$
δn	$\frac{\mu\lvert Im\Sigma\rvert \ln(\frac{D^2}{\lvert Im\Sigma\rvert^2})}{\pi^2\hbar^2 v_F^2} + \cdots$	$\frac{sgn(\mu)\lvert\mu\rvert^2}{2\pi\hbar^2 v_F^2} + \cdots$	$\frac{T\mu}{2\pi\hbar^2 v_F^2} + \cdots$
$\sigma_{xx}^{DC}/\sigma_0$	$2 + \frac{8}{9}(\frac{T\tau}{\hbar})^2 + \frac{8}{3}(\frac{\mu\tau}{\hbar})^2 + \cdots$	$\pi\lvert\frac{\mu\tau}{\hbar}\rvert + \cdots$	$\frac{\pi}{2}\frac{T\tau}{\hbar} + \frac{\pi}{4}\frac{\log\frac{2T\tau}{\hbar}}{\frac{T\tau}{\hbar}} + \cdots$
$\sigma_{xy}^{DC}/\sigma_0$	$\frac{32(w_c\tau)^2}{3}\frac{\mu\tau}{\hbar} + \cdots$	$\frac{sgn(\mu)\pi(w_c\tau)^2}{2} + \cdots$	$\frac{\pi(w_c\tau)^2}{2}\frac{\mu}{T} + \cdots$
$\tan\Theta_H$	$\frac{16(w_c\tau)^2}{3}\frac{\mu\tau}{\hbar} + \cdots$	$\frac{(w_c\tau)^2}{2}(\frac{\hbar}{\mu\tau}) + \cdots$	$(w_c\tau)^2(\frac{\hbar}{T\tau})\frac{\mu}{T} + \cdots$
R_H	$-\frac{8(w_c\tau)^2}{3\lvert B\rvert\sigma_0}\frac{\mu\tau}{\hbar} + \cdots$	$\frac{-sgn(\mu)}{\lvert B\rvert\sigma_0}\frac{(w_c\tau)^2}{2\pi}(\frac{\hbar}{\mu\tau})^2 + \cdots$	$\frac{-1}{\lvert B\rvert\sigma_0}\frac{2(w_c\tau)^2}{\pi}(\frac{\hbar}{T\tau})^2\frac{\mu}{T} + \cdots$

regime $\tau(\mu) \sim \mu$ which implies that the conductivity is proportional to carrier density. The Hall coefficient is inversely proportionally to $(\mu/|Im\Sigma|)^2$. The coefficient of proportionality depends only on physical constants and the scattering rate. Futhermore, the Hall coefficient in terms of the carrier density is $R_H = -1/ecn_\mu$ agrees with the other theoretical results[55]

For low carrier densities, the scattering rate is constant and the conductivity acquires a universal constant for low temperatures which is twice the quantum of conductance. The deviations are quadratic in temperature and carrier density. Rather striking is that the hall coefficient is no longer scattering rate independent and is proportional to the carrier density.

In the entropy dominated regime (III) where $\{|\frac{\hbar}{2\tau}| << \mu << T\}$, the electrical conductivity is linear in temperature. The scale for linearity is set by the scattering rate which in this regime is inverse of the chemical potential. In other words the conductivity has a T/μ dependence at high T. The hall coefficient again is independent of the scattering rate. In this limit of high temperatures, for chemical potential larger than the impurity band width, $R_H^{-1} = \delta n_\mu ec\,(T/\mu)^2$.

The hall coefficient is linear with chemical potential at low carrier densities crossing over to a μ^{-1} at large carrier densities. The crossover occurs at when the chemical potential

crosses the impurity band width. As such the R_H has a peak whose position is sample dependent but very weakly dependent on temperature. For ideal graphene, where the carrier density would be zero at the node, one would expect the hall coefficient to diverge and change from positive to negative as the chemical potential crosses zero energy. The fact that in all samples the divergence is cut off at some energy scale and the hall coefficient is zero at the node[34, 35, 6]. For a pure Dirac spectrum the crossover occurs when the chemical potential crosses temperature. For unitary scatters the crossover scale is independent of temperature for temperatures smaller than the impurity band width.

3.6 Thermoelectric transport coefficients

The thermoelectric conductivity tensor is [18]:

$$\beta_{i,j}(q,\Omega) = \frac{\Pi^{E,e}_{i,j}(q,\Omega+i\delta)}{\Omega} \tag{3.35}$$

where the $\Pi^{E,e}_{i,j}$ is the correlation function of charge and energy current densities. In the presence of an external magnetic field the canonical momentum operators are used to define the appropriate current vertices. Since two bands touch in graphene, both electrons and holes contribute. The two contributions add for off diagonal transport but have opposite signs for thermopower. In particular thermopower vanishes at the node and falls off as μ/T for large temperatures, unlike typical metals which would be a constant equal to the entropy per particle of a classical electron gas.

The calculation of the thermoelectric tensor is technically more complicated as the conventional Kubo formulas need to be generalized to include the effect of magnetization[57, 58, 59]. Fortunately the correction due to magnetization is cM/T[57, 55], which in the

limit of weak magnetic field is proportional to B^2 and is neglected to leading order in magnetic field.

The kernels appearing in the calculations for thermoelectric transport are related to those that determine electrical conductivity and can be expressed as: $\beta^K_{\alpha\beta} = ((\mu - \varepsilon)/e) * \sigma^K_{\alpha\beta}$[18]. For magnetic field perpendicular to the graphene sheet the kernels are (see appendix B)[4, 53, 55, 18]

$$\begin{aligned}
\beta^{DC}_{xx} &= \frac{N_v N_s e^2}{4\pi h} \int d\varepsilon \frac{\partial n_F}{\partial \mu} \beta^K_{xx}(\varepsilon) && (3.36)\\
\beta^{DC}_{xy} &= \frac{-N_v N_s e^3 |\overrightarrow{B}| v_F^2}{2c\pi} \int \frac{d\varepsilon}{\pi} \frac{\partial n_F(\varepsilon)}{\partial \mu} \beta^K_{xy}(\varepsilon) && (3.37)\\
\beta^K_{xx}(\varepsilon) &= (\frac{\mu - \varepsilon}{e})(1 + \frac{A^2 + B^2}{AB} \arctan \frac{A}{B}) && (3.38)\\
\beta^K_{xy}(\varepsilon) &= (\frac{\mu - \varepsilon}{e})\{\frac{1}{8AB}(\frac{B^2 - A^2}{B^2 + A^2} \\
&- \frac{B^2 + A^2}{2AB} \arctan \frac{2AB}{B^2 - A^2}) \\
&- \frac{AB}{3(A^2 + B^2)^2}\} && (3.39)
\end{aligned}$$

We proceed to analyze the properties in the various regimes as before. All expressions are quoted in terms $\beta_0 = \frac{k_B T \sigma_0}{e}$, $w_c^2 = 2e|\overrightarrow{B}|v_F^2/c\hbar$ and $S_0 = k_B/e$.

3.6.1 Thermoelectric transport and Scaling Behavior

A plot of the numerical evaluation of the thermoelectric power and Nernst signal are displayed in fig.3.7 and 3.8. The asymptotic dependences in the regimes identified in the previous section are shown in table 3.3

At high temperatures the thermopower is related to the entropy per unit charge. Since both electron and hole states are thermally populated the net charge is an imbalance

Table 3.3: Thermoelectric coefficients

Quantity	$(I): T, \|\mu\| < \left\|\frac{\hbar}{\tau}\right\|$	$(II): T, \left\|\frac{\hbar}{\tau}\right\| < \|\mu\|$	$(III): \left\|\frac{\hbar}{\tau}\right\| < \|\mu\| < T$
δn	$\frac{\mu\|Im\Sigma\|\ln(\frac{D^2}{\|Im\Sigma\|^2})}{\pi^2\hbar^2 v_F^2} + \cdots$	$\frac{sgn(\mu)\|\mu\|^2}{2\pi\hbar^2 v_F^2} + \cdots$	$\frac{T\mu}{2\pi\hbar^2 v_F^2} + \cdots$
β_{xx}^{DC}/β_0	$\frac{-16\pi^2}{9}(\frac{\tau T}{\hbar})^2\frac{\mu}{T} + \cdots$	$-sgn(\mu)\frac{\pi^3}{3}\frac{\tau T}{\hbar} + \cdots$	$-\frac{\pi}{2}(\frac{T\tau}{\hbar}) + \cdots$
β_{xy}^{DC}/β_0	$\frac{-32\pi^2(w_c\tau)^2}{9}\frac{\tau T}{\hbar} + \cdots$	$sgn(\mu)\frac{\pi^2}{12}(w_c\tau)^2(\frac{\hbar}{\mu\tau})^2\frac{T}{\mu} + \cdots$	$-\frac{\pi(w_c\tau)^2}{4} + \cdots$
$\tan\Theta_{H,TE}$	$2(w_c\tau)^2\frac{\hbar}{\mu\tau} + \cdots$	$-\frac{(w_c\tau)^2}{4}(\frac{\hbar}{\mu\tau})^3 + \cdots$	$-\frac{(w_c\tau)^2}{2}\frac{\hbar}{\tau\mu} + \cdots$
S_{xx}/S_0	$-\frac{8\pi^2}{9}(\frac{\tau T}{\hbar})^2\frac{\mu}{T} + \cdots$	$-\frac{\pi^2}{3}\frac{T}{\mu} + \cdots$	$-\frac{\mu}{T} + \cdots$
e_y/S_0	$-\frac{16\pi^2(w_c\tau)^2}{9}\frac{\tau T}{\hbar} + \cdots$	$\frac{\pi^2(w_c\tau)^2}{6}\frac{\hbar}{\mu\tau}\frac{T}{\mu} + \cdots$	$-\frac{(w_c\tau)^2}{2}\frac{\hbar}{\tau T} + \cdots$

between the two. At the Dirac point, the system is particle hole symmetric and the thermopower goes to zero[34, 35, 36, 37]. At small carrier densities the difference between positive and negative charge occupations is linear in the chemical potential and the thermopower is $\propto \mu/T$. This dependence on chemical potential is very similar to the high temperature classical limit. The thermopower is linear in μ and the coefficient of μ/T is a measure of the relaxation time[53, 60, 56].

Consider the dependence of the thermopower on chemical potential for temperatures smaller than the impurity band width. For small chemical potentials the thermopower grows linearly and reaches a maximum approximately at a chemical potential of order of the impurity band width. For larger values it decreases as T/μ in agreement with the other theoretical results[53, 60, 56]. As temperature is increased and becomes larger than the impurity bandwidth, the thermopower qualitatively shows the same dependence but the peak now is at a chemical potential of order the temperature. In other words as one increases the temperature the position of the peak in thermopower as a function of chemical potential will remain roughly constant until the temperature becomes larger than the impurity bandwidth. For larger temperatures, the peak will move to larger values of chemical potential.

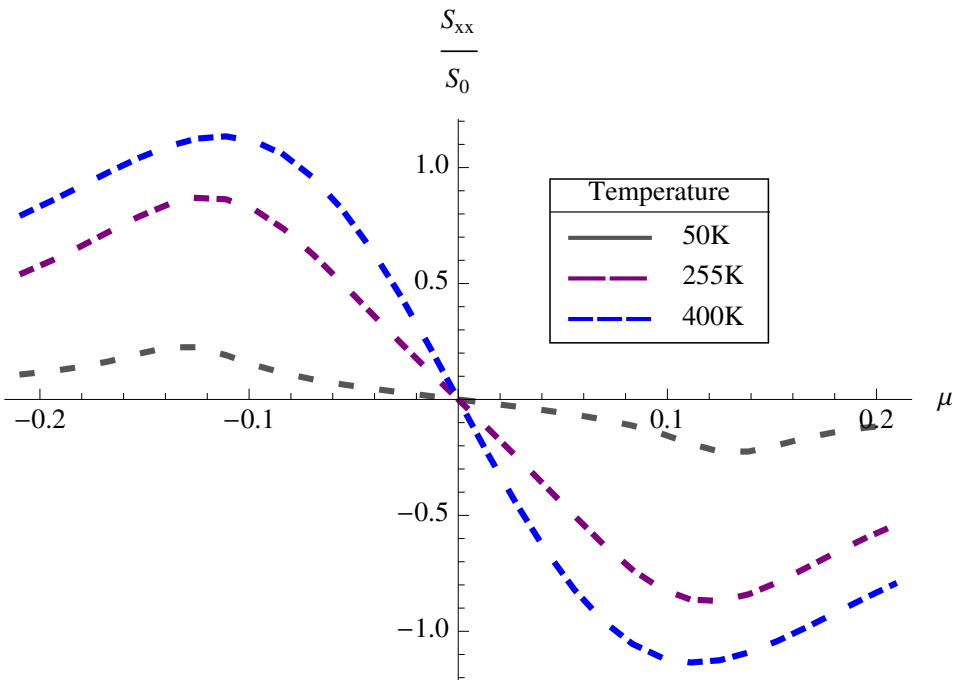

Figure 3.7: S_{xx} as a function of chemical potential. The impurity concentration is $n_i = 0.012$, while the temperature for each curve is given in the legend.

For chemical potentials larger than the impurity bandwidth the Nernst signal is proportional to the thermopower. In this regime the scattering rate is inversely proportional to the chemical potential. Thus for unitary scatterers the ratio of the thermopower to the Nernst signal is a constant proportional to the applied magnetic field. As the chemical potential is lowered and crosses the impurity band width the two start to deviate. Within this scenario, for a fixed magnetic field, the ratio goes to zero as μ/τ. The slope of the ratio as a function of chemical potential is a direct measure of the scattering rate. Within Born approximation the scattering rate is proportional to the density of state which for graphene is linear in energy. Thus one would expect a divergent Nernst coefficient at the node. This divergence is cutoff and the value of Nernst is proportional to τ^3.

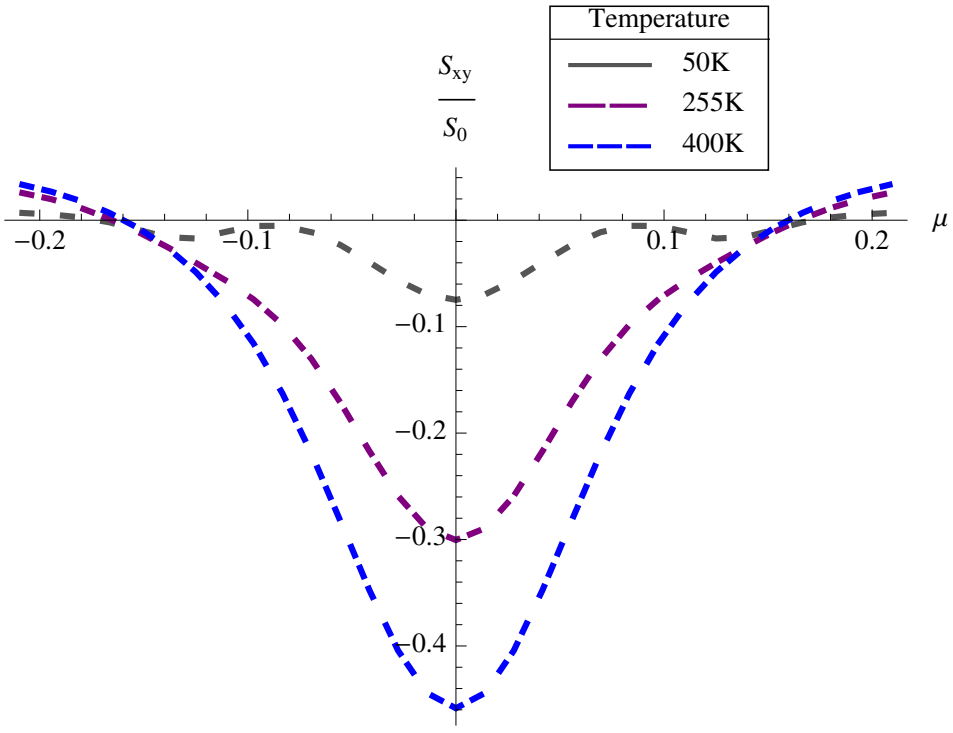

Figure 3.8: S_{xy} as a function of chemical potential. The impurity concentration is $n_i = 0.012$, while the temperature for each curve is given in the legend.

In the clean limit, $\tau \to \infty$, the Nernst diverges as the carrier density goes to zero[56]. The presence of unitary scatters makes it finite and is proportional to τ^3 at the node. The Nernst signal is still orders of magnitude larger than typical metals but the observed values of order $30\mu V/KT$ implies a scattering rate of order $0.1eV$ for unitary impurities. The larger the mean free path, larger is the Nernst signal and therefore one expects a large Nernst signal for large electrical conductivity at the node. As we will see later this is a key puzzle in graphene.

3.7 Thermal transport

Having discussed the electrical and thermoelectric transport we now consider thermal transport. With the boundary condition where the electrical conductivity is zero, the three are related.

$$K = (\frac{1}{T})(\kappa^{(3)} - \beta^{(2)}\frac{\beta^{(1)}}{\sigma^{(0)}}) \tag{3.40}$$

where κ is the energy conductivity tensor which is related energy current-current correlation function.

$$\kappa_{i,j}(q,\Omega) \quad = \quad \frac{\Pi^{E,E}_{i,j}(q,\Omega + i\delta)}{\Omega} \tag{3.41}$$

As in the case of thermoelectric conductivities, the effect of magnetization is of order B^2 and is dropped in our analysis. For a magnetic field perpendicular to the graphene sheet, the longitudinal and transverse components of thermal conductivity tensor are

(see appendix C for details)[4, 53, 55, 18]

$$\kappa_{xx}^{DC} = \frac{Ne^2}{4\pi h}\int d\varepsilon \frac{\partial n_F}{\partial \mu}\kappa_{xx}^{K}(\varepsilon) \tag{3.42}$$

$$\kappa_{xy}^{DC} = \frac{-Ne^3|\overrightarrow{B}|v_F^2}{2c\pi}\int \frac{d\varepsilon}{\pi}\frac{\partial n_F(\varepsilon)}{\partial \mu}\kappa_{xy}^{K}(\varepsilon) \tag{3.43}$$

$$\kappa_{xx}^{K}(\varepsilon) = (\frac{\mu-\varepsilon}{e})^2(1+\frac{A^2+B^2}{AB}\arctan\frac{A}{B}) \tag{3.44}$$

$$\begin{aligned}\kappa_{xy}^{K}(\varepsilon) &= (\frac{\mu-\varepsilon}{e})^2\{\frac{1}{8AB}(\frac{B^2-A^2}{B^2+A^2} \\ &- \frac{B^2+A^2}{2AB}\arctan\frac{2AB}{B^2-A^2}) \\ &- \frac{AB}{3(A^2+B^2)^2}\}\end{aligned} \tag{3.45}$$

The thermal conductivity can be expressed in terms of the thermopower and Nernst as

$$K_{xx}^{DC} = \frac{\kappa_{xx}^{DC}}{T} + \beta_{xy}^{DC}e_y - \beta_{xx}^{DC}S_{xx} \tag{3.46}$$

$$K_{xy}^{DC} = \frac{\kappa_{xy}^{DC}}{T} - \beta_{xx}^{DC}e_y - \beta_{xy}^{DC}S_{xx} \tag{3.47}$$

where K_{xx} is the longitudinal thermal Conductivity and K_{xy} is the transverse thermal Conductivity. Given the large Nernst signal and anomalous temperature and carrier density dependence of thermopower, thermoelectric contribution to thermal conductivity is significant in graphene. Analogous to the hall coefficient we define the thermal hall coefficient,

$$R_{T.H} = \frac{-K_{xy}}{B(K_{xx}^2+K_{xy}^2)} \tag{3.48}$$

The average energy and the specific heat dependence on chemical potential, temperature and scattering rate are given in section 3.2.1. We now analyze thermal transport and all results are quoted in terms of : $k_0 = \frac{\pi^2}{3}S_0\frac{k_BT\sigma_0}{e} = \frac{\pi^2}{3}S_0b_0$ and $S_0 = \frac{k_B}{e}$.

Table 3.4: Thermal transport

Quantity	$(I): T, \lvert\mu\rvert << \lvert\frac{\hbar}{2\tau}\rvert$	$(II): T, \lvert\frac{\hbar}{2\tau}\rvert << \lvert\mu\rvert$	$(III): \lvert\frac{\hbar}{2\tau}\rvert << \lvert\mu\rvert << T$	$(IV): \lvert\mu\rvert << \lvert\frac{\hbar}{2\tau}\rvert << T$
δn	$\frac{\mu\lvert Im\Sigma\rvert \ln(\frac{D^2}{\lvert Im\Sigma\rvert^2})}{\pi^2\hbar^2 v_F^2} + \cdots$	$\frac{sgn(\mu)\lvert\mu\rvert^2}{2\pi\hbar^2 v_F^2} + \cdots$	$\frac{T\mu}{2\pi\hbar^2 v_F^2} + \cdots$	$\frac{\mu\lvert Im\Sigma\rvert \ln(\frac{D^2}{\lvert Im\Sigma\rvert^2})}{\pi^2\hbar^2 v_F^2} + \cdots$
$\frac{c_v}{k_B}$	$\frac{\pi^2}{3}(\frac{k_B T\lvert Im\Sigma\rvert \ln(\frac{D^2}{\lvert Im\Sigma\rvert^2})}{\pi^2\hbar^2 v_F^2}) + \cdots$	$\frac{4\pi^2}{3}(\frac{k_B T\lvert\mu\rvert}{2\pi\hbar^2 v_F^2}) + \cdots$	$\frac{1}{2}(\frac{(k_B T)^2}{2\pi\hbar^2 v_F^2}) + \cdots$	$\frac{1}{3}(\frac{k_B T\lvert Im\Sigma\rvert \ln(\frac{D^2}{\lvert Im\Sigma\rvert^2})}{\pi^2\hbar^2 v_F^2}) + \cdots$
$\kappa_{xx}^{DC}/\kappa_0$	$2 + \frac{8}{9}(\frac{T\tau}{\hbar})^2 + \frac{8}{3}(\frac{\tau\mu}{\hbar})^2 + \cdots$	$\pi\frac{\tau\lvert\mu\rvert}{\hbar} + \cdots$	$\frac{3}{4\pi}(\frac{\tau T}{\hbar}) + \cdots$	$\frac{2}{\pi^2} + \frac{8}{\pi^2}(\frac{\tau\mu}{\hbar})^2 + \cdots$
$\kappa_{xy}^{DC}/\kappa_0$	$\frac{32(w_c\tau)^2}{3}\frac{\tau\mu}{\hbar} + \cdots$	$\frac{\pi}{2}(w_c\tau)^2 sgn(\mu) + \cdots$	$-\frac{\mu}{T}\frac{3}{2\pi}(w_c\tau)^2 + \cdots$	$\frac{32(w_c\tau)^2}{3\pi^2}\frac{\tau\mu}{\hbar} + \cdots$
$\tan\Theta_{H,T}$	$\frac{16(w_c\tau)^2}{3}\frac{\tau\mu}{\hbar} + \cdots$	$\frac{(w_c\tau)^2}{2}\frac{\hbar}{\tau\mu} + \cdots$	$-2(w_c\tau)^2\frac{\hbar}{\tau T}\frac{\mu}{T} + \cdots$	$\frac{16(w_c\tau)^2}{3}\frac{\tau\mu}{\hbar} + \cdots$
$R_{H,T}$	$-\frac{8}{3}\frac{(w_c\tau)^2}{\lvert B\rvert k_0}\frac{\tau\mu}{\hbar} + \cdots$	$-\frac{1}{2\pi}\frac{(w_c\tau)^2}{\lvert B\rvert k_0}(\frac{\hbar}{\tau\mu})^2 sgn(\mu) + \cdots$	$-\frac{8\pi(w_c\tau)^2}{3\lvert B\rvert k_0}(\frac{\hbar}{\tau T})^2\frac{\mu}{T} + \cdots$	$-\frac{8\pi^2(w_c\tau)^2}{3\lvert B\rvert k_0}\frac{\tau\mu}{\hbar} + \cdots$

3.7.1 Thermal Transport Quantities and Scaling Behavior

The asymptotic behavior of diagonal and off diagonal heat transport are given in table 3.4. Numerical results for thermal transport are displayed in fig.3.9 and fig. 3.10. The thermal conductivity depends on the correlations of the energy current as well as thermopower and Nernst. The anomalous behavior of the thermoelectric coefficients in graphene have dramatic effect on heat transport. In particular Wiedemann-Franz law is not universally obeyed. At low temperature thermal conductivity is qualitatively similar to electrical conductivity and the corrections are of order $(T\tau)^2$. At the node and for very large carrier densities Wiedemann-Franz law is obeyed. In the intermediate regime the deviation grows as the temperature approaches the impurity bandwidth. In particular a peak develops at the node as the temperature is increased and becomes of order the impurity bandwidth.

In fig.3.10 the thermal hall coefficient is plotted units of $R_{0,T,H} = 1/Bk_0$. In regimes I, II and III it is proportional to the hall coefficient with the constant of proportionality being $\sigma_0/\kappa_0 = \pi^2 k_B^2 T/3e^2$.

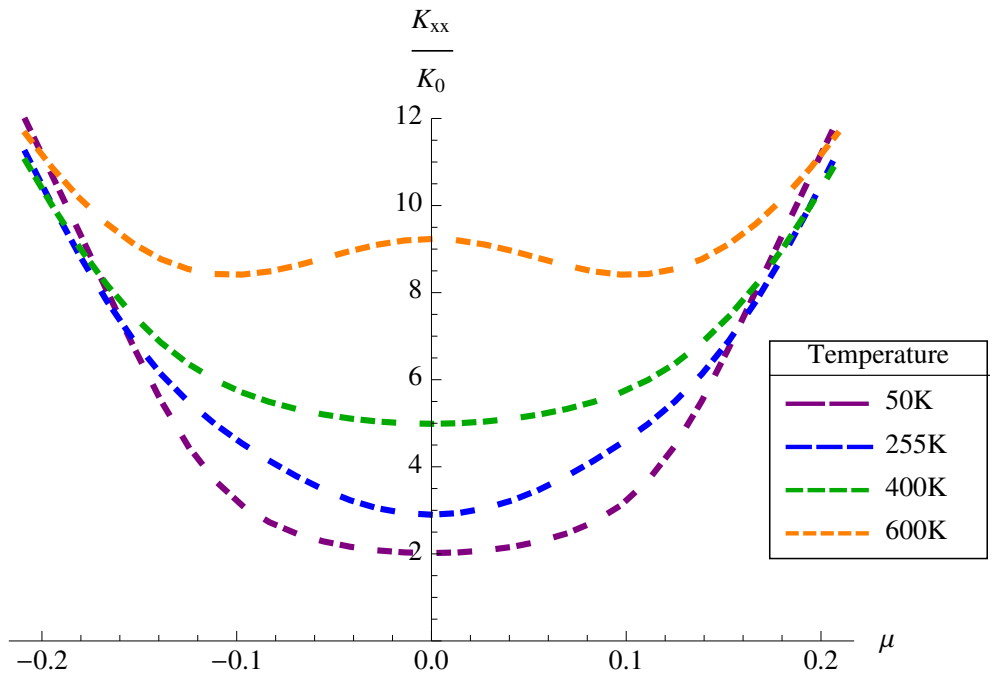

Figure 3.9: K_{xx} as a function of chemical potential. The impurity concentration is $n_i = 0.012$, while the temperature for each curve is given in the legend.

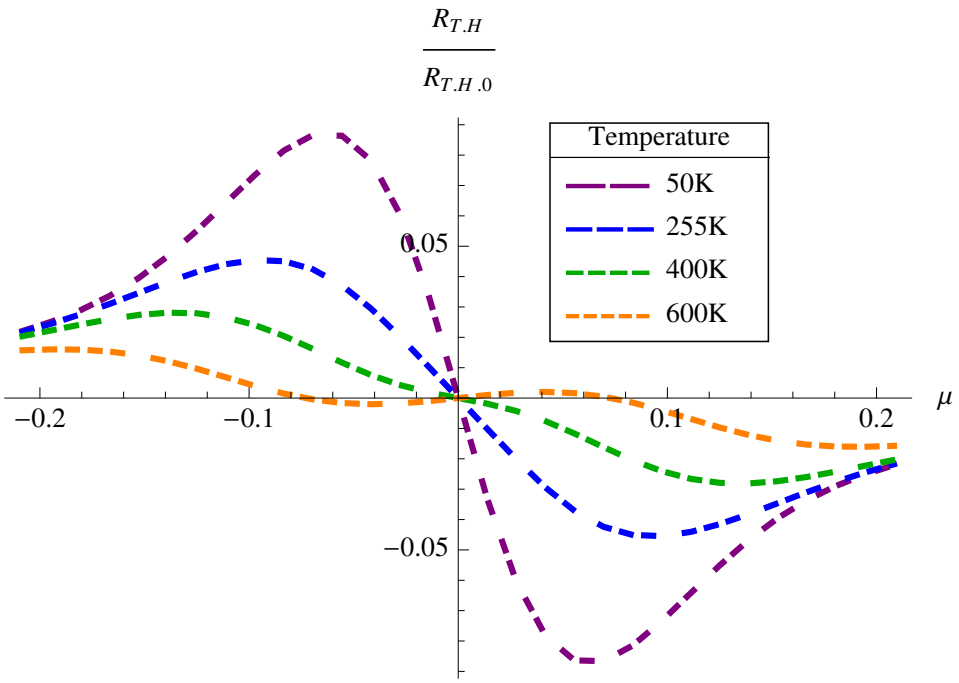

Figure 3.10: $R_{T.H.}$ as a function of chemical potential. The impurity concentration is $n_i = 0.012$, while the temperature for each curve is given in the legend.

3.8 Comparison of Experiments Data and Numerical Results

3.8.1 Unitary Scatterers

We compare the transport dominated by unitary scatterers with experimental data on graphene[34] . Since much of the data is obtained as a function of gate voltage and temperature, we need to determine the dependence of chemical potential on gate voltage. Experimental control over carrier concentration is achieved capacitively in a parallel plate geometry. For the experimental range of parameters used, we can assume that the capacitance of the device is constant which implies that the gate voltage is linearly proportional to the number of charge carriers: $Q = CV_g$.

The only fitting parameter is the impurity concentration. Other relevant parameters are: (1) band width ($D = 1.8eV$), (2) Lattice constant ($a = 1.42\mathring{A}$) and fermi velocity ($v_F = 0.8 \times 10^6$m/s). All the data is taken at 255K. The best fit for thermopower and Nernst were obtained for an impurity concentration of = 0.012. The impurity band width is $\sim \sqrt{n}D$[53]. An impurity density smaller by a factor of three is needed to fit longitudinal conductivity. Further measurements are needed to verify this discrepancy as the measurements are made using a two probe geometry.

Given this impurity concentration we can estimate the impurity band width to be of order $0.1eV(1000K)$. Since most measurements are done at low temperatures, we are always in a regime where $T << |Im\Sigma|$. In this regime the scattering rate is very weakly dependent on gate voltage upto chemical potentials of order $0.1eV$.

3.8.1.1 Electrical Conductivity

The longitudinal conductivity has a plateau around zero gate voltage crossing over to the a linear dependence at higher gate voltages. This is consistent with a small impurity bandwidth beyond which the scattering rate is inversely proportional to energy. Since both the slopes and the crossover scale is determined by the same parameter, the lack agreement is a clear evidence for the departure from the unitary scattering dominated scattering theory.

The observed data is asymmetric which is specific to the device studied here. The behavior at high carrier densities is consistent with a small impurity concentration of about 0.002 but the value at the node requires an impurity concentration that is an order of magnitude smaller. As mentioned the data are obtained from a two probe measurement which renders this an inconclusive test. Note our goal is to compare data of all measured transport coefficients within a single formulation. This imposes a severe constraint in that the same sample has to be connected with both thermal and electrical probes in a hall bar geometry. For comparison we also plot the expected conductivity for an impurity concentration of 0.012 and 0.015. These large impurity concentrations are in better agreement with the Nernst signal.

3.8.1.2 Hall resistance

The fit to the observed hall coefficient is shown in fig.3.12. The hall varies linearly with gate voltage for small carrier densities and fall off as $1/\mu^2$ beyond a scale set by the impurity bandwidth. Given our analytic form for small carrier densities we notice that the slope is a measure of the scattering rate which is roughly constant up to the impurity bandwidth. In this regime the scattering rate is 0.2 eV. Both the position of the peak and

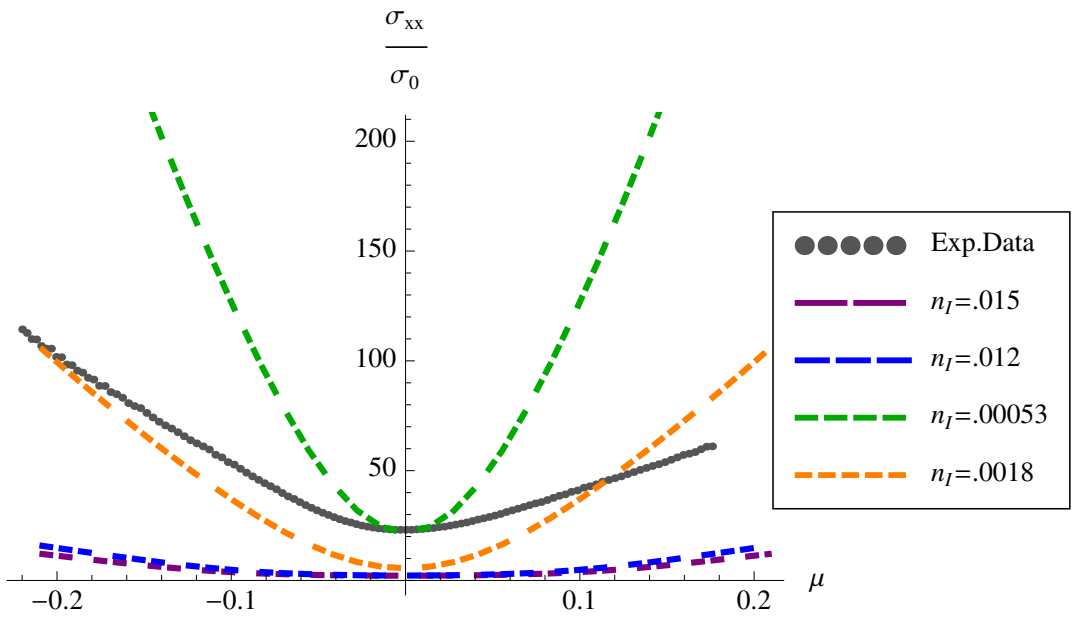

Figure 3.11: Comparison of calculation and experimental data of longitudinal conductivity. The observed conductivity is much larger than those predicted for an impurity concentration of 0.012 and 0.015. An impurity concentration closer to 0.002 is consistent with the data.

the slope near the node are reproduced with the same impurity concentration 0.015. We also plot the hall resistance for a impurity concentration of 0.015. While the agreement in slope near the node is worse for the larger impurity concentration, the overall fit is not significantly worse suggesting that the hall resistance is rather insensitive to impurity concentration in this regime.

3.8.1.3 Thermopower

The measured thermopower in graphene is a linear function of gate voltage for small carrier densities (see fig.3.13). The slope is proportional to τ^2. By fitting our numerical solution to the data we find that the impurity concentration of 0.015 can account for the slope and the position of the peak in thermopower. We also plot the dependence of thermopower for an impurity concentration of 0.012. The fit to data is for the larger

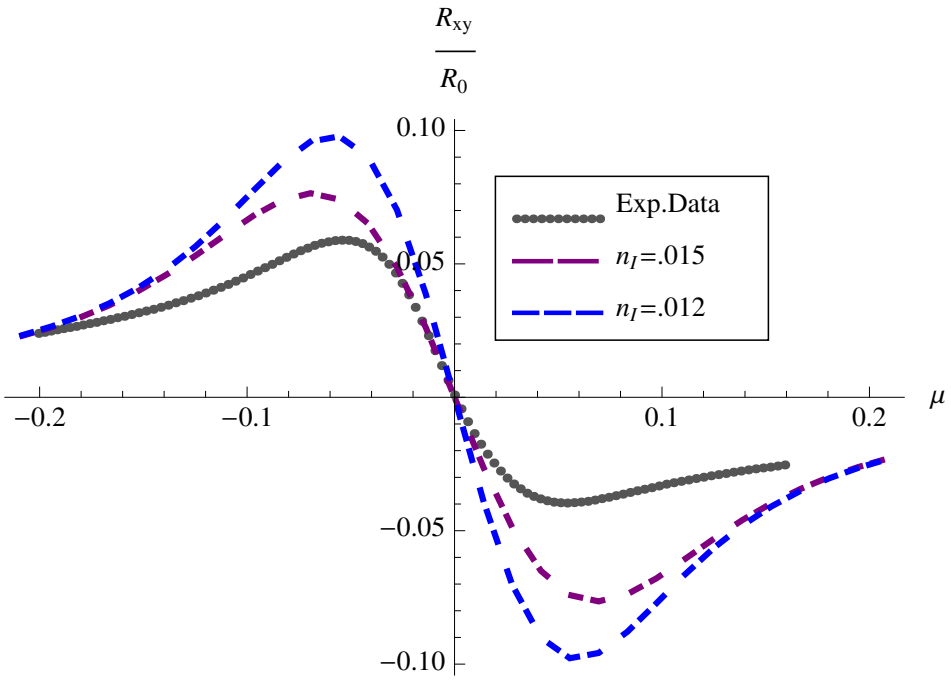

Figure 3.12: The calculated Hall coefficient and experimental data is plotted in units of $R_0 = \frac{\pi h}{|B|e^2}$ as a function of chemical potential. The data is best fit for an impurity concentration of 0.015. The overall features are not too sensitive to the impurity concentration as can be seen by the predicted behavior for n=0.012.

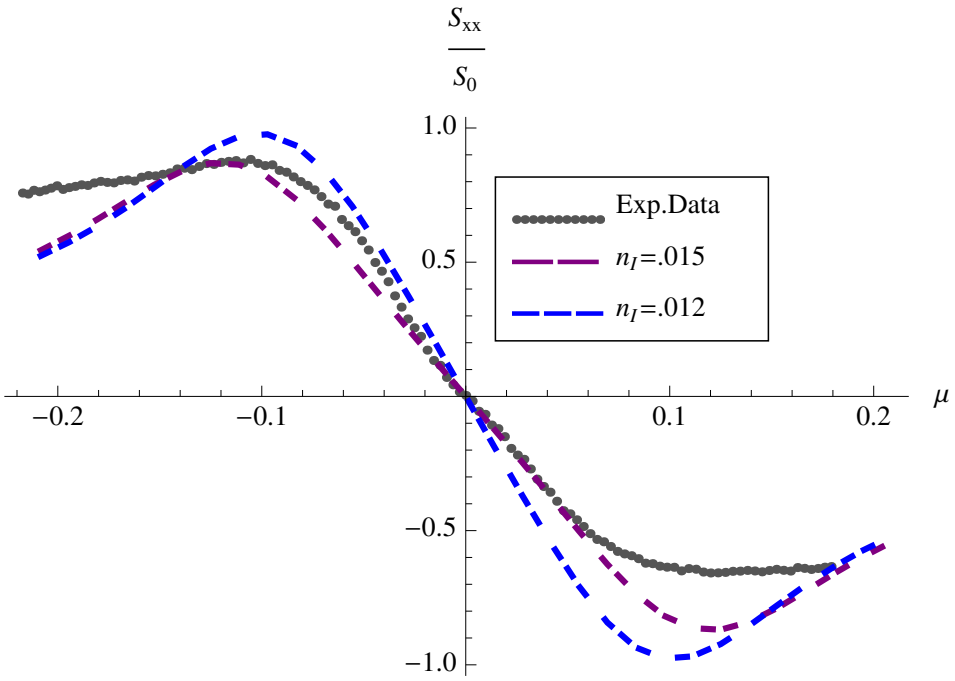

Figure 3.13: The calculated S_{xx} and experimental data as a function of chemical potential. The data can be fit by impurity concentrations of order 0.012-0.015

impurity concentration is not that sensitive to the impurity concentration for this range of parameters.

3.8.1.4 Nernst Signal

The Nernst signal in graphene is shown in fig.3.14. It is negative at zero gate voltage changing sign for large carrier densities. The peak value is large and about $50\mu V/KT$. Theoretically it is proportional to τ^3 and is predicted to change sign as a function of chemical potential and gate voltage. The best fit to the data is obtained for an impurity concentration of 0.015. For a smaller impurity concentration of 0.012 the theoretical value is smaller by a factor of 2 as compared to the data at the node.

The above analysis suggests that a large impurity concentration is needed to account for the observed Nernst signal. Given a band width of 0.22 eV we can account for the

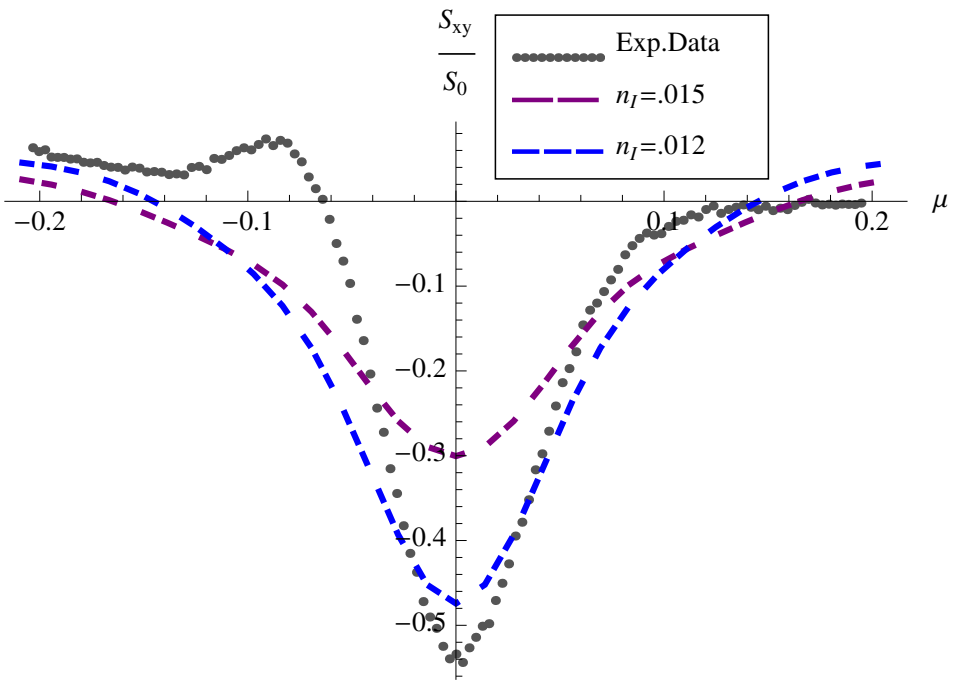

Figure 3.14: Experimental data as a function of chemical potential and calculated S_{xy}. The value at the node is extremely sensitive to the impurity concentration and a best fit obtained for n=0.012.

thermopower, hall resistance and Nernst signals. Such a large impurity bandwidth is inconsistent with electrical conductivity data. In particular the conductivity will be constant up to a gate voltage of $\sim$ 20V and will cross over to a linear in gate voltage dependence for larger values.

3.8.2 Coulomb Scatterers

It is clear from the analysis in the previous section that unitary scatterers fail to accurately reproduce conductivity data. Coulomb scatterers have been shown to reproduce conductivity data at large carrier densities. The fits to the data with Coulomb scatterers is presented in this section. One caveat to note in these fits is that the experimental data for Hall and Nernst are outside the regime of validity of our theoretical calculations. In particular the scattering length is much longer than

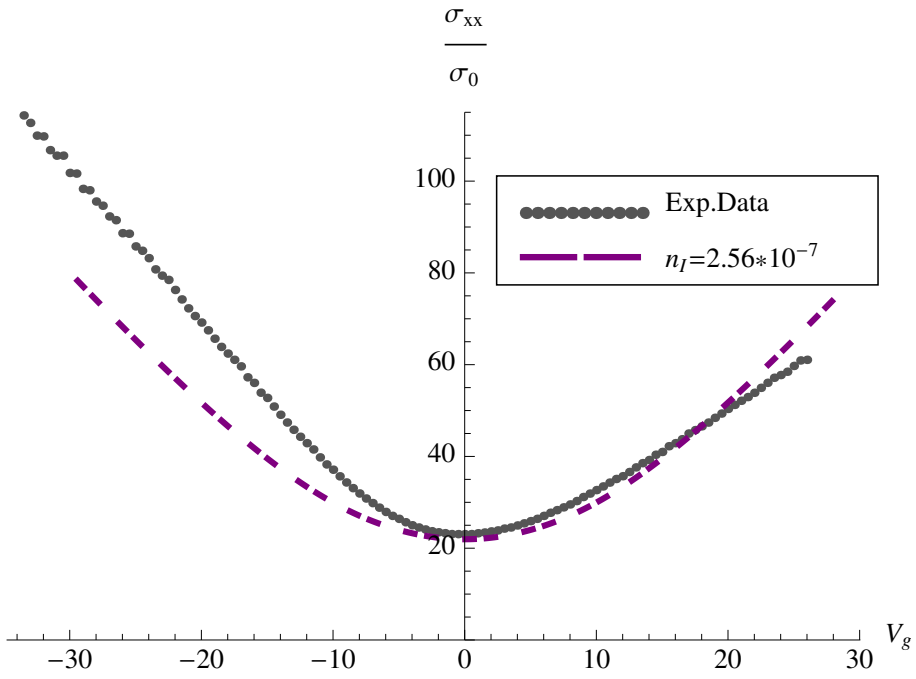

Figure 3.15: The conductivity data and calculations for a charge impurity concentration of $n_c = 2.56 \times 10^{-7}$. Coulomb scatterers provide excellent quantitative and qualitative agreement in the entire range of carrier densities measured.

the cyclotron frequency. For Coulomb scattering one needs to include the physics of Landau levels while our results are valid in the regime of weak magnetic fields where a hydrodynamic theory is justified.

3.8.2.1 Electrical Conductivity

The conductivity data can be reproduced over the entire range from low to high carrier concentration (see fig.3.15). The impurity concentration required is $n_c = 2.7 \times 10^{-7}$. The finite conductivity at the node is a result of the self consistent treatment of the impurity potential. Even for weak potentials, the induced impurity states provide finite conductivity and screening at the node. The agreement with data suggests that Coulomb and not unitary scatterers are the predominant source of scattering in these systems.

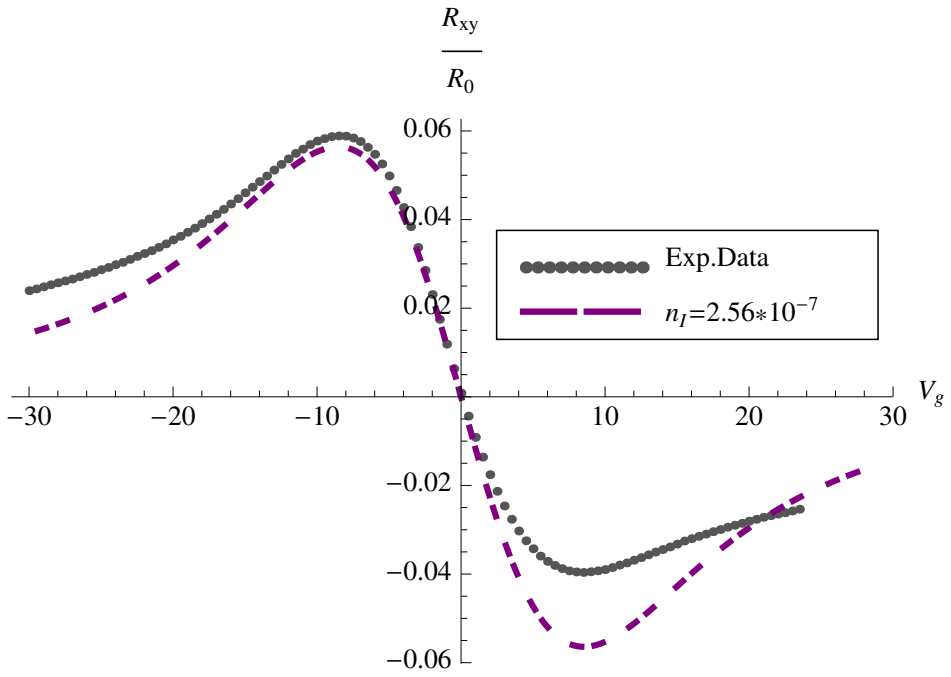

Figure 3.16: Hall resistivity data fit to calculations for a charge impurity concentration of $n_c = 2.56 \times 10^{-7}$.

3.8.2.2 Hall Resistance

For the same impurity concentration we find excellent agreement with Hall resistance data (see fig.3.16). The fit obtained is better than that for unitary scatters suggesting that the longitudinal and transverse charge transport is determined by the long range Coulomb impurities that live in the substrate.

3.8.2.3 Thermopower

Thermopower data reveal significant deviations from predictions from Coulomb scattering dominated transport (see fig.3.17). The peak and the slope are overestimated by a factor of ~ 2. Since thermopower is sensitive to higher derivatives of the scattering rate with respect to energy as compared to electrical conductivity, this disagreement reflects the difference in the dependence of the imaginary part of the self energy of unitary and

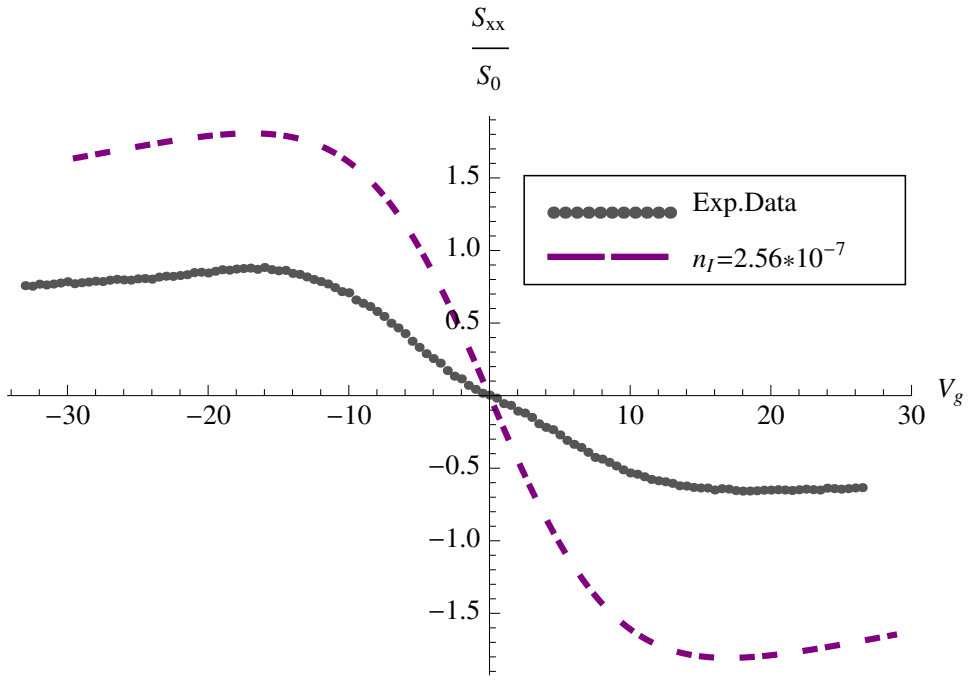

Figure 3.17: Thermpower data fit to calculations for a charge impurity concentration of $n_c = 2.56 \times 10^{-7}$.

charge scattering potentials (see fig.3.1 and fin.3.3). In particular the self energy in the former varies by a factor of ~ 2 from 0 to 0.2 eV while the latter changes by a factor of ~ 8 from 0 to 0.1 eV. The weaker dependence of unitary scatterers provides a much better fit to the data.

3.8.2.4 Nernst Signal

The observed peak in the Nernst signal at the node is an order of magnitude smaller than that expected from charge scatterers (see fig.3.18). This result is consistent with the observation that charge scatterers are not sufficient to accurately reproduce thermopower data, since both depend on the variation of the scattering rate as a function of energy. A simplifying assumption made in these calculations is that the self energy is independent of momentum. Including the momentum dependence similar agreement with

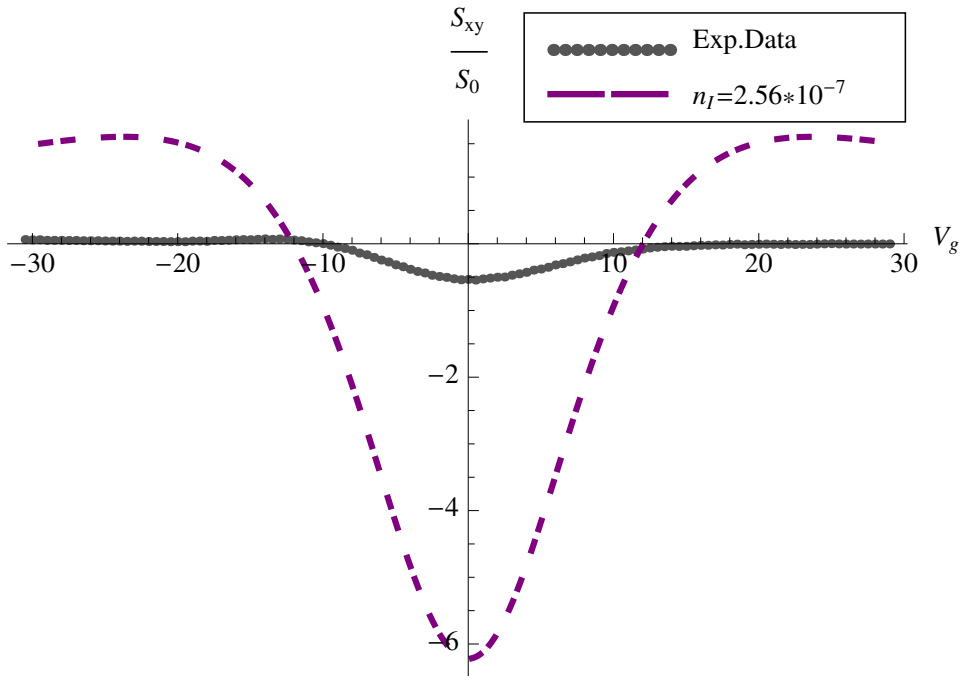

Figure 3.18: Nernst signal data fit to calculations for a charge impurity concentration of $n_c = 2.56 \times 10^{-7}$.

conductivity [46] and Hall coefficient [61] has been obtained for finite range scatterers. The inclusion of momentum dependence also yields better agreement with thermopower data [62] while the discrepancy with Nernst data cannot be resolved with this generalization [63].

3.9 Conclusion

We have derived the dependence of transport coefficients of graphene on temperature, chemical potential and impurity band width (impurity concentration) in the presence of unitary scatterers. Analytic forms are presented in regimes of parameter space where one of the three is the dominant energy scale. The numerical solution is fit to available data on conductivity, hall resistance, thermopower and Nernst signal measured on a single device. Our analysis suggests that unitary scatterers alone cannot account for

all the observed data. For a given impurity concentration, hall resistance, thermopower and Nernst are in agreement with the dependences expected form unitary scatterers. However the impurity concentration is too large to fit conductivity data. Since the predicted conductivity in this regime is much smaller, the influence of contact resistance in the two probe measurement cannot account for this discrepancy. On the other hand, if we choose the impurity concentration that best captures the dependence of conductivity, the predicted Nernst signal at the node is too small.

Long range Coulomb scatterers results in conductivity and hall resistivity that agrees qualitatively and quantitatively with the features observed in experimental data. Thermopower data is better fit with long range scatterers provided on takes into account the dependence of self energy on momentum, which we have ignored in our calculations. The only major discrepancy between the predictions of Coulomb impurities and observations is in the Nernst data. One possible source of this discrepancy is that, for the magnetic field applied, the scattering rate is smaller that the Landau level splitting. This regime is outside the regime of validity of our calculations.

Chapter 4

Conclusions

In this thesis, we have generalized the method used and developed by Khodas-Finkelstein to calculated the electrical, thermoelectric and thermal transverse conductivities. The importance of generalizing the Khodas-Finkelstein Formalism is that it gives a general method for canceling singular terms in each current-current correlation function by differentiation the phase factors in eqn.2.12 in the each current density operator. These phase factors can be rearranged in the charge-charge, energy-charge and energy-energy current correlation tensor in two ways: the formation of gauge invariant closed current loops cancels the singular terms in the correlation function, while terms that do not yield closed loops are used to extend the diamagnetic part of the current operator used in each correlation tensor. The main theoretical results were given at the end of chapter 2 (sections 2.5.1,2.5.2,2.5.3). Furthermore, it was shown that this method yielded the same results obtain by Mahan, i.e., I derived that in the dc limit the relation $L^n(\mu,T) = \int d\varepsilon(\frac{\varepsilon-\mu}{-e})^n \sigma_K^{dc}(\varepsilon,\mu,T)$ is still valid when relating each type of conductivity: here $\sigma_K^{dc}(\varepsilon,\mu)$ is the kernel of the electrical conductivity tensor , $L^{n=1}(\mu,T)$ refers to the kernel of the thermoelectric conductivity tensor and $L^{n=2}(\mu,T)$ refers to the kernel of

the heat conductivity tensor.

In chapter 3 we use this method to calculate the following transport quantities of graphene: Electrical, Thermoelectric, and Thermal conductivity. Also I derived the dependence of transport coefficients of graphene on temperature, chemical potential and impurity band width (impurity concentration) in the presence of both unitary and screened Coulomb scatterers. The Analytic forms of the transport coefficients are given in tables for regimes of parameter space where one of the three is the dominant energy scale. In calculating these transport quantities the full Green's function was approximated by the impurity averaged Green's function and we assumed a weakly applied magnetic field. The validity of these assumptions are as follows:

$$(I) \quad \frac{N_i}{V} << 1 \quad , \qquad w_c\tau << 1 \tag{4.1}$$

here N_i is the number of impurities, V is the volume, ω_c is the cyclotron frequency, and τ is the mean free time. The dilute limit of impurities ($\frac{N_i}{V} << 1$) restricts the sample size to be much larger than the coherence length of electrons. The restriction placed on the magnetic field ($w_c\tau << 1$) guarantees momentum is still a good quantum number. However, In fitting our numerical solution to available data on conductivity, hall resistance, thermopower and Nernst signal measured on a single device, these restriction are pushed to the limit when comparing data to numerical results of long range Coulomb scatterers.

In our analysis the following two results occurred: (1) the numerical solution can describe experimental data qualitatively, however, (2) unitary scatterers alone cannot account for all the observed data while long range Coulomb scatterers yields a better fit. For a given impurity concentration, unitary scatterers can fit hall resistance,

thermopower and Nernst. However, using the same impurity concentration for unitary scatterers, the impurity concentration is to large to fit conductivity data. On the other hand, if we choose the impurity concentration that best captures the dependence of conductivity, the predicted Nernst signal at the node is too small.

For long range Coulomb scatterers our numerical solutions for conductivity and hall resistivity agree qualitatively and quantitatively with the features observed in experimental data. Long range Coulomb scatterers provide a better fit for thermopower then unitary scatterers, however, when the dependence of self energy on momentum is included a qualitatively and quantitatively agreement with the features observed in experimental data occurs. On the other hand, the predictions of Coulomb impurities for Nernst data only a qualitatively agreement occurs for general features. The restriction placed on the magnetic field limits the validity of our calculations for Coulomb scatterers and Landau level splitting is necessary for a proper analysis. Parts of this work has been submitted to Physical Review B and are currently in the review process.

Bibliography

[1] L. Pauling, Journal of the American Chemical Society **53**, 1367 (1931).

[2] P. R. Wallace, Phys. Rev. **71**, 622 (1947).

[3] A. H. Castro Neto, F. Guinea, N. M. R. Peres, K. S. Novoselov, and A. K. Geim, Reviews of Modern Physics **81** (2009).

[4] N. M. R. Peres, F. Guinea, and A. H. Castro Neto, Phys. Rev. B **73**, 125411 (2006).

[5] A. K. Geim and K. S. Novoselov, Nat Mater **6**, 183 (2007).

[6] K. S. Novoselov, Nature **438**, 197 (2005).

[7] Y.-W. Tan *et al.*, Phys. Rev. Lett. **99**, 246803 (2007).

[8] M. Katsnelson, Materials Today **10**, 20 (2007).

[9] J. Martin *et al.*, Nat Phys **4**, 144 (2008).

[10] T. Ihn *et al.*, Materials Today **13**, 44 (2010).

[11] A. Deshpande, W. Bao, F. Miao, C. N. Lau, and B. J. LeRoy, Physical Review B **79** (2009).

[12] S. Adam, E. H. Hwang, V. M. Galitski, and S. Das Sarma, Proceedings of the National Academy of Science **104**, 18392 (2007), 0705.1540.

[13] E. H. Hwang and S. Das Sarma, Physical Review B **77** (2008).

[14] K. Nomura, M. Koshino, and S. Ryu, Physical Review Letters **99** (2007).

[15] J. Bang and K. J. Chang, Physical Review B **81** (2010).

[16] M. Khodas and A. M. Finkel'stein, Phys. Rev. B **68**, 155114 (2003).

[17] P. S. Pershan and W. B. Lacina, Physical Review **168** (1968).

[18] G. D. Mahan, (Plenum Press, New York :, 1981).

[19] F. J. Dyson, Physical Review **75** (1949).

[20] P. C. Martin and J. Schwinger, Physical Review **115** (1959).

[21] J. Schwinger, Physical Review **75** (1949).

[22] V. Edelstein, JETP Letters **67**, 159 (1998).

[23] B. Laikhtman and E. L. Altshuler, Annals of Physics **232**, 332 (1994).

[24] B. L. Altshuler, D. Khmel'nitzkii, A. I. Larkin, and P. A. Lee, Physical Review B **22** (1980).

[25] J. M. Luttinger, Physical Review **121** (1961).

[26] J. Schwinger, Physical Review **82** (1951).

[27] R. Kubo, Journal of the Physical Society of Japan **12**, 570 (1957).

[28] I. Paul and G. Kotliar, Phys. Rev. B **67**, 115131 (2003).

[29] G. Katsnelson, N. K.S., and A. Geim, Nat Phys **2**, 620 (2006).

[30] A. F. Young and P. Kim, Nat Phys **5**, 222 (2009).

[31] N. Stander, B. Huard, and D. Goldhaber-Gordon, Phys. Rev. Lett. **102**, 026807 (2009).

[32] K. S. Novoselov, Science , 1137201 (2007).

[33] X. Du, I. Skachko, F. Duerr, A. Luican, and E. Y. Andrei, Nature **462**, 192 (2009).

[34] P. Wei, W. Bao, Y. Pu, C. Lau, and J. Shi, Phys. Rev. Lett. **102**, 166808 (2009).

[35] Y. M. Zuev, W. Chang, and P. Kim, Phys. Rev. Lett. **102**, 096807 (2009).

[36] J. G. Checkelsky and N. P. Ong, Phys. Rev. B **80**, 081413 (2009).

[37] A. Balandin *et al.*, Nano Lett. **8**, 902 (2008).

[38] S. Adam, E. Hwang, E.H.and Rossi, and S. Das Sarma, Solid State Communications **149**, 1072 (2009), Recent Progress in Graphene Studies.

[39] S. Das Sarma, S. Adam, E. H. Hwang, and E. Rossi, ArXiv e-prints (2010), 1003.4731.

[40] C. Bena, Phys. Rev. B **79**, 125427 (2009).

[41] L. Fritz, J. Schmalian, M. Muller, and S. Sachdev, Phys. Rev. B **78**, 085416 (2008).

[42] E. H. Hwang, S. Adam, and S. Das Sarma, Phys. Rev. Lett. **98**, 186806 (2007).

[43] N.-H. Shon and T. Ando, Journal of the Physical Society of Japan **67**, 2421 (1998).

[44] T. Ando, Y. Zheng, and H. Suzuura, Journal of the Physical Society of Japan **71**, 1318 (2002).

[45] M. Koshino and T. Ando, Phys. Rev. B **73**, 245403 (2006).

[46] X.-Z. Yan, Y. Romiah, and C. S. Ting, Phys. Rev. B **77**, 125409 (2008).

[47] M. Katsnelson, Euro. Phys. Jour. B **51**, 157 (2006).

[48] L. Zhu, R. Ma, L. Sheng, M. Liu, and D.-N. Sheng, Phys. Rev. Lett. **104**, 076804 (2010).

[49] J. Chen *et al.*, Nat Phys **4**, 377 (2008).

[50] Y. Y. Wang, Z. H. Ni, Z. X. Shen, H. M. Wang, and Y. H. Wu, Applied Physics Letters **92**, 043121 (2008).

[51] Z. H. Ni *et al.*, ACS Nano **3**, 569 (2009).

[52] S. Schmitt-Rink, K. Miyake, and C. Varma, Phys. Rev. Lett **57**, 2575 (1986).

[53] T. Lofwander and M. Fogelstrom, Phys. Rev. B **76**, 193401 (2007).

[54] N. W. Ashcroft and D. N. Mermin, , 1 ed. (Thomson Learning, Toronto, 1976).

[55] H. Fukuyama, Journal of the Physical Society of Japan **76**, 043711 (2007).

[56] V. P. Gusynin and S. G. Sharapov, Phys. Rev. B **73**, 245411 (2006).

[57] H. Oji and P. Streda, Phys. Rev. B **31**, 7291 (1985).

[58] N. R. Cooper, B. I. Halperin, and I. M. Ruzin, Phys. Rev. B **55**, 2344 (1997).

[59] L. Smrcka and P. Streda, J. Phys. C: Solid State Phys. **10**, 2153 (1977).

[60] E. H. Hwang, E. Rossi, and S. Das Sarma, Phys. Rev. B **80**, 235415 (2009).

[61] X.-Z. Yan and C. S. Ting, Phys. Rev. B **80**, 155423 (2009).

[62] X.-Z. Yan, Y. Romiah, and C. S. Ting, Phys. Rev. B **80**, 165423 (2009).

[63] X.-Z. Yan and C. S. Ting, Phys. Rev. B **81**, 155457 (2010).

Appendix A

Transport tensors of Graphene in a Homogeneous Magnetic Field

In this appendix were derive the Electrical, Thermoelectric, and Thermal conductivity tensor of Graphene in the Dc limit. The starting point of this section is the impurity self averaging current-current correlation tensor of graphene which has the form

$$\Pi^{e,e}_{x,x}(\overrightarrow{q} \to 0; i\Omega) = \frac{N_v e^2}{\beta} \sum_{\overrightarrow{p}, iw_n} \{(\overrightarrow{v}^2_{\overrightarrow{p},x}) \widetilde{G}_{AA,\overrightarrow{p}}(iw_n + i\Omega) \widetilde{G}_{AA,\overrightarrow{p}}(iw_n)\} \tag{A.1}$$

$$\begin{aligned}\Pi^{e,e}_{x,y}(\overrightarrow{q} \to 0; i\Omega) = \\ \frac{-N_v e^3 i|\overrightarrow{B}|}{c\beta m} \sum_{\overrightarrow{p}, iw_n} (\overrightarrow{v}_{\overrightarrow{p}})^2 \widetilde{G}_{AA,\overrightarrow{p}}(iw_n + i\Omega) \widetilde{G}_{C,\overrightarrow{p}}(iw_n + i\Omega) \widetilde{G}_{AA,\overrightarrow{p}}(iw_n) \\ + \frac{N e^3 i|\overrightarrow{B}|}{c\beta m} \sum_{\overrightarrow{p}, iw_n} (\overrightarrow{v}_{\overrightarrow{p}})^2 \widetilde{G}_{AA,\overrightarrow{p}}(iw_n + i\Omega) \widetilde{G}_{AA,\overrightarrow{p}}(iw_n) \widetilde{G}_{C,\overrightarrow{p}}(iw_n)\end{aligned} \tag{A.2}$$

$$G_{(AA,BB)}(\overrightarrow{K}, \mathrm{i}\varepsilon) = \frac{(\mathrm{i}\varepsilon - \Sigma(\mathrm{i}\varepsilon))}{(\mathrm{i}\varepsilon - \Sigma(\mathrm{i}\varepsilon))^2 - |\phi(\overrightarrow{K})|^2} \tag{A.3}$$

$$G_C(\overrightarrow{K}, \mathrm{i}\varepsilon) = \frac{|\phi(\overrightarrow{K})|}{(\mathrm{i}\varepsilon - \Sigma(\mathrm{i}\varepsilon))^2 - |\phi(\overrightarrow{K})|^2} \tag{A.4}$$

The impurity self averaging Green's function[4] of graphene has two bands, the number of bands has been accounted for by the factor of N_v multiplying the correlation function. Performing the sum over frequency and taking the real part of the electrical conductivity tensor we get

$$\sigma_{xx} = \frac{N_v e^2}{V}\sum_{\overrightarrow{p}}\int\frac{d\varepsilon}{\pi}(\frac{n_F(\varepsilon)-n_F(\varepsilon+\Omega)}{\Omega})\overrightarrow{v}^2_{\overrightarrow{p},x}ImG_{AA,p}(\varepsilon)ImG_{AA,p}(\varepsilon+\Omega) \tag{A.5}$$

$$\sigma_{xy} = \frac{-N_v e^3|\overrightarrow{B}|v_F^2}{c\Omega V}\sum_{\overrightarrow{p}}\int\frac{d\varepsilon}{\pi m}(n_F(\varepsilon)(\Sigma_{xy}^{(1,a)}-\Sigma_{xy}^{(2,a)})-n_F(\varepsilon+\Omega)(\Sigma_{xy}^{(1,b)}-\Sigma_{xy}^{(2,b)}))$$

$$\Sigma_{xy}^{(1,a)} = Im\widetilde{G}_{AA,\overrightarrow{p}}(\varepsilon)\{Re\widetilde{G}_{AA,\overrightarrow{p}}(\varepsilon+\Omega)Re\widetilde{G}_{C,\overrightarrow{p}}(\varepsilon+\Omega)-Im\widetilde{G}_{AA,\overrightarrow{p}}(\varepsilon+\Omega)Im\widetilde{G}_{C,\overrightarrow{p}}(\varepsilon+\Omega)\}$$

$$\Sigma_{xy}^{(2,a)} = Re\widetilde{G}_{AA,\overrightarrow{p}}(\varepsilon+\Omega)\{Im\widetilde{G}_{AA,\overrightarrow{p}}(\varepsilon)Re\widetilde{G}_{C,\overrightarrow{p}}(\varepsilon)+Re\widetilde{G}_{AA,\overrightarrow{p}}(\varepsilon)Im\widetilde{G}_{C,\overrightarrow{p}}(\varepsilon)\}$$

$$\Sigma_{xy}^{(1,b)} = Im\widetilde{G}_{AA,\overrightarrow{p}}(\varepsilon+\Omega)\{Re\widetilde{G}_{AA,\overrightarrow{p}}(\varepsilon)Re\widetilde{G}_{C,\overrightarrow{p}}(\varepsilon)-Im\widetilde{G}_{AA,\overrightarrow{p}}(\varepsilon)Im\widetilde{G}_{C,\overrightarrow{p}}(\varepsilon)\}$$

$$\Sigma_{xy}^{(2,b)} = Re\widetilde{G}_{AA,\overrightarrow{p}}(\varepsilon)\{Im\widetilde{G}_{AA,\overrightarrow{p}}(\varepsilon+\Omega)Re\widetilde{G}_{C,\overrightarrow{p}}(\varepsilon+\Omega)+Re\widetilde{G}_{AA,\overrightarrow{p}}(\varepsilon+\Omega)Im\widetilde{G}_{C,\overrightarrow{p}}(\varepsilon+\Omega)\}$$

(A.6)

Integrating over momentum and taking the limit of an ideal Dirac spectrum the diagonal conductivity in the dc limit is

$$\sigma_{xx}^{DC} = \frac{N_s N_v e^2}{4\pi h}\int d\varepsilon\frac{\partial n_F}{\partial\mu}(1+\frac{A^2+B^2}{AB}\arctan\frac{A}{B}) \tag{A.7}$$

where A and B are defined as $\varepsilon - Re\Sigma(\varepsilon)$ and $Im\Sigma(\varepsilon)$. The hall term can be simplified by letting $\Omega \to 0$ and using the following Identities:

$$Im(|G_{BB}|^2 G_C) = (ReG_{BB}^2 + ImG_{BB}^2)ImG_C \tag{A.8}$$

$$Im(G_{BB}^2\frac{\partial G_C}{\partial\varepsilon}) = (ReG_{BB}^2 - ImG_{BB}^2)\frac{\partial ImG_C}{\partial\varepsilon} + 2ReG_{BB}ImG_{BB}\frac{\partial ReG_C}{\partial\varepsilon}) \quad \text{(A.9)}$$

$$\sigma_{xy}^{DC} = \frac{N_v e^3|\overrightarrow{B}|v_F^3}{cV}\sum_{\overrightarrow{p}}\int\frac{d\varepsilon}{\pi|\overrightarrow{p}|}\{\frac{\partial n_F(\varepsilon)}{\partial\mu}(|\widetilde{G}_{AA,\overrightarrow{p}}(\varepsilon)|^2 Im\widetilde{G}_{C,\overrightarrow{p}}(\varepsilon))\}$$
$$- \frac{N_v e^3|\overrightarrow{B}|v_F^3}{cV}\sum_{\overrightarrow{p}}\int\frac{d\varepsilon}{\pi|\overrightarrow{p}|}\{n_F(\varepsilon)Im(\widetilde{G}_{AA,\overrightarrow{p}}^2(\varepsilon)\frac{\partial\widetilde{G}_{C,\overrightarrow{p}}(\varepsilon)}{\partial\varepsilon})\} \quad \text{(A.10)}$$

Calculating the angular integral first the hall term reduces to

$$\sigma_{xy}^{DC} = \frac{N_s N_v e^3|\overrightarrow{B}|v_F^3}{2c\pi}\int dp\int\frac{d\varepsilon}{\pi}\{\frac{\partial n_F(\varepsilon)}{\partial\mu}(|\widetilde{G}_{AA,\overrightarrow{p}}(\varepsilon)|^2 Im\widetilde{G}_{C,\overrightarrow{p}}(\varepsilon))\}$$
$$- \frac{N_s N_v e^3|\overrightarrow{B}|v_F^3}{2c\pi}\int dp\int\frac{d\varepsilon}{\pi}\{n_F(\varepsilon)Im(\widetilde{G}_{AA,\overrightarrow{p}}^2(\varepsilon)\frac{\partial G_C}{\partial\varepsilon})\} \quad \text{(A.11)}$$

where the integrals of the green's functions are

$$\int dx(|\widetilde{G}_{AA,x}(\varepsilon)|^2 Im\widetilde{G}_{C,x}(\varepsilon)) = \frac{-1}{8AB}(\frac{B^2-A^2}{B^2+A^2} - \frac{B^2+A^2}{2AB}\arctan\frac{2AB}{B^2-A^2}) \quad \text{(A.12)}$$

$$\int dx Im(\widetilde{G}_{AA,x}(\varepsilon)^2\frac{\partial\widetilde{G}_{C,x}(\varepsilon)}{\partial\varepsilon}) = \frac{-1}{3}\frac{\partial}{\partial\varepsilon}(\frac{AB}{(A^2+B^2)^2}) \quad \text{(A.13)}$$

Integrating by parts,

$$\sigma_{xy}^{DC} = \frac{-N_s N_v e^3|\overrightarrow{B}|v_F^2}{2c\pi}\int\frac{d\varepsilon}{\pi}\frac{\partial n_F(\varepsilon)}{\partial\mu}\{\frac{1}{8AB}(\frac{B^2-A^2}{B^2+A^2} - \frac{B^2+A^2}{2AB}\arctan\frac{2AB}{B^2-A^2})\}$$
$$+ \frac{N_s N_v e^3|\overrightarrow{B}|v_F^2}{2c\pi}\int\frac{d\varepsilon}{\pi}\frac{\partial n_F(\varepsilon)}{\partial\mu}\{\frac{AB}{3(A^2+B^2)^2}\} \quad \text{(A.14)}$$

The Thermoelectric conductivity tensor can be calculated similar to the Electrical conductivity tensor from the energy-charge current correlation tensor eqn.(2.33,2.34). In the Dc limit the Thermoelectric conductivity tensor is equal to the electrical conductivity kernel multiplied by energy minus the chemical potential divided by the electron charge. Thus the thermoelectric conductivity in the dc limit is

$$\beta_{xx}^{DC} = \frac{-N_s N_v e}{4\pi h} \int d\varepsilon \frac{\partial n_F}{\partial \mu}(\varepsilon - \mu)(1 + \frac{A^2 + B^2}{AB} \arctan \frac{A}{B}) \tag{A.15}$$

$$\beta_{xy}^{DC} =$$
$$\frac{-N_s N_v e^2 |\overrightarrow{B}| v_F^2}{2c\pi} \int \frac{d\varepsilon}{\pi} \frac{\partial n_F(\varepsilon)}{\partial \mu}(\varepsilon - \mu)\{\frac{1}{8AB}(\frac{B^2 - A^2}{B^2 + A^2} - \frac{B^2 + A^2}{2AB} \arctan \frac{2AB}{B^2 - A^2})\}$$
$$+ \frac{N_s N_v e^2 |\overrightarrow{B}| v_F^2}{2c\pi} \int \frac{d\varepsilon}{\pi}\{(\varepsilon - \mu)\frac{\partial n_F(\varepsilon)}{\partial \mu} - n_F(\varepsilon)\}(\frac{AB}{3(A^2 + B^2)^2}) \tag{A.16}$$

Following the same analysis used in calculating both Electrical and Thermoelectric conductivity tensors, the Heat conductivity tensor is calculated from the energy-energy current correlation tensor eqn.(2.40,2.41). The Heat conductivity tensor in the Dc limit is just the electrical conductivity kernel multiplied by the square of the quantity energy minus the chemical potential divided by the electron charge. The Heat conductivity in the dc limit is

$$\kappa_{xx}^{DC} = \frac{N_s N_v}{4\pi h} \int d\varepsilon \frac{\partial n_F}{\partial \mu}(\varepsilon - \mu)^2(1 + \frac{A^2 + B^2}{AB} \arctan \frac{A}{B}) \tag{A.17}$$

$$\kappa_{xy}^{DC} =$$
$$\frac{-N_s N_v e |\overrightarrow{B}| v_F^2}{2c\pi} \int \frac{d\varepsilon}{\pi} \frac{\partial n_F(\varepsilon)}{\partial \mu}(\varepsilon - \mu)^2\{\frac{1}{8AB}(\frac{B^2 - A^2}{B^2 + A^2} - \frac{B^2 + A^2}{2AB} \arctan \frac{2AB}{B^2 - A^2})\}$$
$$+ \frac{N_s N_v e |\overrightarrow{B}| v_F^2}{2c\pi} \int \frac{d\varepsilon}{\pi}((\varepsilon - \mu)^2 \frac{\partial n_F(\varepsilon)}{\partial \mu} - 2(\varepsilon - \mu) n_F(\varepsilon))\{\frac{AB}{3(A^2 + B^2)^2}\} \tag{A.18}$$